

Anhydrous Protein Ions

Cherokee S. Hoaglund-Hyzer, Anne E. Counterman, and David E. Clemmer*

Department of Chemistry, Indiana University, Bloomington, Indiana 47405

Received February 2, 1999 (Revised Manuscript Received June 9, 1999)

Contents

I. Introduction	3037	V. Other Biopolymers: DNA and Oligosaccharides	3073
A. Scope and Organization of This Review	3038	VI. New Analytical Methods that Are Based on Gas-Phase Ion Properties	3073
B. Brief Description of the Protein Folding Problem and the Importance of Water	3039	VII. Summary and Future Prospects	3075
II. Electrospray Ionization	3040	VIII. Acknowledgment	3076
A. General Experimental Features	3040	IX. References	3076
B. Evidence that Ions Are Formed through Evaporation of Solvated Droplets	3040		
C. Influence of Gas-Phase Ion Stability on the ESI Charge State Distribution	3041		
D. Influence of Solution Conformation upon Charge State Distributions	3042		
E. Do Gas-Phase Proteins Retain a Memory of the Solution Conformation?	3043		
III. Chemical Probes of Conformation	3044		
A. Proton-Transfer Reactivity Studies	3044		
1. Proton Affinities of the 20 Common Amino Acids and Small Peptides	3044		
2. Multiply Charged Peptides and Proteins	3045		
3. General Considerations of Apparent Gas-Phase Basicity Measurements of Multiply Protonated Proteins	3045		
B. Hydrogen–Deuterium Exchange as a Probe of Gas-Phase Ion Conformation	3048		
1. Small Peptides and Exchange Mechanism	3049		
2. Multiply Charged Peptides and Proteins	3049		
C. Capture of Target Molecules by Peptide Ions	3051		
D. Molecular Adduction	3051		
IV. Physical Methods for Probing Biomolecular Ion Structure	3052		
A. Collision-Induced Dissociation (CID) Studies Designed To Locate Charge Sites	3052		
B. Collision Induced Dissociation as a Probe of Gas-Phase Protein Conformations	3053		
C. Photodissociation and Spectroscopic Probes	3053		
D. Blackbody Infrared Radiative Dissociation (BIRD)	3053		
E. Thermal Dissociation at High Pressures	3054		
F. Kinetic Energy Release Distributions (KERD)	3054		
1. Stability of the Melittin α -Helix in Solution, Crystal, and the Gas Phase	3055		
2. Evidence for Persistence of Multistrand β -Pleated Sheets	3055		
G. Collision Cross Sections	3055		
1. Ion Scattering in Triple Quadrupole Instruments	3055		
2. Ion Mobility Measurements	3057		
H. Microscopy Studies of Surface Imprints	3071		

I. Introduction

The recent development of electrospray ionization (ESI)¹ and matrix-assisted laser desorption ionization (MALDI)² sources for creation of macromolecular ions has brought about a renaissance in the field of mass spectrometry (MS). It is now common to determine molecular weights of large molecules such as proteins to within a few daltons (or less)! MS-based methods for sequencing are proliferating and replacing (or complementing) traditional biochemical methods for many applications. However, analysis of covalent structure is only part of the story. A number of studies have investigated the use of MS strategies for examining noncovalent biomolecular structure. Mounting evidence suggests that some conformational properties of biomolecules in solution are preserved during the ionization process and persist over the transient time that ions exist in mass spectrometers. The persistence of solution-like structure in the gas phase provides opportunities to examine conformation and folding as well as binding interactions (e.g., enzyme–substrate, receptor–ligand interactions) in an entirely new environment.

In the past 5 years, a new field involving structural studies of biomolecular ions has emerged. At first glance, the relevance of biomolecular ion structure in the gas phase to studies of functional molecules in solution may seem far removed, perhaps not unlike questions about the relevance of structural measurements of protein crystals 20–30 years ago. Studies of biomolecular ions in the gas phase provide information about the nature of conformation in the absence of solvent; thus, the roles of intramolecular interactions and solvent can be discerned by comparison of similarities between gas- and solution-phase structure. Additionally, the utility of MS strategies for sampling noncovalent binding between molecules in solution hinge on a fragile balance of interactions associated with the assembled pair as the ions travel through the mass analyzer. As these strategies become widely used, the differentiation



Cherokee S. Hoaglund-Hyzer received her B.S. in Chemistry and Mathematics from Adrian College in Adrian, MI, in 1996. She is in her third year of graduate school at Indiana University pursuing her Ph.D. in Analytical Chemistry with a minor in Biochemistry and is currently working on development of combined ion mobility/mass spectrometry instrumentation for the analysis of biological mixtures.



Anne E. Counterman earned her B.S. in Chemistry and Chemical Engineering at the University of Delaware in Newark, DE, in 1996 and is currently a third-year graduate student at Indiana University pursuing her Ph.D. in Analytical Chemistry with a minor in Physical Chemistry. Her research interests include using ion mobility/time-of-flight methods to explore the influence of amino acid sequence upon gas-phase peptide ion conformations.

between specific and nonspecific interactions will become increasingly important.

A. Scope and Organization of This Review

In this review, we present a comprehensive assessment of what is currently known about the structures of solvent-free protein ions (including peptides). Although there has been substantial progress in understanding the structures of anhydrous proteins, it is clear that this field is in its infancy and that the questions that have arisen far outnumber the answers that have been obtained. Studies of gas-phase protein ions are based on a long and rich history of gas-phase studies of smaller ions. We refer to this work frequently in order to clarify the understanding of larger systems; however, the review does not attempt to include all of the relevant work on smaller systems. Many of the experiments described in this work take advantage of spectacular advances in analytical instrumentation. When possible, we describe advantages of particular methods and discuss recent variations or improvements to techniques that



David E. Clemmer obtained his B.S. in Chemistry from Adams State College in Alamosa, CO, and his Ph.D. in Physical Chemistry from the University of Utah under the sponsorship of Peter B. Armentrout. He was a Japan Society Fellow for the Promotion of Science in Himeji, Japan, and worked with Martin F. Jarrold at Northwestern University. In 1995 he joined the faculty at Indiana University where he is currently Assistant Professor of Chemistry. His research involves understanding the formation of structure in large low-symmetry systems in the gas phase and the development of analytical methods for characterizing large mixtures.

are particularly relevant to studies of gas-phase ion structure. However, we do not present the basic operating principles of these methods. Several reviews of instrumentation are especially relevant to this work, including several papers on quadrupole mass filters,³⁻⁵ ion traps,⁶⁻⁹ Fourier transform ion cyclotron resonance (FTICR),¹⁰⁻¹³ ion mobility spectrometry,¹⁴⁻¹⁶ dissociation methods,¹⁷ and microscopies.^{18,19}

The gas-phase structural work also benefits from sophisticated molecular modeling software used for generating trial conformations. It is possible to generate thousands of energy-minimized trial conformers for comparison with experimental results. Much of the experimental work that is presented below has been complemented by theory. With so little known about the validity of calculations of in vacuo conformations, the interplay between molecular modeling results and methods for collision cross-section calculation is important. The ability to compare calculations with experiment should aid in refinement of the force fields used for these calculations. A number of force fields, including several variations of AMBER,²⁰ CHARMM,²¹ CVFF,²² and GROMOS,²³ have recently been used to generate trial in vacuo conformations for comparison with experimental results. Below we describe only those theoretical studies that have been compared directly with experimental results for biomolecular ions.

This manuscript is organized as follows. We start by describing the formation of macromolecular ions from charged droplets that are produced by ESI. Special attention is given to the final stages of the ESI process, where the naked ion is formed—the transition region where the interactions that are responsible for stabilizing structures in solution shift to those that are present in the anhydrous gas-phase ion. Much of this presentation relies on results obtained from structural studies of the gas-phase ions, which are described in detail in later sections.

Our presentation of structural studies of protein ions is organized in terms of the techniques used to obtain structural information. These techniques have been grouped into two categories: chemical probes, in which structural characteristics are deduced by monitoring the products of ion–molecule reactions, and physical probes, such as measurements of dissociation patterns and measurements of cross sections. A large portion of the review is devoted to ion mobility measurements of collision cross sections. Although the application of this method to biomolecular ion structure came much later than many other methods, it currently provides the most definitive information about ion shape and has played an important role in understanding earlier studies and defining the elements of structure that are important in the gas phase. It is fortunate that at this stage several systems have been investigated by multiple methods, allowing information obtained from different techniques to be compared. In several cases, the complementary nature of different methods makes it possible to draw conclusions that were not apparent in the original experiments.

Several authoritative reviews of the strategies for elucidating structure that are described here, proton-transfer reactions, isotopic H–D exchange, MS dissociation methods, and ion scattering and ion mobility measurements of collision cross section, have been given recently. Proton-transfer reactivity has been reviewed recently by Williams²⁴ (1996), Green and Lebrilla²⁵ (1997), and Harrison²⁶ (1997). The Green and Lebrilla paper also presents a thorough discussion of isotopic H–D exchange as a probe of gas-phase ion structure. McLuckey (1997) has discussed time scale considerations relevant to dissociation methods.¹⁷ Douglas (1998) has recently described collision dynamics in quadrupoles.²⁷ Clemmer and Jarrold (1997) reviewed the early work involving the use of ion mobility spectrometry for measurements of biomolecular ion cross section.¹⁶ When possible, we refer to the coverage of topics in these thorough writings. However, the substantial progress made in this field during the past few years and the degree of understanding that has been obtained leaves much to be covered here. Additionally, new experimental techniques have evolved, including exciting measurements of surfaces after exposure to high-energy bombardment. This review attempts to relate the results obtained from ion–molecule reactions to physical measurements. When possible, we have also drawn comparisons between noncovalent structures in the gas phase and those that are found in solution; however, in the interest of providing a comprehensive assessment of the gas-phase studies, the discussion of solution-phase work is presented in brevity and neglects many elegant experiments. Several recent reviews that address the influence of bulk solvent upon conformation,^{28,29} protein folding in solution,^{30–33} and the prediction of conformation from sequences³⁴ will be useful to the interested reader. Finally, the properties of biomolecular ions in the gas phase have recently been exploited as analytical tools for rapid characterization of protein conformation in solution and also for analysis of biomolecular mixtures. A brief

discussion of the application of these principles as new analytical methods is given. Opportunities for extending these methods in the future are mentioned.

B. Brief Description of the Protein Folding Problem and the Importance of Water

In the 1950s, the observation that denatured ribonuclease A spontaneously refolded into the native conformation (under physiological conditions) demonstrated that primary sequence and environment are sufficient to specify conformation.^{35,36} A tremendous effort has been devoted to elucidating the factors that define conformation.^{30,37–41} Understanding the details of folding and delineating the delicate balance between intramolecular, solvent–molecule, and solvent–solvent interactions that define the properties of the native state, as well as intermediate structures that are present during folding, is referred to as the “protein folding problem”. One property of proteins that complicates work in this area is the transient nature of folding intermediates. In even the best cases, structural information is limited to a few partially folded states (which are believed to be folding intermediates or kinetically trapped metastable structures). Folding mechanisms must explain the processes that allow an inexhaustible number of different random or partially folded states to reach the native structure.³² Ideally, one would like to take snapshots of many structures as they fold in order to determine the step-by-step motions that allow many different conformers to be funneled into the native state.⁴⁰

An important factor in folding involves solvent–molecule interactions. Proteins appear to form physiologically relevant conformations in the presence of a minimum hydration shell.²⁸ A typical protein crystal (which often has a conformation that is similar to the solution structure) is comprised of 25–90% solvent.⁴² This solvent shell is believed to be at least partially responsible for the observation that crystal conformations normally resemble solution structures obtained by nuclear magnetic resonance (NMR) methods. The intrinsic propensity of the polypeptide chain to form the native structure (regardless of solvent contributions) will also contribute to structural similarities. The magnitude of the energetic contributions of solvent was recently illuminated in a comparison of folding free energies for cytochrome *c* in vacuo,⁴³ where estimates range from –2182 to –3497 kJ mol⁻¹,^{21,44,45} with the –37.1 kJ mol⁻¹ value from solution.⁴⁴ This difference arises because in the gas-phase strong intramolecular interactions are not mitigated by solution effects.

The exact roles of solvent and structural changes that occur when critical levels of solvent are removed constitute active research areas. Recent studies have considered structural changes that occur when proteins are lyophilized by examining anhydrous powders and thin films. Techniques such as Fourier transform infrared (FTIR) spectroscopy,⁴⁶ Raman spectroscopy,⁴⁷ and H–D exchange NMR methods⁴⁸ have shown structural changes upon removal of solvent.⁴⁹ For example, Griebenow and Klibanov have shown that the fraction of β -sheet content increases

at the expense of α -helix propensity upon lyophilization and that there is an increase in protein order.⁴⁶ These results can be understood by considering that in the anhydrous solid, protein molecules are forced into contact with one another and intermolecular β -sheet formation is not prohibited entropically, as is the case for the isolated proteins in solution. An understanding of the origins of this phenomenon is particularly important, since the aggregation of polypeptides through β -sheet interactions has recently been proposed to explain plaque and fibrils⁵⁰ associated with Alzheimer's^{51,52} as well as newly discovered prion-based diseases.^{53,54} Very recently, evidence that most proteins have an intrinsic ability to transform into fibrils has been presented.⁵⁵

Inference of the contributions of solvent to structures from comparisons of protein conformation of anhydrous powders to solution structures for the isolated molecules is complicated by intermolecular interactions (in the former system). This comparison is simplified by examining the isolated anhydrous molecules in the gas phase. Until recently, these studies were impossible because of the low vapor pressures of large molecules such as proteins (e.g., a value of 10^{-480} atm has been reported for a 14 000 amu molecule).⁵⁶ When heated, these molecules denature, making them even less volatile; the molecules decompose rather than vaporize.⁵⁶ ESI has offered a simple, efficient means of producing gaseous, anhydrous biomolecules for study by mass spectrometry. New chemical and physical probes are being invented to explore the behavior of these ions. Early on in these studies it became apparent that the answers to seemingly simple questions were not obvious. For example, it was initially unclear if ionized proteins formed unique conformations. It turns out that there are favored structures in the gas phase. Moreover, recent studies show that in some cases gas-phase proteins can retain a degree of memory of their solution structures. Anhydrous proteins also fold and unfold, and new conformations are established in a grossly simplified environment where only intramolecular constraints are relevant.

Wolynes has commented that an understanding of the nature of gas-phase conformations addresses fundamental questions about evolutionary constraints on folding kinetics.⁵⁷ It may be the case that the framework of intramolecular interactions within proteins in solution persists in the gas phase. Inasmuch as this is true, gas-phase conformation should resemble the ensemble of equilibrium structures that is present in solution. Alternatively, in the apolar vacuum, proteins may turn inside out in order to maximize intramolecular interactions between polar groups.⁵⁷ A discussion of new methods and studies that provide initial insight into protein structure in this unusual environment is the subject of this review.

II. Electrospray Ionization

In this section we describe electrospray ionization (ESI). An especially relevant question that arises in studies of conformations of gas-phase ions involves the mechanism of the ESI process. Mounting evi-

dence indicates that distributions of gas-phase protein ion conformations may reflect the ensemble of solution states that exists during the final stages of ESI. An understanding of what factors influence ion conformation as they are produced provides some insight into what types of structural elements may be preserved in vacuo. We do not include a discussion of the mechanisms for other recently developed sources for producing macromolecular ions because most structural work has utilized ESI.^{58,59}

A. General Experimental Features

Several excellent reviews have covered work involving the generation of charged droplets and the general features associated with ion formation.^{60–63} Charged droplets containing molecular ions are initially formed by pumping a solution through a narrow capillary tube that is electrically biased with respect to an entrance orifice of a mass spectrometer. The electrode shapes, geometries, and potentials are important for generating a stable spray of droplets; however, many different experimental configurations can be used. Two widely held views of the mechanism for ESI are that solvent-free molecular ions are formed either after a series of droplet fissions, followed by solvent evaporation from the ion (proposed by Dole,^{56,64,65} Fenn,^{1,60,66,67} and their collaborators), or by ion evaporation from the droplet surface (proposed by Iribarne and Thomson⁶⁸), a process driven by repulsive Coulombic interactions. The mechanistic details of ESI are still under investigation.

The generally accepted features of ESI are as follows. Initial electrospray generates charged droplets which, when small enough, undergo a series of Coulomb-driven fissions, producing even smaller charged droplets. Evaporation of solvent and ions leads to droplets of decreasing size and ultimately to formation of the gas-phase ion. Smith et al. have noted that in the ion evaporation model of Iribarne and Thomson it is often assumed that biomolecular ions are evaporated from the droplet surface in a highly charged entirely desolvated state.⁶³ Exactly what happens in the final stages leading to ion formation is poorly understood; these final steps of ESI are critical in determining the initial gas-phase ion conformation. In this transition region, the protein structure evolves from the equilibrium distribution of conformations in solution (defined by solvent–solvent, solvent–molecule, and intramolecular interactions) to a distribution of gaseous, anhydrous molecular ions with structures that depend only on intramolecular constraints.

B. Evidence that Ions Are Formed through Evaporation of Solvated Droplets

Increasingly, studies suggest that in the final stages of ESI, ion–solvent adducts are formed and that dissociation of solvated molecules produces the solvent-free ion. Several groups have recorded the distribution of ion mobilities through a high pressure of gas immediately following ESI of protein solutions. A general feature of these studies is the observation

of a broad peak at drift times that are much longer than expected for arrival of desolvated charge states of proteins. Dole,⁶⁹ Smith,⁷⁰ Hill,⁷¹ Guevremont,⁷² and their collaborators have observed such features and suggested that these are probably attributable to highly solvated ions. Hill and co-workers have heated the drift tube buffer gas (which is similar to heating the ESI interface region) and shown that the broad features are transformed into a series of sharp peaks that can be assigned as individual charge states of the desolvated protein.⁷¹ These data are consistent with desolvation of highly solvated ions to produce naked biomolecular ions.

In other studies, highly solvated biomolecules that are formed from the ESI source have been observed directly. Chait and co-workers show that under some source conditions, peptide ions with waters attached could be resolved.⁷³ Williams used a quadrupole mass filter instrument to record mass spectra as a function of ESI source temperature.⁷⁴ As the ESI source temperature was decreased, peptide ions with distributions of solvent clusters (up to 50 attached water molecules) were observed. Beauchamp and co-workers have used FTICR methods to observe clusters with more than 100 water adducts attached to peptide ions and have used off-resonance ejection of specific sizes to demonstrate that evaporation occurs sequentially.⁷⁵ The consensus of these studies is that a gentle transition involving the stepwise evaporation of water is operative during the final stages of ion formation. This evaporation process cools the biomolecular ion and may cause some solution structure to be "frozen" in the gas-phase ions. Beauchamp has termed this a "freeze-drying" process.⁷⁵

C. Influence of Gas-Phase Ion Stability on the ESI Charge State Distribution

As a rule of thumb, the maximum charge state for protein ions produced by ESI is usually no greater than the total number of basic Arg, Lys, and His residues and N-termini in the sequence.^{70,76} A few exceptions exist. For example, Smith et al. have observed that as many as 59 charges can attach to actin, even though it has only 46 basic residues.⁷⁷ It is useful to consider the thermodynamic and kinetic processes that produce the protonated biomolecule from the charged droplet. In solution, the net charge on the protein will depend on the number of accessible acidic (Asp, Glu, and C-terminal) and basic (Lys, Arg, His, and N-terminal) sites (defined by the protein sequence and structure) and the solution pH.⁷⁸ During the final stages of evaporation of the charged, solvated biomolecule, the retention or elimination of a charge from the protein should depend on the relative protonation thermochemistry of the protein and the solvent molecules, as well as factors associated with the rate of drying. Many conformations are probably present and are likely to change as solvent evaporates. Adducted solvent molecules will influence the conformation as well as the thermochemistry of protonation sites.

To a first approximation, the geometries of a solvent-free protein should be determined by the change in the charge repulsion associated with dif-

ferences in the dielectric constants for the surrounding media (~ 80 for water,⁷⁹ and 1.0 for a vacuum). Smith treated the protonation of a polypeptide by considering a model in which charges were placed equidistant on a string.⁸⁰ The authors note that this model is mainly qualitative; the issue of protonation is much more complicated for a heterogeneous system such as a protein. Jarrold and co-workers have recently calculated that for the +7 charge state of cytochrome *c* (which they considered to have 31 basic sites: 2 Arg, 19 Lys, 3 His, 3 Gln, 1 Trp, and 4 Pro residues), there are $31!/(7!(31 - 7)!)$ or 2 629 575 possible charge site assignments.⁸¹ Williams previously calculated that there are $\sim 10^{14}$ unique ways to assign 13 charges along the small (76 residue) ubiquitin protein (if one considers the possibility that the backbone amide N-H groups may be protonated);⁸² for carbonic anhydrase (260 residues) there are $\sim 10^{50}$ ways to assign 45 charges.

Although detailed assignments of charges to specific sites are usually not possible, the maximum observable charge state can be predicted by a model developed by Williams and co-workers (described in detail in section III.A.3). In initial studies, this model was used to consider the influence of Coulomb repulsion on the gas-phase basicity of 13 common proteins for which rigid linear string geometries were assumed. The calculated apparent gas-phase basicities decrease with increasing charge state; when the basicities of a high charge state fall below the gas-phase basicities of the solvent molecules, the solvent is protonated. The authors were able to predict the maximum charge state of the proteins to within an average of 6%, demonstrating that the thermochemistry of the gas-phase ions are important in the ESI process.

Additional insight into the charging phenomenon is obtained by combining measurements of collision cross sections for different charge states with charging limits imposed by calculations of gas-phase basicities for different geometries. The gas-phase basicities of the compact crystal conformation of cytochrome *c* are predicted to fall below the gas-phase basicities of methanol and water for charge states higher than +8 and +10, respectively.⁸³ Structures that are more extended in nature, such as linear string-like or α -helical conformations, will have greater distances between charges and thus lower Coulomb energies; these should form higher charge states. Ion mobility measurements of cross sections for cytochrome *c* show evidence for compact conformers for the +10 and lower charge states; substantially more extended forms exist as higher charge states. Several factors may explain this. From gas-phase basicity arguments, it should not be possible to add protons to a compact conformer containing 10 charges because of the high Coulomb repulsion between charges (i.e., low gas-phase basicity) of the compact conformer for higher charge states.

The combined interpretation of apparent gas-phase basicity and ion mobility measurements is consistent with a series of recent measurements by Smith, Whitesides, and their co-workers.⁸⁴ In these studies, capillary electrophoresis (CE) and ESI-MS were

combined to study charge ladders of a series of related proteins. The "charge ladder" expression refers to neutralization (via covalent modification) of different numbers of basic sites prior to ESI. Modified proteins, which should have similar conformations, vary by the number of remaining charged residues (which can be estimated from the CE measurement). ESI mass spectra obtained for proteins having different numbers of covalent modifications were remarkably similar; the authors conclude that the ESI charge state is defined by electrostatic interactions between charges on the gas-phase protein surface and not the number of solution charged sites.

D. Influence of Solution Conformation upon Charge State Distributions

Charge state distributions generated by ESI do depend on the conformation of the biomolecule in solution. Smith and co-workers^{85,86} have shown that mass spectra obtained upon electrospraying disulfide-intact proteins favor substantially lower charge states than data obtained when 1,4-dithiothreitol was used to reduce the disulfide bonds. An example is shown in Figure 1 for ESI of albumin (bovine, mol wt = 66 kDa, which has 17 disulfide bonds) where the +67 and lower charge states are observed when the disulfide bonds are intact; when the disulfide bonds are reduced, as many as 100 protons are attached to the protein. When the disulfide bonds are reduced, interior regions of the protein are exposed to solvent, such that many additional basic sites are accessible for protonation during ESI.

Chowdhury, Katta, and Chait have investigated electrosprayed cytochrome *c* as a function of solution pH.⁸⁷ Cytochrome *c* is a small protein containing 104 residues and a heme prosthetic group that is covalently attached at the 14 and 17 cysteine residues. In the native conformation, the heme iron is coordinated to a ring nitrogen of the histidine 18 residue and a sulfur of the methionine 80 residue.^{88,89} Studies of cytochrome *c* in solution using a number of techniques, including circular dichroism⁹⁰ and NMR,⁹¹ demonstrate that under acidic conditions at least three conformations exist. Figure 2 shows the mass spectra obtained upon electrospraying a 1×10^{-5} M cytochrome *c* solution containing (a) 4% acetic acid, pH = 2.6; (b) 0.2% acetic acid, pH = 3.0; and (c) no acetic acid, pH = 5.2. The mass spectrum in part a (low pH, where three states were known to exist in solution) shows eight peaks (+11 to +18, where +16 is most intense). When the pH is increased to 3.0, a second charge state distribution which is almost entirely comprised of the +8 charge state is observed. When no acid is added (pH = 5.2), the charge state distribution centered around the +16 ion decreases and a new distribution which favors the +10 ion is observed. These results can be interpreted by noting that different conformations in solution have different numbers of exposed basic sites. The results demonstrate the viability of ESI to sample properties of noncovalent solution conformation.

Factors such as temperature, solvent composition, and ionic strength can also influence biomolecular conformation in solution. Loo et al. have examined

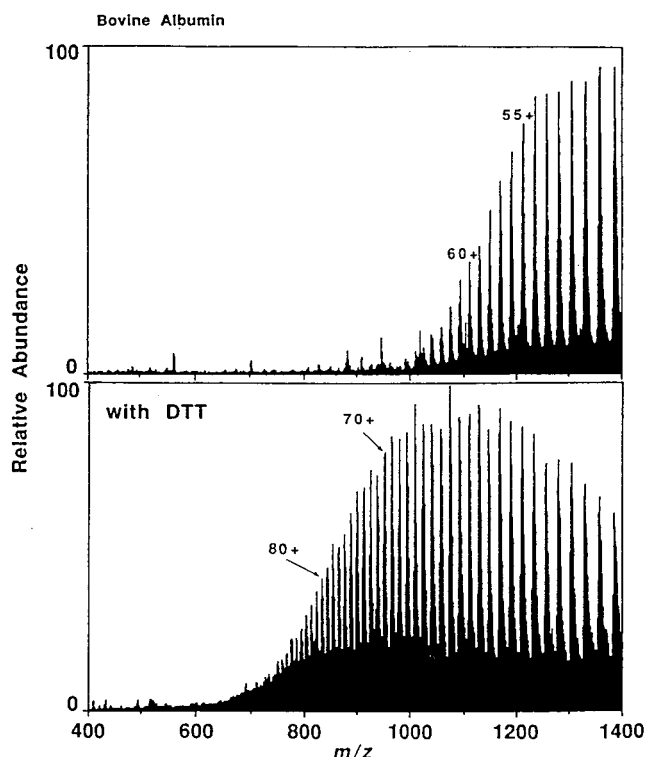


Figure 1. ESI mass spectra of bovine serum albumin ($M_r = 66$ kDa), a 585 residue protein that contains 17 disulfide bonds: (top) native form; (bottom) after disulfide bond reduction with 1,4-dithiothreitol (DTT). (Reproduced with permission from ref 70. Copyright 1991 John Wiley & Sons.)

the changes in ESI charge state distributions for lysozyme (hen, mol wt = 14,306) and ubiquitin (bovine and yeast, 8564.8) that are observed upon varying the pH and the fraction of several organic solvents (methanol, acetonitrile, 2-propanol, and acetone) used.⁹² When the fraction of these organic solvents was increased, a shift to higher charge states was observed in the ESI-MS data. The transition from low to high charge states was found to vary depending upon which organic solvent was used, a result which indicated that the protein had denatured in solution. Even changes induced by mild denaturants are discernible by ESI analysis. Le Blanc et al.,⁹³ as well as Mirza, Cohen, and Chait,⁹⁴ examined the influence of solution temperature upon charge state distributions for a number of proteins including cytochrome *c* and lysozyme (a 129 residue protein with four Cys–Cys disulfide bonds) and found that thermal denaturation is also discernible. At low solution temperatures, low charge states are favored; at high temperatures where thermal denaturation can occur, high charge states are observed.

Mirza and Chait⁹⁵ have used a heated capillary ESI source to test the possibility that proteins may denature in the ESI droplet as it travels through the capillary interface into the mass spectrometer. Charge state distributions of proteins electrosprayed from native solution conditions were insensitive to the heated capillary temperature, a result that is substantially different from the effect of heating the ESI solution. The authors concluded that the transport time (calculated to be ~ 0.6 ms) of charged droplets through the tube was too short for the transfer of

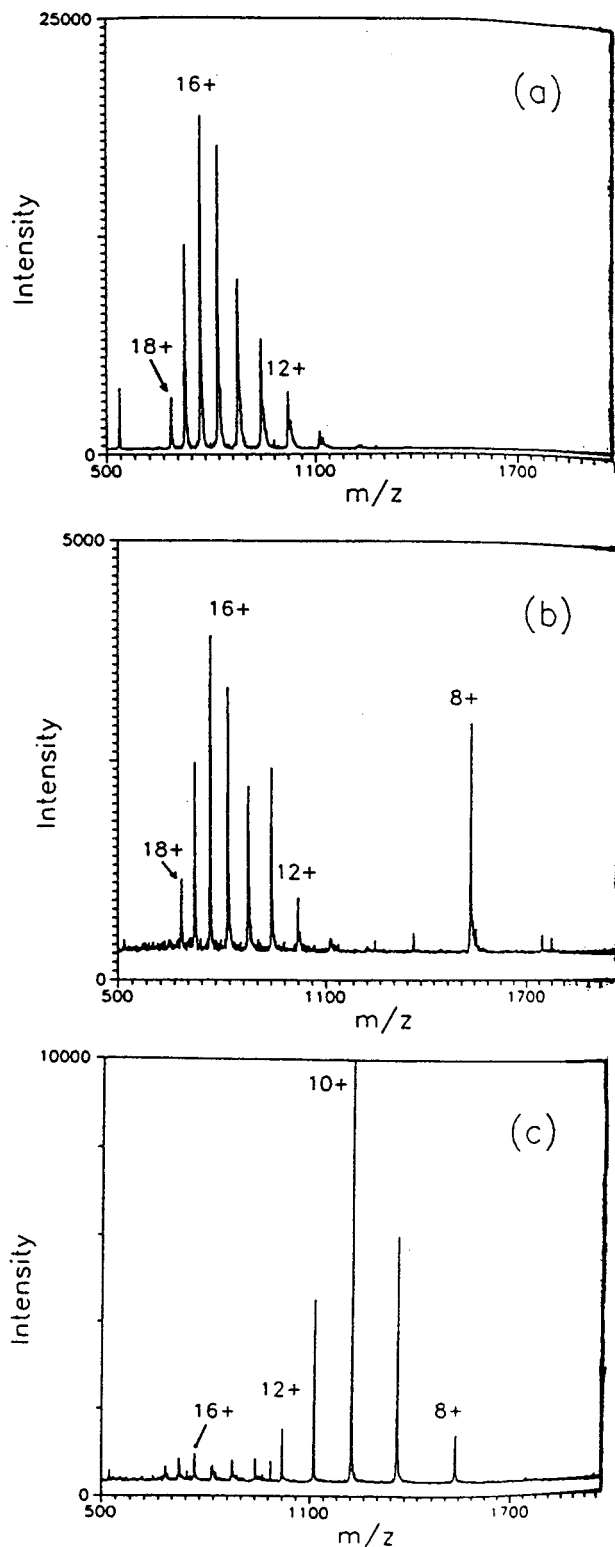


Figure 2. Electrospray mass spectra of bovine cytochrome *c* charge state distributions at various pH values. Protein concentration is 1×10^{-5} M in (a) 4% acetic acid, pH = 2.6, (b) 0.2% acetic acid, pH = 3.0, and (c) no acid, pH = 5.2. (Reproduced with permission from ref 87. Copyright 1990 American Chemical Society.)

heat required for denaturation in the solution droplet. Ogorzalek Loo and Smith⁹⁶ have also examined the influence of capillary temperature upon charge state distributions and did observe a shift in charge state distribution for electrosprayed cytochrome *c* at high capillary temperatures, an indication that these

solution conditions may lead to 'solution-like' denaturation.

E. Do Gas-Phase Proteins Retain a Memory of the Solution Conformation?

There is now strong evidence suggesting that under some ESI conditions, gas-phase ions retain a memory of the distribution of conformations that are present in solution. Ogorzalek Loo and Smith investigated the proton-transfer reactivity of disulfide-reduced and disulfide-intact ions of three proteins (α -lactalbumin, proinsulin, and albumin).⁹⁶ For a specific charge state, disulfide-reduced ions are substantially less reactive than disulfide intact ions. Disulfide-reduced ions can adopt extended structures that lower Coulombic repulsion. Similar studies of non-disulfide-bound protein ions (ubiquitin, cytochrome *c*, and myoglobin) showed no significant differences in the proton-transfer reactivities for ions formed from different solution compositions.⁹⁶ However, several other studies suggest that solution composition can influence gas-phase ion conformation for these proteins. Douglas,⁹⁷ Jarrold,⁹⁸ and their collaborators have measured cross sections for cytochrome *c* ions that were electrosprayed from different solution conditions. Both experiments show that collision cross sections measured for the +9 and +10 ions are smaller when the solution composition is more aqueous and larger when large fractions of nonpolar solvents are used. Suckau et al. found less extensive isotopic exchange for low charge state ions when cytochrome *c* was electrosprayed from more aqueous solutions than for high charge states found from solutions containing a larger fraction of organic solvent.⁹⁹

Li et al. have carried out high-pressure ion mobility studies for ubiquitin ions as a function of solvent composition and capillary temperature.¹⁰⁰ These results show that the distributions of the gas-phase ion conformations for all charge states differ depending on the solvent conditions used; ions from more aqueous solutions were more compact than those from solutions containing a significant fraction of organic solvent. Studies as a function of capillary temperature showed no significant changes in the charge state distributions, consistent with the results of Mirza and Chait.⁹⁵ However, mobility studies showed that as the capillary temperature was increased, the ion mobility distributions for different solution conditions became more similar.¹⁰⁰ For some charge states, elongated conformers were favored regardless of the initial solution conditions. Similar work in which ions are injected into drift tubes at high injection energies (760 eV) also showed favored gas-phase states that are independent of ESI solvent compositions.¹⁰¹ These results show that the conditions of heated capillaries and high injection energies (as well as other gas-phase perturbations) may cause gas-phase ions to lose memory of their solution states. Finally, Williams and co-workers used blackbody infrared radiative dissociation (BIRD) techniques to investigate the energetics of noncovalent heme binding in holo-myoglobin and holo-hemoglobin.¹⁰² They observed that the ordering of the stability of heme

attachment was the same in the gas-phase ions as is observed in solution and that the stabilities decreased when ions were produced from denaturing solutions.

In summary, it appears that ion structure in the final stages of ESI are influenced by both the properties of solution and the nature of the gas-phase ion that is formed. The solution environment influences the conformation of the ion in the droplet. As the last solvent molecules evaporate, the relationship of stable solution structures to the stability of the gas-phase conformer and thermochemistry of proton attachment becomes important in defining the initial gas-phase structure. In many cases, it appears that the initial structure is metastable. High-energy collisions or heated capillary interfaces may give rise to new gas-phase conformations.

III. Chemical Probes of Conformation

Once proteins are introduced into the gas phase, it is possible to select specific m/z ions for exposure to chemical reagents in order to probe reactivity patterns. The chemical changes observed provide information about the properties of the gas-phase ions, including the types of chemical moieties present and the conformation. Our discussion of reactivity studies is divided into three sections: (1) proton-transfer reactions; (2) isotopic hydrogen–deuterium (H–D) exchange; and (3) molecular adduction of solvents to the biomolecular surface.

A. Proton-Transfer Reactivity Studies

Accurate measurements of the kinetics and thermochemistry associated with proton transfer between peptide and protein ions and small neutral molecules can be used to extract information about conformation. These measurements are nontrivial, even for small ion–molecule systems; large multiply charged ions present additional challenges. By convention, the proton affinity (or gas-phase basicity) associated with a molecule **B** corresponds to $-\Delta H$ (or $-\Delta G$) for the attachment of a proton to molecule **B** by the reaction $\mathbf{B} + \mathbf{H}^+ \rightarrow \mathbf{BH}^+$. For small molecular ions, a number of methods have been used to determine proton affinities (or gas-phase basicities), including equilibrium binding studies,^{103,104} the kinetic method,¹⁰⁵ and bracketing.^{106,107} Complete discussions of the application of all three of these methods for determining thermochemistry for biomolecular ions has been given in recent reviews by Harrison²⁶ and Green and Lebrilla.²⁵ Proton affinities of individual amino acids and gas-phase basicities for a few small peptides are discussed in brevity in this section; these values are of interest because they refine our intuition about where charges should be located in larger proteins and the structural features that are associated with the charged site. Larger systems have been reviewed by Williams²⁴ and are discussed in more detail below (section III.A.3). The interested reader should refer to the aforementioned reviews^{25,26} for a complete discussion of this work.

1. Proton Affinities of the 20 Common Amino Acids and Small Peptides

Extensive work involving measurements of the gas-phase basicities of individual amino acids has been

Table 1. Proton Affinities (in kcal mol⁻¹) of Common Amino Acids

amino acids	PA ^a
Gly	211.9
Ala	215.5
Cys	215.9
Asp	217.2
Val	217.6
Glu	218.2
Ser	218.6
Leu	218.6
Ile	219.3
Pro	220.0
Thr	220.5
Phe	220.6
Tyr	221.3
Asn	222.0
Met	223.6
Gln	224.1
Trp	226.8
His	236.1
Lys	238.0
Arg	251.2

^a All values are taken from the 1998 compilation by Hunter and Lias (ref 117). A compilation of amino acid proton affinities based on the 1984 scale of Lias, Liebman, and Levin (ref 116) is given in a review by Harrison (ref 26). The experimental values are reported in refs 110, 108, 113, and 114. Values are listed in order of increasing proton affinity.

carried out.^{26,108–115} Some of this work was tabulated in a 1984 compilation of ion thermochemistry provided by Lias, Liebman, and Levin;¹¹⁶ a more recent compilation by Hunter and Lias¹¹⁷ is available online.¹¹⁸ A summary of proton affinity data for individual amino acids is given in Table 1; values range from ~212 to 251 kcal mol⁻¹. The proton affinities for the arginine, histidine, and lysine amino acids are substantially greater than those for other residues, consistent with the pK_a s for amino acids in solution.¹¹⁹ The effect of charge stabilization in the gas-phase amino acids has been considered in detail. Theoretical studies indicate that with the exception of arginine, histidine, and lysine, the preferred site of protonation for the common amino acids is the N-terminus.^{26,120–123} The large values of the proton affinities for lysine and histidine (and large entropies, $\Delta S(\text{Lys}) = 10.1 \text{ cal mol}^{-1} \text{ K}^{-1}$ and $\Delta S(\text{His}) = 4.2 \text{ cal mol}^{-1} \text{ K}^{-1}$) have been interpreted in terms of the formation of favorable interactions in which the two amines are associated with the proton, forming a cyclic structure.^{124,125} Intramolecular charge solvation effects are also an important structural feature of larger peptide ions.

A number of small singly protonated glycine-based peptides,^{123,126–128} polyalanine, polyvaline, and other small peptides have also been investigated.^{129–132} The consensus of work on the small homopolymers is that the preferred site of protonation is the N-terminus. Table 2 provides a list of measured gas-phase basicities for 34 dipeptides and 16 tripeptides, as well as several larger peptides.¹¹⁷ The observation that the gas-phase basicity of peptides generally increases with increasing chain length can be attributed to stabilization of the charge through interactions with other residues. In particular, charge stabilization associated with interaction of the protonated site with the electronegative carbonyl groups of other

Table 2. Gas-Phase Basicities (in kcal mol⁻¹) of Peptides

peptide	GB ^a	peptide	GB ^a
AV	208.9	GGA	218.6
DV	208.9	GGP	218.8
GV	208.9	GPG	218.8
VD	208.9	AGG	219.4
VG	208.9	GGL	219.4
VS	208.9	GLG	220.3
GS	210.5	PGG	221.1
LV	211.2	LGG	221.5
VA	211.2	HGG	226.1
VV	211.2	GHG	228.4
VL	211.2	GKG	228.4
SG	211.9	G GK	229.1
SS	211.9	KGG	229.1
FV	213.6	GGH	234.1
YV	213.6	G GK	245.8
MV	214.9	GKKG	241.0
GP	216.4	GKKGK	241.6
PV	217.3	KGGGK	245.7
VF	217.3		
VM	217.3	GG	210.8
VW	217.3	GGG	219.1
VY	217.3	GGGG	221.8
VP	219.6	GGGGG	220.1
VE	220.1	GGGGGG	227.1
KV	220.9	GGGGGGG	234.4
VK	220.9	GGGGGGGG	236.8
PG	221.1	GGGGGGGGG	240.1
PP	225.8	AA	216.4
GK	226.0	AAA	220.9
KG	226.1	AAAA	225.8
GH	228.4	AAAAA	229.9
HG	228.4	AAAAAA	234.5

^a All values are taken from the 1998 compilation by Hunter and Lias (ref 117). A recent review by Harrison (ref 26) tabulates most of these values based on the 1984 basicity scale of Lias, Liebman, and Levin (ref 116). Individual experimental values can be found in refs 114, 123, 126, and 127.

residues is significant.^{123,126,127} The high gas-phase basicities for sequences containing Arg, His, and Lys is evidence that these groups are the preferred charge sites.

2. Multiply Charged Peptides and Proteins

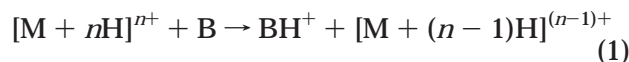
McLuckey, Van Berkel, and Glish reported the first proton-transfer studies for macromolecular ions using ion trap techniques.¹³³ In this work, different charge states of cytochrome *c* were selected in the trap and exposed to dimethylamine vapor. Rate constants for proton transfer were found to decrease with decreasing charge state. The authors noted that as charges are removed, remaining protons will be held more strongly.

Several groups have initiated proton-transfer reactions by introducing reagents into moderate pressure regions that are present prior to the mass spectrometer.^{101,134} Smith and co-workers have developed a 'Y' tube inlet reactor, where reagents are entrained in the flow of gas in the ESI source capillary. This configuration has been used in a number of studies to investigate the abstraction of protons from positively charged ions by neutral bases⁹⁶ and the addition of protons to negatively charged (deprotonated) ions by acids.¹³⁵ Although the reaction conditions are somewhat ill-defined (i.e., there is no initial ion selection and the gas composition is a mixture of

base, electrospray solvent, and ambient laboratory air), the proton-transfer reactions compete efficiently with other processes such as adduction, making this a relatively simple means of studying ion-molecule reactions. As mentioned in section II.E, disulfide-intact ions are substantially more reactive than disulfide-reduced ions.¹³⁶ Disulfide-reduced ions are free to adopt more open conformations, which can reduce Coulombic repulsion. Subsequent gas-phase basicity (section III.A.3),¹³⁷ ion mobility cross section (section IV.G.2.g),¹³⁸ and microscopy ion impact (section IV.H)^{139,140} studies of disulfide-intact and -reduced lysozyme are in agreement with this. Smith and co-workers have also investigated proton-transfer reactions with charge-transfer reagents having varying proton affinities as a function of capillary temperature.¹⁴¹

3. General Considerations of Apparent Gas-Phase Basicity Measurements of Multiply Protonated Proteins

Thermochemical values for large multiply charged ions have been obtained from bracketing measurements involving the reaction



These reactions are influenced by the presence of a reverse activation barrier that arises due to long-range Coulomb repulsion of the two charged products. Williams and co-workers have described the origin of this barrier using the qualitative potential energy surfaces shown in Figure 3.⁸³ The discussion given here assumes that $\Delta S = 0$; thus, the terms gas-phase basicity (GB) and proton affinity (PA) are equivalent. While ΔS is often close to zero for proton-transfer reactions of singly charged ions (i.e., $AH^+ + B \rightarrow A + BH^+$), ΔS can be significant for addition of a proton to a neutral molecule (i.e., $B + H^+ \rightarrow BH^+$).

For the surfaces shown in Figure 3, the proton affinities of the M, A, and B reagents are ordered as $PA(M) = PA(A) < PA(B)$ and $PA(MH^+) = PA(C)$.

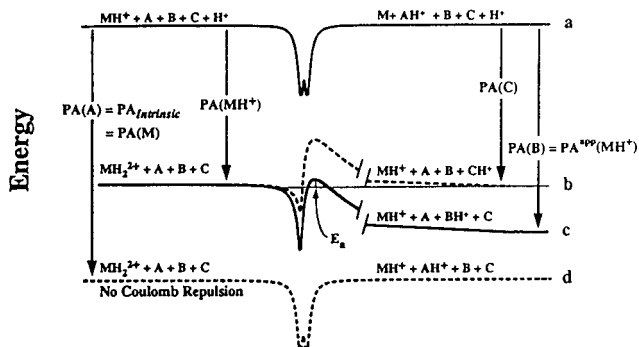


Figure 3. Qualitative interaction potentials for proton-transfer reactions of singly and doubly protonated M and neutral reference bases (A, B, and C), where M is a symmetrical molecule with two identical sites of protonation separated by $>10 \text{ \AA}$. The surfaces that are shown correspond to: (a) reaction of MH^+ with A, $PA(M) = PA(A)$; (b) reaction of MH_2^{2+} with C, $PA(MH^+) = PA(C)$; (c) reaction of MH_2^{2+} with B, $PA^{app}(MH^+) = PA(B)$; (d) the hypothetical reaction of MH_2^{2+} with A in the absence of Coulomb repulsion. (Reproduced with permission from ref 83. Copyright 1995 American Chemical Society.)

Proton transfer from MH^+ to A is thermoneutral and proceeds on a totally symmetric surface (Figure 3a). Proton transfer from MH_2^{2+} to C is also thermoneutral; however, a reverse activation barrier arises for the interaction of the MH^+ and CH^+ products because of the long-range Coulomb potential (Figure 3b). Thus, the rate of the forward reaction will be limited due to the presence of the substantial reverse activation barrier. Because B has a higher proton affinity, the overall proton-transfer reaction from MH_2^{2+} will be exothermic; this lowers the reverse activation barrier (Figure 3c) and should increase the reaction rate (relative to proton transfer to A).

The net result of multiple charging is a shift of the measurable thermochemistry by the Coulomb barrier. Figure 3d shows the surfaces that would be operative if Coulomb repulsion was neglected. Thermochemistry relative to this surface corresponds to the intrinsic thermochemistry of the species in the system. Experimentally, Coulomb repulsion and entropy cannot be removed from measurements; therefore, measured values are reported as apparent gas-phase basicities (i.e., the negative of the free energy associated with addition of a proton to a reagent M by the reaction $\text{M} + \text{H}^+ \rightarrow \text{MH}^+$).

The presence of the reverse activation barrier introduces some ambiguity in gas-phase basicity measurements.²⁴ Bracketing measurements require the establishment of a cutoff associated with the minimum rate constant that can be measured for a thermodynamically allowed process. Below this rate, the reaction is normally assumed to be endoergic. In the case of proton transfer between a singly charged ion and a neutral base, this cutoff is usually clear. Plots of the reaction efficiency as a function of the gas-phase basicity of the neutral molecule have relatively well-defined break points that usually occur over a few kcal mol^{-1} . The presence of the reverse activation barrier in the case of multiply charged ions makes the break point substantially less clear. Cassady has provided a detailed comparison of the break points for the +13 charge state of ubiquitin and for the singly protonated GlySer dipeptide.¹⁴² A sharp decrease in the reaction efficiency of the $[\text{GlySer} + \text{H}]^+$ ion is observed between gas-phase basicity values of 207 and 212 kcal mol^{-1} . The profile for the highly charged ubiquitin ion has a break point that occurs over a substantially larger range; the curve has an inflection point at 220 kcal mol^{-1} but continues to decline gradually until 196 kcal mol^{-1} . Ultimately the choice of break point will influence the absolute values of the thermochemistry more than relative values (between charge states). Gronert has suggested that break points along the reaction efficiency curve between 0.1 and 0.2 be used.¹⁴³

Since the first measurements of apparent gas-phase basicities for protein ions by Cassady et al.,^{144,145} this group has studied a number of systems including different charge states of ubiquitin, insulin chain B, renin substrate (a tetradecapeptide),¹⁴² and several related triply-protonated dodecapeptides containing 4 Lys and 8 Gly residues of varying sequence by FTICR techniques.¹⁴⁶ Gas-phase basicities for these systems as well as those discussed

below are provided in Table 3. Particularly interesting is the observation of multiple reaction rates for certain charge states of ubiquitin and insulin chain B. These were interpreted in terms of multiple isomers (different protonation configurations) or conformations of the gas-phase ions. For the dodecapeptides, the efficiency of proton transfer was found to depend on the locations of basic residues and increased in the following order: $[(\text{K}_2\text{G}_4)_2 + 3\text{H}]^{3+} < [(\text{KGG})_4 + 3\text{H}]^{3+} < [\text{K}_4\text{G}_8 + 3\text{H}]^{3+}$. These results emphasize the influence of Coulomb repulsion on the efficiency of deprotonation.

a. Information About Conformation and Charge Shielding. Williams and co-workers have measured the apparent gas-phase basicities of different charge states of cytochrome *c*,⁸³ lysozyme,¹³⁷ and a number of peptides^{82,147,148} and developed a model that allows gas-phase basicities for trial conformations to be calculated from intrinsic basicities and the Coulomb repulsion of sites.⁸² The apparent gas-phase basicity of the protein is related to the intrinsic basicity of the site involved in proton transfer as given by

$$\text{GB}^{\text{app}} = \text{GB}_{\text{intrinsic},t} - \sum_{i=1}^n \frac{q^2}{(4\pi\epsilon_0)\epsilon_r r_{i,t}} \quad (2)$$

where $\text{GB}_{\text{intrinsic},t}$ corresponds to the intrinsic proton-transfer reactivity of a protonation site *t* and the remaining terms account for the sum of Coulomb repulsion energies experienced by the protonation site from other protons where ϵ_0 is the permittivity of free space, ϵ_r is the dielectric constant, *n* is the number of charges on the ion, and $r_{i,t}$ is the distance between charges assigned to the *i* and *t* locations. Measurements of gas-phase basicities for peptide ions allow values of $\text{GB}_{\text{intrinsic},t}$ to be estimated.⁸² The model implicitly assumes that protonation sites can be represented as point charges. From eq 2, it is clear that as protons are removed from a multiply protonated ion, the basicity of the ion will approach the value of the intrinsic basicity.¹⁴⁹ By comparing calculated basicities for trial conformations (using assumed values of the dielectric polarizability, ϵ_r) with the experimental thermochemistry, it is possible to propose structural information. Similarly, by assuming a conformation, it is possible to elucidate values of dielectric polarizabilities. This model does not explicitly account for the fact that structures may change when charges are removed.

The first application of this model involved the proton-transfer reactions of doubly protonated gramicidin S.¹⁴⁷ The authors derived a lower limit of 27.9 kcal mol^{-1} for the Coulomb energy associated with the doubly protonated ion. This value was combined with geometric information about the distances between charged residues (using complementary molecular modeling methods) to deduce an upper limit for the dielectric polarizability for this ion of 1.2.

Figure 4 shows an extension of this method to examine the +3 to +15 charge states of cytochrome *c*.⁸³ The experimental gas-phase basicities are compared with calculated apparent gas-phase basicities for three different ion conformations: linear extended conformers, using $\epsilon_r = 2.0$; linear α -helical forms,

Table 3. Apparent Gas-Phase Basicities for Individual Peptide or Protein Charge States

molecule	z^a	GB(app), ^b kcal mol ⁻¹	
FYGPV ^c		234.3	
YDWGFM ^c		234.3	
CYIQNC ^c		237.4	
GAGGVGKS ^c		241.5	
YGGFLK ^c		> 243.3	
gramicidin S ^c		219.1	
RST ^d	1	221.6	
	2	205.3	
	3	< 195.6	
insulin chain B ^d	1	> 232.6	
	2	212.2	
	3	203.4, 0.68 ^c	
	3	204.1, 0.32 ^c	
	4	198.2, 0.38 ^c	
	4	203.4, 0.62 ^c	
(KGG) ₄ e	2	208.7	
	3	202.8	
(K ₂ G ₄) ₂ e	2	209.6	
	3	202.8	
K ₄ G ₈ e	2	207.3	
	3	187.3	
ubiquitin (bovine) ^d	3	224.0(0.62)	
		231.5(0.30)	
		> 232.6(0.08)	
	4	224.0(0.59)	
		227.0(0.41)	
	5	224.4(0.80)	
		225.1(0.20)	
	6	218.1	
	7	211.8	
	8	211.7	
	9	211.8	
	10	211.5	
	11	205.6(0.50)	
		208.9(0.50)	
	12	205	
cytochrome <i>c</i> (horse) ^f	3	234.3	
	4	234.3	
	5	228.1	
	6	228.3	
	7	223.3	
	8	219.1	
	9	216.2	
	10	216.2	
	11	212.2	
	12	212.2	
	13	206.3	
	14	206.3	
	15	191.5	
		disulfide-intact	disulfide-reduced
lysozyme (hen egg white) ^g	3	234.3(0.46)	241.5(0.55)
	4	234.3	238.6
	5	234.3	234.3
	6	234.3	229.3(0.51)
			234.3(0.49)
	7	229.3(0.7)	229.3(0.7)
		234.3(0.3)	234.3(0.3)
	8	226.4(0.9)	223.3(0.2)
		229.3(0.1)	226.5(0.4)
			229.3(0.4)
	9	223.3(0.85)	206.3(0.3)
		229.3(0.15)	214.7(0.7)
	10	219.1	201.0(0.6)
			211.2(0.4)
	11	216.2(0.1)	
		219.1(0.7)	
		223.4(0.2)	
	12	214.7(0.4)	
		219.1(0.6)	
	13	214.7	
	14	211.2	
	15	211.2	

^a Protonation state. ^b Measured value of apparent gas-phase basicity. If multiple reactive conformations were observed, the fraction of the population having the listed gas-phase basicity is given in parentheses. The basicities given here are based on the scale of Lias, Liebman, and Levin (ref 116). ^c Schnier et al., ref 82. ^d Zhang and Cassady, ref 142. Values were converted from apparent gas-phase acidities, GA(app) (as originally reported) by using the simple relation GB(app)[M + (n - 1)H]⁽ⁿ⁻¹⁾⁺ = GA(app)[M + nH]ⁿ⁺. RST = renin substrate tetradecapeptide. ^e Cassady et al., ref 146. ^f Schnier et al., ref 83. ^g Gross et al., ref 137.

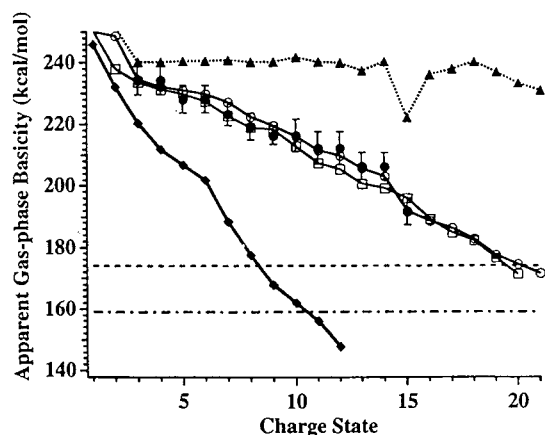


Figure 4. Apparent gas-phase basicity as a function of charge state for cytochrome *c* ions, measured (●), and calculated assuming three different ion conformations: linear extended ($\epsilon_r = 2.0$, ○; $GB_{\text{intrinsic}}$, ▲), linear α -helix ($\epsilon_r = 4.1$, □), and the X-ray crystal structure ($\epsilon_r = 2.0$, ◆). The dashed line indicates the gas-phase basicity of methanol ($174.1 \text{ kcal mol}^{-1}$), and the dash-dot line indicates the gas-phase basicity of water ($159.0 \text{ kcal mol}^{-1}$). The origin of the dip in $GB_{\text{intrinsic}}$ at $n = 15$ is deprotonation of backbone sites in the lowest energy configurations for this charge state. (Reproduced with permission from ref 24 which was adapted from ref 83. Copyright 1996 John Wiley & Sons.)

using $\epsilon_r = 4.1$; and the X-ray crystal structure, using $\epsilon_r = 2.0$. The authors note that in order for the crystal model to fit the experimental results, a value of $\epsilon_r = 12 \pm 2$ is required. Comparisons with theoretical values of $\epsilon_r = 2-4$ for protein cores^{150,151} led the authors to conclude that values of $\epsilon_r = 12$ are too high to fit the data. On the basis of these results, the authors were unable to distinguish between helical ($\epsilon_r = 4.1$) and linear string ($\epsilon_r = 2.0$) forms and postulated that a structure that was intermediate between these forms would also be consistent with these results. The authors indicated that because the data for all charge states can be reproduced by their model using one conformation and a single ϵ_r value, all charge states have a common ion structure. However, they also noted that tertiary structure could exist in lower charge states. These compact conformers would require a higher ϵ_r value. The latter interpretation (i.e., that compact conformers at lower charge states have higher values of ϵ_r) is most consistent with measurements of collision cross sections (sections IV.G.1 and IV.G.2) and H–D isotopic exchange studies (section III.B.2) for cytochrome *c*.

If one assumes that the different ion charge states in Williams' studies have cross sections that are similar to those from ion mobility work, then it appears that eq 2 predicts higher values of ϵ_r for low charge state ions than would be expected from calculations of protein cores. Recent work on peptides indicates that charges are highly solvated by electronegative residues, consistent with this idea.¹⁵²⁻¹⁵⁵ The combined measurements of gas-phase basicity and cross sections (section IV.G.2.g) suggest that charges in compact conformations of low charge states of proteins are also heavily shielded. Detailed delineation of the important interactions that shield charges for different charge states and conformations

of gas-phase proteins should provide insight into interactions of charges in condensed phase systems.

Gas-phase basicities of the $[M + H]^+$, $[M + X]^+$, $[M + 2H]^+$, and $[M + H + X]^{2+}$ ions of gramicidin S (where X = Li, Na, or K) have also been reported.¹⁴⁸ The rate of proton-transfer from $[M + H + X]^{2+}$ to dipropylamine was shown to decrease with increasing size of the attached alkali cation; the authors interpreted this as an indication that the each metal cation was similarly attached on the external surface of the cyclic peptide structure.

b. Evidence for Protein Folding Transitions.

Gross et al. extended comparisons of calculated and experimental gas-phase basicities to investigate the conformations of disulfide-intact and disulfide-reduced lysozyme ions.¹³⁷ Measurements of charge-transfer reaction kinetics indicated that multiple structures within individual charge states were present. For the +9 and +10 charge states, the gas-phase basicities for disulfide-reduced ions were substantially greater than values for the disulfide-intact ions. Comparison of the experimental gas-phase basicities with values that were calculated for extended linear string models and the lysozyme crystal coordinates showed that high charge states of the disulfide-reduced ions have open conformations. Lower charge states for disulfide-intact ions were in better agreement with more compact structures. When protons were removed from high charge states of the disulfide-reduced ions, charge states below +8 were measured to have similar (or indistinguishable) reactivities. This indicated that the once extended forms of disulfide-reduced ions had transformed into more compact conformers by folding in the gas phase. The results are particularly important because the folding has occurred in the complete absence of solvent. In this case, the driving force for folding is the relief of repulsive Coulombic barriers by the removal of charges. Measurements of collision cross sections recorded by Valentine et al. for disulfide-intact and -reduced lysozyme after ions were exposed to proton-transfer reagents (discussed in detail in section IV.G.2.g)¹³⁸ corroborate many of the ideas proposed by Gross et al.

B. Hydrogen–Deuterium Exchange as a Probe of Gas-Phase Ion Conformation

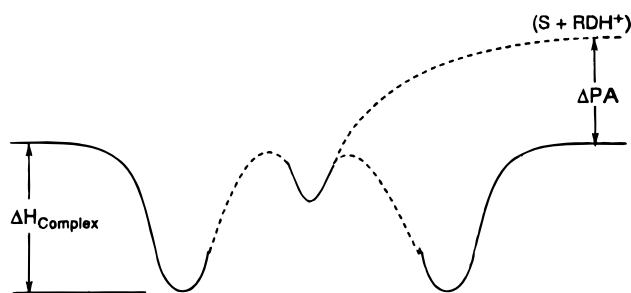
Isotopic H–D exchange of peptides and proteins in solution can be monitored by a number of techniques including NMR and MS and has recently been used to infer information about folding.⁴⁹ Several discussions covering the application of MS for studies of H–D exchange of proteins in solution have been given.¹⁵⁶⁻¹⁶² In this section, the use of H–D exchange as a probe of gas-phase ion conformation is described. This work is deeply rooted in fundamental studies involving smaller ion–molecule systems.^{163,164} In particular, the mechanism of H–D exchange has been investigated previously and has been reviewed in detail by Green and Lebrilla.²⁵ Here, we provide a brief discussion of the exchange mechanism and focus on work involving larger protein ion systems. The experimental work involving H–D exchange of protein ions in the gas phase shows that this method is

a tremendously sensitive probe of structure. However, at this stage, the mechanism of exchange in these larger systems remains largely unknown. For example, in large proteins it seems likely that intramolecular scrambling (which will depend on the locations of charged sites and conformation of the protein) will play an important role in establishing the maximum exchange level. Because of this, the relationship between exchange level and conformer shape (i.e., the accessibility of sites for exchange imposed by the conformation) remains elusive. That said, the method is evolving rapidly; as new MS techniques for determining sites of exchange emerge, it is likely that the approach will be sensitive to subtle details of gas-phase conformation.

1. Small Peptides and Exchange Mechanism

In the generally accepted mechanism for gas-phase H–D exchange between a small ion and a deuterated reagent molecule, exchange occurs via a three-step process such as that depicted by the qualitative energy diagram shown in Scheme 1 (Reproduced with

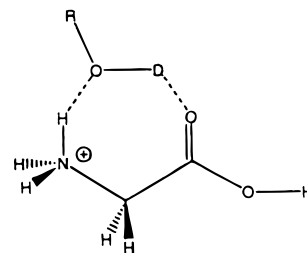
Scheme 1



permission from ref 25. Copyright 1996 John Wiley & Sons).²⁵ In this diagram, the reagents SH^+ and RD interact to form a long-lived collision intermediate ($\text{SH}^+ \cdots \text{RD}$). Intramolecular proton transfer within this intermediate forms the $\text{S} \cdots \text{RDH}^+$ intermediate, which upon dissociation can lead to isotopic scrambling ($\text{SD}^+ + \text{RH}$) or the original reagents ($\text{SH}^+ + \text{RD}$). Except for small differences associated with zero-point energies of the deuterated and nondeuterated forms of the reactants and products, the overall process is thermoneutral. The difference in proton affinities of the S and R reagents influences H–D exchange because this affects the stability of the $\text{S} \cdots \text{RDH}^+$ intermediate necessary for isotopic scrambling. For small molecules, H–D exchange is facile when the difference in S and R proton affinities is less than $\sim 20 \text{ kcal mol}^{-1}$.²⁵

A number of studies involving amino acid and peptide ions, including those by Beauchamp,^{165,166} Fenselau,¹⁶⁷ Lebrilla,^{168,169} and their collaborators, have shown that facile exchange can occur when substantially larger proton affinity differences ($> 50 \text{ kcal mol}^{-1}$) exist. This has been rationalized by noting that hydrogen bonding can stabilize intermediates. The exchange mechanism for amino acids and small peptides has been investigated extensively by Lebrilla's and Beauchamp's groups. Gard et al. have proposed that exchange of amino acids with deuter-

Scheme 2



ated methanol may involve extensively hydrogen bonded intermediates such as that shown in Scheme 2 (Reproduced with permission from ref 168. Copyright 1998 Elsevier.) for glycine.^{168,169} FTICR and semiempirical calculations for exchange of glycine oligomers containing 1–5 residues with D_2O , CD_3OD , CD_3COOD , and ND_3 have been used to examine several types of mechanisms.^{165,166} Of particular interest to larger systems are results for D_2O in which a relay mechanism, where the D_2O shuttles a proton from the N-terminus to a slightly less basic site in the molecule was proposed. Wytttenbach and Bowers¹⁷⁰ have recently used this mechanism to explain Zhang's and Marshall's FTICR results for exchange of bradykinin with D_2O .¹⁷¹ This work assumes that exchange occurs on the peptide surface and requires distances between the charged site and the less basic site of less than 4 Å. When the deuterated solvent bridges these sites, it abstracts the proton and a deuteron is shuttled to the less basic site. An important feature of this mechanism was the development of a molecular modeling based algorithm for determining surface availability as structures fluctuate. This allows all protonation sites to be accessed over the long (2 h) experimental time scales. Recently, Lee et al. have used crown ether complexation to restrict the participation of the charged site in exchange.¹⁷² These studies implicate a salt-bridge mechanism in which the charged site plays an ancillary role in exchange by stabilizing the ion pair.

2. Multiply Charged Peptides and Proteins

Isotopic H–D exchange methods have recently been applied to a number of peptide and protein systems in order to investigate ion conformation. Smith and co-workers investigated deuterium incorporation by electrospraying disulfide-intact and -reduced forms of proinsulin and α -lactalbumin.⁸⁶ These ions were exposed to D_2O vapor as they traveled through the desolvation region of the ESI source. The different levels of exchange that were observed were interpreted in terms of the reactivities of the disulfide-intact and -reduced ion conformations. Interestingly, ions with intact disulfide bonds (which are expected to have compact conformations) exchanged more hydrogens than ions with disulfide bonds reduced (which were expected to have more open gas-phase conformations). The authors speculated that the reactivity of the compact conformers was greater because of the increased Coulomb energy. These arguments are consistent with the discussion of the idea that increased Coulomb repulsion would lower the ion's proton affinity (as discussed in section

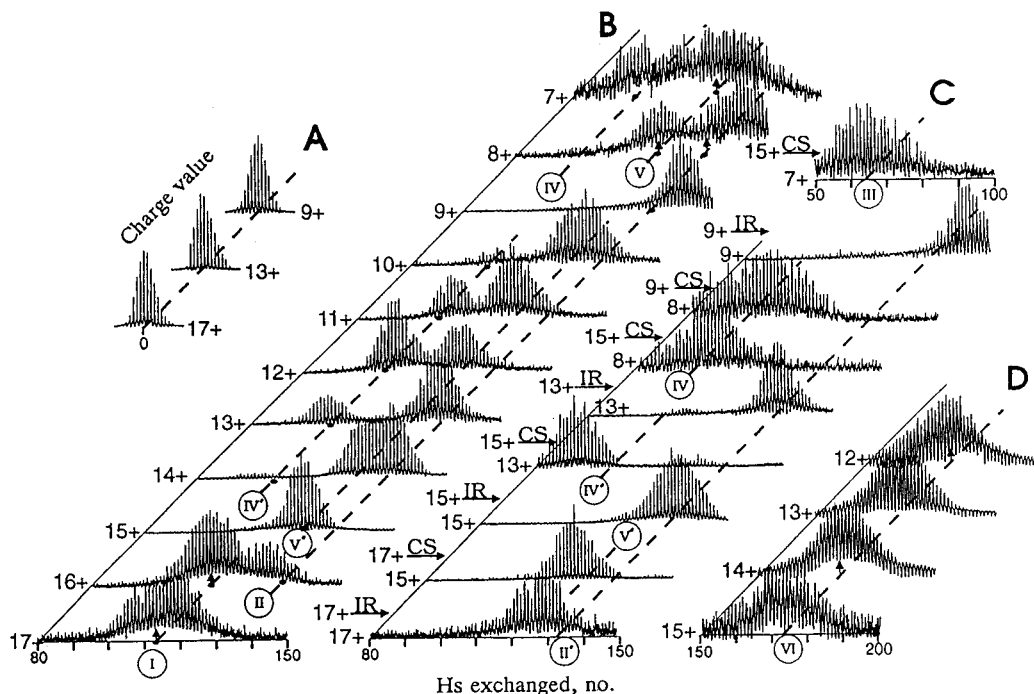


Figure 5. FTICR isotopic peak distributions for various charge states of electro sprayed equine cytochrome *c*. (A) Typical precursor $[M + nH]^{n+}$ (most abundant isotopic peak contains seven ^{13}C atoms and ^{56}Fe). (B) Spectrum observed after exchange with gaseous D_2O , and (C) data recorded after ions have been exposed to IR irradiation or charge stripping (CS). (D) Spectrum obtained following quadrupolar axialization collisions. (Reproduced with permission from ref 175. Copyright 1993 Dover.)

III.A.3);⁸² the lower difference in proton affinities for the compact conformer and D_2O would decrease the barrier to exchange as shown in Scheme 1.

In 1993, McLafferty and co-workers used FTICR techniques to investigate the conformations of five proteins (cytochrome *c*, ubiquitin, myoglobin, and two forms of RNase); trapped ions were exposed to dilute concentrations of D_2O vapor (ca. 10^{-7} Torr), and exchange levels were monitored for extended time periods (seconds to 30 min).⁹⁹ The most extensive studies were performed for cytochrome *c*, the neutral protein has 198 heteroatom hydrogens. These experiments provided evidence for distinct gas-phase conformations that were stable over the extended time scale of the experiment. In the initial report, four stable gas-phase conformers were observed over the range of charge states (+6 to +16) that were examined. These studies were both inspiring and controversial; the ability to investigate conformations of solvent-free proteins over extended time periods in such detail was unprecedented. The authors interpreted their results as an indication that there was a direct correspondence between the gas-phase exchange levels and known solution conformers. In a later paper,¹⁷³ McLafferty et al. concluded that there were no close similarities between gaseous and solution cytochrome *c* conformers. Another important result of the initial study was that H–D exchange levels were relatively insensitive to the ion charge state, an indication that the gas-phase conformations were not influenced substantially by changes in Coulomb repulsion. This result seemed to conflict with cross-section measurements of Covey and Douglas near the same time (section IV.G.1)⁹⁷ which showed that conformations expand with increasing charge. Later, combined H–D exchange ion mobility

studies found that exchange of elongated conformers was independent of charge state even when cross sections increased by more than 20% (section IV.G.2.h).¹⁷⁴

Wood et al. reinvestigated the cytochrome *c* system in order to explore how physical and chemical perturbations of the ions influence conformation.¹⁷⁵ This study used a new experimental apparatus, and the exchange levels that were measured were higher than in the initial study. Some of the results that were found upon exposing ions to various perturbations are shown in Figure 5 as a plot of the number of hydrogens that have exchanged. Part A shows typical isotopic distributions for several charge states: +9, +13, and +17. The results obtained after exposure of ions to D_2O vapor are shown for the +7 to +17 charge states in part B. The data for the +7 charge state shows that a wide range of exchange levels are observed (from ~ 90 to 130). Higher charge states show evidence for well-defined exchange levels for multiple conformations; for example, the +11 to +13 charge states each show two resolved features that exchange ~ 102 and ~ 124 sites. Part C shows the exchange levels that are observed after ions have been exposed to either infrared laser radiation or to butylamine (which leads to proton-transfer reactions). When the +13 state was exposed to infrared radiation, only a single exchange level (centered at ~ 132 exchanged sites) was observed. The authors interpreted this result as an indication that the ions have undergone unfolding transitions, similar to thermal denaturation in solution; still higher levels are observed after ions are exposed to quadrupolar axialization collisions (Part D). When protons are stripped from high charge states (such as the +15 state shown in part C), the new lower charge state

ions that are formed favor states that exchange at substantially lower levels. These results indicate that the ions have undergone folding transitions. Subsequent ion mobility studies of cytochrome *c* also found evidence for multiple stable conformations and evidence for folding and unfolding transitions.¹⁷⁴ Observations of folding and unfolding transitions in this unusual environment and the plethora of powerful laser, collisional, and reactivity strategies associated with MS opened up a wide range of new opportunities for understanding solvent and intramolecular contributions to conformation and folding.⁵⁷

Several additional studies showing evidence for multiple stable conformer forms of peptides and protein ions have been presented. In further studies of cytochrome *c*, McLafferty et al. investigated the temperature dependence of exchange and proposed locations of exchange sites based on MS/MS experiments.¹⁷³ Cassady's¹⁴⁵ and Marshall's¹⁷⁶ groups have investigated ubiquitin and found evidence for multiple conformations. Evidence for unfolding transitions that occur as a function of ESI capillary temperature, which bear remarkable similarity to ion mobility results (section IV.G.2.g), have been presented.¹⁷⁶ Freitas et al. have investigated the exchange levels for several peptide ion systems and noted that the reproducibility of three experiments on separate days is better than $\pm 10\%$.¹⁷⁷ So far, most H–D exchange results (and also ion mobility results) for peptides smaller than ~ 10 residues behave as though a single conformation is favored (i.e., there is no direct evidence for multiple resolvable features associated with different stable conformers). Of particular interest are results for the angiotensin II peptide (*L*-Asp–Arg–Val–Tyr–Ile–His–Pro–Phe) which shows two types of exchange processes, indicating that two stable conformations are present. Recent ion mobility data for angiotensin II show that two conformations can be resolved.¹⁷⁸ Finally, H–D exchange has recently been applied to studies of negatively charged oligonucleotides.^{179,180}

C. Capture of Target Molecules by Peptide Ions

Initial insight into the conformation of peptide ions came from the observation that small polypeptide ions could capture target gases at moderate collision energies (12–24 eV in the center-of-mass frame) by Cheng and Fenselau.¹⁸¹ These studies came about at a time when several groups had shown that C_{60}^+ could incorporate target molecules during high-energy collisions.^{182–184} The authors interpreted the observation of target capture by peptide ions as evidence that gas-phase polypeptide ions are self-solvated, leading to conformations that approach spherical shapes. They referred to this shape as a “loose-woolen ball”. This interpretation was an important first step in understanding that peptide ions did not have floppy string-like structures.

D. Molecular Adduction

Arguably the most relevant noncovalent adduct that can be investigated in the gas phase is the partially solvated biomolecule produced by ESI. By

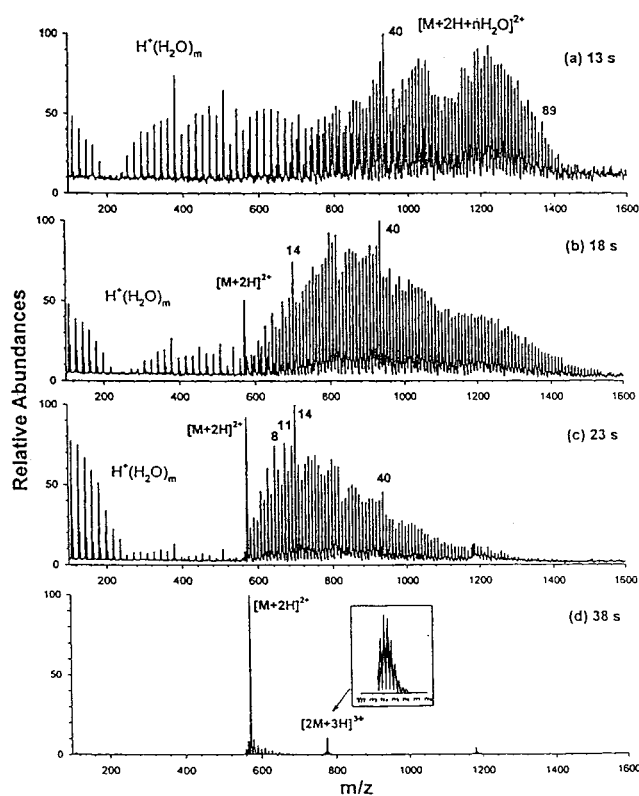


Figure 6. FTICR mass spectra showing water clusters detected at various delay times for gramicidin S. Solution contains $50 \mu\text{M}$ analyte in 0.01% acetic acid solution. Magic number clusters are observed with $n = 40$ (where n is the number of adducted waters) often being most prominent in the mass spectra. (Reproduced with permission from ref 75. Copyright 1998 American Chemical Society.)

varying the temperature of the ESI capillary, Williams and co-workers were able to control solvent adduction to gramicidin S {a cyclic decapeptide, $(-\text{Pro}-\text{Val}-\text{Orn}-\text{Leu}-D-\text{Phe}-)_2$, where Orn corresponds to ornithine $[\text{R} = (\text{CH}_2)_3\text{NH}_3^+]$.⁷⁴ In this study, mass spectra were recorded using a quadrupole mass filter. Ions were observed with as many as 50 water adducts having an intensity distribution that was approximately Gaussian. Some mass spectra revealed the presence of “magic” numbers of 8, 11, and 14 water molecules attached to the peptide, suggesting that favorable arrangements of water molecules can solvate the charge and peptide surface.

Beauchamp and co-workers have also investigated highly solvated states of gramicidin S by trapping ions for extended timeperiods (1–118 s) in a temperature-controlled high-resolution Fourier transform MS cell.⁷⁵ Figure 6 shows mass spectra of solvated ions that were observed. The authors provide a detailed discussion of the ‘gentle’ source conditions that were used to make these ions. At long times, they also observed the magic numbers reported by Williams;⁷⁴ however, at short trapping times and low cell temperatures, many larger adducts were observed. As solvent evaporates, peaks corresponding to doubly charged ions with 40 waters attached are especially prominent. Theory and experiment have previously shown that proton-bound water clusters, $\text{H}_3\text{O}^+(\text{H}_2\text{O})_n$ (where n is the number of water molecules associated to a central hydronium ion), should be especially stable when $n = 20$, because a clathrate

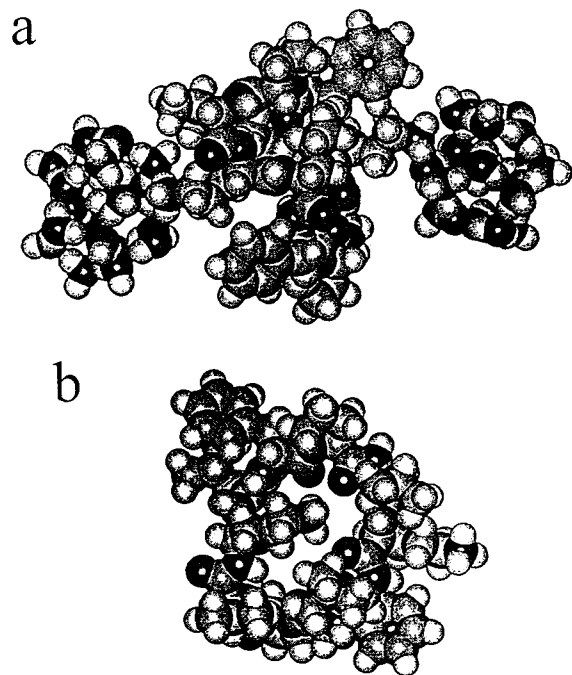


Figure 7. Proposed structures for (a) doubly protonated hydrated gramicidin S in which both protonated ornithines comprise part of a pentagonal dodecahedron clathrate where $n = 40$ and (b) doubly protonated anhydrous gramicidin S in which one of the protonated ornithines is tucked into the ring and stabilized by hydrogen bond formation with the amide carbonyl oxygens. (Reproduced with permission from ref 75. Copyright 1998 American Chemical Society.)

pentagonal dodecahedron structure can be formed around the hydronium ion.^{185,186} At $n = 20$, a completely closed shell with no defects (and relatively high stability) can be formed. In the case of gramicidin S, the stability of the 40 water magic number was proposed to arise from the inclusion of each protonated ornithine as a part of a clathrate. A structure that was proposed by the authors is shown in Figure 7a. The closed nature of the 20 water clathrate structures leads to a relatively stable peptide structure associated with 40 water adducts. Peaks in the mass spectrum for other sizes were less prominent because the partially closed clathrate structures contain defects, making them less stable. Comparison of the solution modeling results in Figure 7b with those for the 40 water adduct show that the solution structure is largely retained for solvent shells of 40 or more waters; below this critical solvent level, the transition from solution to gas-phase structure ensues and at least one charged ornithine residue collapses into the ring.

Studies of adduct formation with species other than water have also been carried out. Stephenson and McLuckey have exposed charge state distributions of ubiquitin ions to hydroiodic acid and reported adduction rate constants.¹⁸⁷ The highly protonated ions are found to be amphoteric, adsorbing HI at levels that increase with decreasing charge state. The authors considered the possibility that HI might bridge across a charged and noncharged basic residue pair in a salt-bridged configuration; however, the observation that the level of adduction increases with decreasing charge state makes this unfavorable, both

energetically (for addition of HI molecules) and entropically.¹⁸⁷ Subsequent work showed that for oligopeptide ions over a range of sizes, the sum of adsorbed HI molecules and the ion charge state is equal to the number of basic Arg, Lys, His, and N-termini.¹⁸⁸ These studies indicate that the HI adducts are bound to nonprotonated basic sites. The ability to examine nonprotonated sites is highly complementary to proton transfer and H–D exchange methods, and the authors have discussed the idea that adduction rate constants should depend on conformation.¹⁸⁸ So far, no studies of the kinetics of adduction to ions that are believed to have vastly different gas-phase conformations have been reported.

Zhan, Rosell, and Fenn have recently reported some early results involving the solvation of leucine–enkephalin by water and several alkanols (methanol; ethanol; 2-propanol; and *n*-, iso-, and *tert*-butyl alcohol).¹⁸⁹ In these studies, ions are exposed to solvent in an interface region between the ESI source and the mass spectrometer. An interesting finding was that some doubly charged dimers (originally hidden in the mass spectrum) were exposed upon solvent uptake. The observation that multiply charged peptide multimers could be hidden in mass spectra has recently been reported using ion mobility techniques.¹⁹⁰ A number of other interesting structural adducts involving peptides bound to metals, cyclodextrins, and crown ethers have been observed; these are discussed in recent reviews of noncovalent ESI complexes.^{62,191,192}

IV. Physical Methods for Probing Biomolecular Ion Structure

The categorization of a method as physical indicates that the molecule has not been altered chemically in order to discern the structure. Generally, MS methods for probing gas-phase ion structure are carried out by monitoring fragmentation patterns that are observed when ions are subjected to high-energy collisions or laser irradiation. Several important observations regarding the noncovalent structures of ions have been made with this approach. Most of the discussion in this section is associated with several methods that probe the overall shape of the intact parent ion.

A. Collision-Induced Dissociation (CID) Studies Designed To Locate Charge Sites

When ions are accelerated to elevated kinetic energies and exposed to a collision, it is possible to induce fragmentation. The differential pressure regions associated with most ESI conformations are well-suited for collisional activation.¹⁹³ Early work on the mechanism of peptide ion dissociation carried out at keV collision energies showed that fragmentation patterns could be dominated by charge remote fragmentation processes.¹⁹⁴ At low collision energies, fragment formation is directed by the location of the charged site.¹⁹⁵ The presence and location of basic residues in the sequence of peptides has

a pronounced effect on the dissociation pattern.^{194–196} Wysocki and collaborators have used surface-induced dissociation (SID) methods¹⁹⁷ to study the energetics of peptide fragmentation.^{198–200} Information about the location of protons can be obtained by comparing the energetics and efficiency of fragmentation channels of related sequences or those that have been modified to prohibit charge localization (e.g., acetylation of specific basic sites). For example, the onset of dissociation channels for peptide sequences having basic Lys or Arg residues occurs at higher energies than for sequences with no basic residues.¹⁹⁹ The highly localized proton requires more energy to become accessible for charge-directed fragmentation in other regions of the peptide than weakly bound protons associated with less basic sites. Vachet, Asam, and Glish have proposed that the inability of protons associated with Arg-containing peptides to facilitate fragmentation at low collision energies results from a local structure where the charge site is stabilized by an intramolecular hydrogen bond associated with the adjacent backbone carbonyl group.²⁰¹ In sequences where the Arg residue is immediately followed by a Pro residue, charge-directed fragmentation was substantially enhanced because of steric inhibition of hydrogen bond formation.

B. Collision-Induced Dissociation as a Probe of Gas-Phase Protein Conformations

Differences in collision-induced dissociation patterns have also been used to demonstrate that gas-phase conformations of large protein ions must have different conformations. Loo, Edmonds, and Smith have used triple quadrupole techniques to examine the fragment ions of disulfide-intact and -reduced ribonuclease A.²⁰² The substantial differences in fragment ion intensities and identities were attributed to differences in the structures of the gas-phase ions with and without the disulfide linkages. In other studies, Wu et al. have examined the fragmentation patterns of bovine, tuna, rabbit, and horse cytochrome *c* by collision-induced dissociation in an FTICR.²⁰³ The +15 charge state of each protein displayed substantially different fragmentation patterns even though there are only minor sequence differences in these related proteins. Variations in these 104 residue sequences by only three residues led to dramatic changes in the dissociation patterns. The authors suggested that the dissociation process was influenced by the conformation of the gas-phase ions and noted differences in the crystal forms of the proteins that are also apparent.

An interesting outcome of charge-solvation has been reported by Zubarev et al.²⁰⁴ Exposure of multiply protonated proteins to low-energy electrons leads to electron capture and charge neutralization. The resulting ions preferentially dissociate to form *c* and *z* ion products, rather than the *b* and *y* products, which are typical of CID. The authors invoke the solvated nature of the initial protonated site to explain this behavior. An electron approaching an $A \cdots H^+ \cdots B$ charge site will attach at the site having a greater electron affinity. In the case of protonated

amine/amide groups solvated by carbonyl groups, the $\cdot C-OH$ radical is preferred, facilitating preferential *c* and *z* ion formation.

C. Photodissociation and Spectroscopic Probes

Photodissociation and photoionization techniques are well-established methods for probing the geometries of small molecules.^{205,206} Spectroscopic probes of the conformations of protein ions have not been conducted. One can speculate that a combined site-specific mutagenesis/fluorescence quenching strategy would be a viable means of obtaining additional information about gas-phase ion structure. This approach has been used to follow folding in solution.²⁰⁷ The ability to resolve rotational bands allows precise determination of geometric structures and bond distances.^{208,209} Photoexcitation with ultraviolet and infrared lasers has been used to induce fragmentation and generate sequence information for macromolecules, including proteins²¹⁰ and DNA fragments.^{211,212} Multiphoton infrared dissociation was combined with CID techniques in high-resolution MS studies of a 50-residue DNA strand, making it possible to deduce the complete sequence.^{211,212}

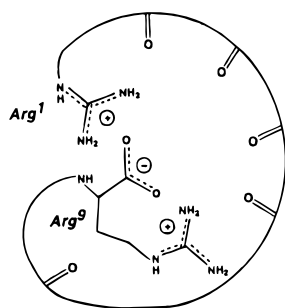
D. Blackbody Infrared Radiative Dissociation (BIRD)

Recently, FTICR techniques have exploited the blackbody radiation from the ICR cell as a means of inducing dissociation. Dunbar, McMahon, and their collaborators showed that the rates of dissociation for small ions that were trapped at low pressures were characteristic of the ICR cell wall temperature.^{213,214} This result is remarkable because these studies are carried out at low pressures, indicating that the molecules were in thermal equilibrium with blackbody radiation associated with the cell walls. Williams and co-workers applied this technique of blackbody infrared radiative dissociation (BIRD) to investigate the fragmentation pathways and energetics of macromolecular ions. The first study by Price, Schnier, and Williams gave a detailed account of the pressure dependence of their dissociation rate constants for macromolecular ions.²¹⁵ Below 10^{-7} Torr they observed that dissociation rate constants were independent of pressure, indicating that the ions were activated by absorption of blackbody radiation that was emitted from the ICR cell walls. The authors reported that the observed fragments as well as activation energies for dissociation depended upon the ion charge state and ascribed this to differences in Coulomb repulsion and conformations of different charge states.

Schnier et al. used the BIRD technique to study conformations of bradykinin (Arg-Pro-Pro-Gly-Phe-Ser-Pro-Phe-Arg) and a series of its analogues in order to investigate the possibility of intramolecular proton transfer from the acidic carboxy terminus (or the Ser residue, a less likely donor) to one of the more basic Arg residues or N-terminal amino group.²¹⁶ The activation energies and Arrhenius preexponential factors, *A*, for bradykinin (and

several other variants) were found to be substantially greater (1.0–1.4 eV and $10^9 - 10^{12}$, for E_a and A , respectively) than those for methyl ester analogues (0.6–0.8 eV and $10^5 - 10^7$, respectively) in which the acidic sites were blocked with respect to intramolecular proton transfer by methylation.²¹⁷ Additionally, the dissociation products for the parent peptide ions and the methyl ester analogues differed. The major dissociation channels of bradykinin and other variants where the carboxyl terminus was not methylated involved loss of NH_3 ; the corresponding methyl esters of these peptides dissociated primarily by loss of CH_3OH . The authors considered several explanations for the changes in Arrhenius factors and dissociation channels. In the end, the decreases in activation energies observed for the methyl ester analogues were explained by noting that methylation eliminates the possibility of salt-bridging, leading to a conformation that is destabilized relative to the transition state for dissociation. The higher pre-exponential factor for bradykinin suggests a 'loose' transition state in which both Arg residues participate in the elimination of NH_3 ; the lower value observed for the methyl ester (and favored methanol loss) suggests that this structure does not involve close interaction of both arginines. Scheme 3 (Repro-

Scheme 3



duced with permission from ref 216. Copyright 1996 American Chemical Society.) shows the proposed salt bridge structure for bradykinin in which the deprotonated carboxylic acid is located between the two protonated Arg residues. The authors have oriented the electronegative carbonyl groups along the backbone of the peptide in the direction of the protonation sites because this should stabilize the net +1 charge, in accord with calculations reported by Bowers' group (section IV.G.2.I).

E. Thermal Dissociation at High Pressures

Several recent studies have measured unimolecular rate constants for ion dissociation by using the heated ESI capillary as a reaction cell. Arrhenius plots of the data allow measurements of the Arrhenius activation barriers and preexponential factors. Rockwood et al. were the first to report that this method could be used to induce dissociation of macromolecular ions.²¹⁸ Busman, Rockwood, and Smith used this approach to study the dissociation energies of +3 to +6 charge states of melittin.²¹⁹ The barriers to unimolecular dissociation were found to decrease with increasing charge state and indicate that high

charge states are destabilized by increased Coulombic repulsion energy. Wysocki and co-workers have used this approach to obtain activation energies for comparison with surface-induced dissociation studies.²²⁰ Although only a few studies have been done to date, it seems likely that the simplicity of this approach will make it useful as a rapid means of sampling gas-phase ion stabilities. The stability of noncovalently bound ions can be assessed with the method.²²⁰

F. Kinetic Energy Release Distributions (KERD)

Mass-analyzed ion kinetic energy spectrometry (MIKES) is a classical MS technique²²¹ that has recently been used to provide information about interchange distances,^{131,222–224} an important constraint in multiply-charged peptide ion conformation. In these experiments, the kinetic energy that is released when multiply charged ions undergo spontaneous unimolecular dissociation is measured. Example MIKE spectra associated with the b_6^+ and $y_2^{''+}$ fragment ions formed upon unimolecular dissociation of doubly-charged angiotensin II are shown in Figure 8.²²² The characteristic "dish topped" shape associated with the kinetic energy release distribution (KERD) for the fragment ion peak indicates that a substantial kinetic energy is imparted to the products during dissociation.

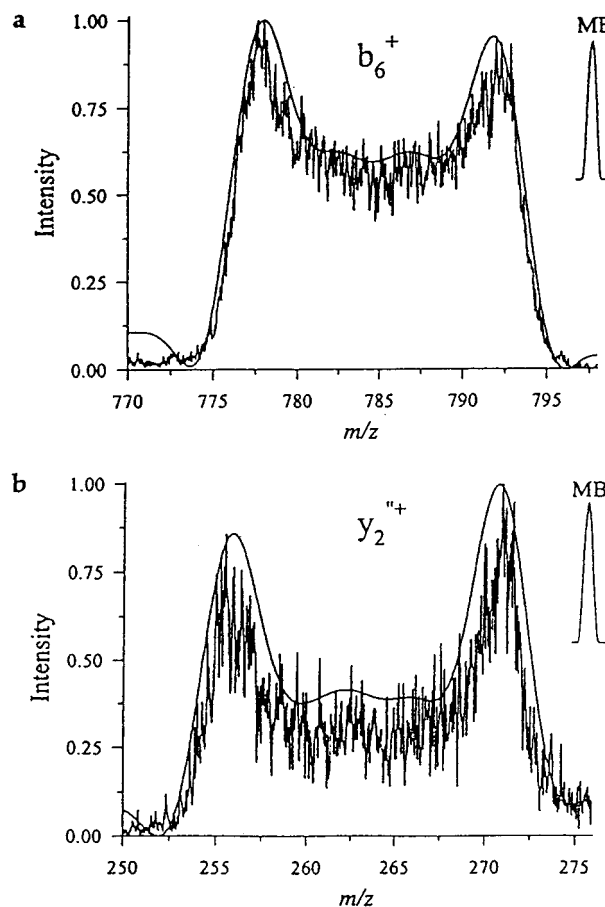


Figure 8. MIKE spectra of the b_6^+ and $y_2^{''+}$ fragment ions produced by the unimolecular dissociation of doubly charged angiotensin II ions. (Reproduced with permission from ref 222. Copyright 1996 American Society for Mass Spectrometry.)

The average kinetic energy released is approximately²²¹

$$\text{KER}_{\text{ave}} \cong \frac{z_2^2 m_1^2 eV}{16z_1 m_2 m_3} \cdot \frac{(\Delta E)^2}{E^2} \quad (3)$$

for a precursor ion having mass m_1 and charge z_1 and product ions having masses of m_2 and m_3 and charges z_2 and $(z_1 - z_2)$, respectively. E is the value measured at the center of the kinetic energy distribution for the precursor ion; ΔE is the peak width at half-maximum for either of the product ions; e is the charge of an electron; and V is the acceleration voltage. The source of kinetic energy associated with the center of mass of the product ions is the relief of electrostatic repulsion between charges at the transition state; thus, Coulomb repulsion energies can be estimated from the data. Kaltashov and Fenselau have shown that the energy released appears to be independent of source conditions,²²⁵ consistent with the notion that the method probes the transition-state structure.

Structural information is obtained by comparing experimental Coulomb repulsion energies to values that are estimated for trial structures. The dynamics of the dissociation process are not rigorously included in the analysis. Additionally, it is assumed that charges interact through the vacuum such that the dielectric polarizability of the system is 1.0. This assumption may not be appropriate because self-solvation of charged sites may shield charges.

1. Stability of the Melittin α -Helix in Solution, Crystal, and the Gas Phase

The KERD method has been used to investigate the structure of gas-phase melittin, a 26 residue peptide that is helical in a wide range of solution environments²²⁶ as well as in the crystal form.²²⁷ Kaltashov and Fenselau determined a value of 1.25 ± 0.12 eV for the kinetic energy released upon dissociation of triply charged melittin to form the y_{18}^{2+} and y_{19}^{2+} ions.²²⁴ This value was compared to values of the Coulomb energy calculated for several trial conformations. A trial helix, generated by molecular modeling (where polar side chains were solvated by backbone carbonyl groups and charges were located at basic residues), was determined to be 1.26 ± 0.06 eV, in close agreement with the experimental value. A value of 1.15 eV was calculated for the crystal form, and 0.52 eV was determined for a fully extended linear string conformation. From the comparison of experimental and calculated Coulomb repulsion energies, the authors concluded that the structure of triply charged melittin at the transition state has an overall shape that is similar to that of a helix. The network of hydrogen bonds associated with the helix should be energetically favorable.

The first evidence for a helical structure in the gas phase for the dissociative transition state of melittin is significant because it links solution and gas-phase structure for a ubiquitous structural element. However, the interpretation of structure from KERD data is not unambiguous. If higher values of the dielectric polarizability are used in the calculation of Coulomb

energies, closer distance constraints between charges would be imposed on the transition-state conformer. In this case a more compact conformation would be required to reproduce the experimental result. Additionally, those ions that can dissociate during the microsecond time scales of these experiments must have relatively high internal energies; it seems likely that other nonhelical structures (having similar charge positions at the transition state) also contribute to the KERD spectrum. It is not easy to test the validity of this approach because there is virtually nothing known about the structures of biomolecular ions during dissociation. One check comes from subsequent ion mobility measurements of the collision cross section for this ion. These experiments also suggest that triply-charged melittin has a helical conformation (even though the latter measurement should probe a distribution of stable conformations).²²⁸ Thus, there is evidence that the helicity of melittin that is observed in a wide range of solvents and in the crystal may also be prevalent in a range of stable and metastable gas-phase states.

2. Evidence for Persistence of Multistrand β -Pleated Sheets

In recent work, Li, Fenselau, and Kaltashov have used KERD to examine the gas-phase conformations of sequences that exist as single β -strands and multistrand β -pleated sheets in solution.²²⁹ Sequences having single β -strand solution structures were found to form compact gas-phase ion conformations; the authors reported that sequences having multistrand β -pleated sheet conformations in solution were likely to retain this type of structure in the gas phase. It was concluded that intramolecular hydrogen bonding was the major factor that determined the structure of these ions.

G. Collision Cross Sections

The collision cross section of a biomolecular ion depends directly on its conformation. At a given pressure, large ions with open structures will undergo more collisions than those with compact geometries. Thus, measurements that depend on the number of collisions that are experienced by different conformers can be used to discriminate between conformer shapes. A general limitation of these measurements is that many conformations could have similar cross sections. For biopolymer systems, the number of possible conformers with the same cross section decreases to unique values as shapes approach the limiting cases of the most extended and most compact structures. This section presents several different methods for measuring cross section as well as discussions of how these studies have been used to elucidate relatively detailed information regarding structure and dynamics of folding.

1. Ion Scattering in Triple Quadrupole Instruments

Triple quadrupole methods have been used extensively to study ion–molecule reactions,²³⁰ as a means of generating fragmentation patterns for known m/z ions,²³¹ and, more recently, for measurements of

macromolecular ion collision cross sections. In the cross-section measurements, specific protein ion charge states are selected in the first quadrupole and injected into a second quadrupole collision cell containing a known pressure of an inert buffer gas. Cooks and co-workers observed that the abundances of different charge state peaks in mass spectra of protein ions depend on the nature and pressure of the target gas as well as the nature of the protein ions.²³² Under certain buffer gas pressures and voltages used to inject ions into the collision cell, they observed bimodal distributions of charge states. In the absence of collision gas, high charge state ions are observed; as the Ar pressure increases, the relative abundance of low charge state ions increases. They interpreted these results by considering that different conformations of the gas-phase ions could have different collision cross sections. High-cross-section ions undergo more collisions with the buffer gas than low-cross-section ions and therefore lose kinetic energy more rapidly than the smaller ions.

Covey and Douglas recorded intensity distributions for protein ions as a function of ion kinetic energy and buffer gas pressure and developed a model that related the energy lost to the ion's collision cross section as given by⁹⁷

$$\frac{E}{E_0} = \exp[-\sigma S \ln \alpha'] \quad (4)$$

where E is the laboratory energy of the ion, E_0 is the laboratory energy before any collisions, σ is the collision cross section, and S is the target thickness ($S = Nl$; N is the number density of molecules or atoms in the collision cell and l is the collision cell length). The ratio of laboratory energy after one collision to that before any collisions, E_1/E_0 , is denoted α and can be calculated by $(m_1^2 + m_2^2)/M^2$ (m_1 is the ion mass, m_2 is the mass of the neutral collision gas, and $M = m_1 + m_2$). By fitting the experimental stopping profiles measured for individual charge states, it is possible to deduce the collision cross sections of each ion. An example of the stopping curves obtained for various target thickness values for the +11 charge state of apomyoglobin is given in Figure 9. Here, a cross section (determined by fitting eq 4) of 3020 \AA^2 was reported. Cross sections for different charge states were reported for five proteins ranging in molecular weight from ~ 3 to 66 kDa, including motilin, ubiquitin, cytochrome *c*, myoglobin, and bovine serum albumin.

An important outcome of this work was that it was the first to show that collision cross sections increase with increasing charge state, a result that the authors attributed to increased Coulombic repulsion. For example, the charge states of cytochrome *c* ions, electrosprayed from a 89.95:8.95:0.1 water:acetonitrile:acetic acid solution varied from 2370 \AA^2 for the +9 ion up to 4310 \AA^2 for the +20 charge state. Douglas later revised these values²³³ by inclusion of an aerodynamic drag coefficient. This modification showed that the previously reported values had been overestimated by $\sim 25\%$. Recently, the scattering process of the ion-neutral collision has been considered in detail by measuring energy losses for cyto-

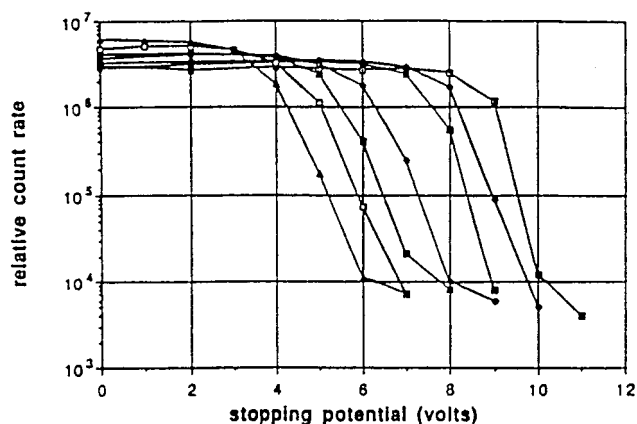


Figure 9. Stopping curves for the +11 charge state of myoglobin ($m/z = 1542$) at target thickness values of 0 (\square), 9.64×10^{13} (\blacklozenge), 1.47×10^{14} (\blacksquare), 2.61×10^{14} (\blacklozenge), 3.35×10^{14} (\blacksquare), 4.25×10^{14} (\square), and 5.33×10^{14} (\blacktriangle) cm^{-2} . (Reproduced with permission from ref 97. Copyright 1993 American Society for Mass Spectrometry.)

chrome *c* and myoglobin using Ne, Ar, and Kr as stopping gases.²³⁴ The results show that a diffuse scattering model provides a more accurate representation of the experimental data than a model based on specular scattering.²³⁴

Collings and Douglas have examined the gas-phase ion structures of holo- and apo-myoglobin²³⁵ and disulfide-intact and -reduced bovine pancreatic trypsin inhibitor (BPTI).²³⁶ In all cases, collision cross sections were found to increase with increasing charge state. The cross sections for apo-myoglobin were larger when ions were electrosprayed from a strongly denaturing solution, rather than from a solution that should favor native conformations. An additional comparison of the cross sections for disulfide-intact and disulfide-reduced BPTI ions showed that ions had larger cross sections when the disulfide bonds were reduced. Here, the removal of the covalent disulfide linkages allowed ions to adopt a more extended gas-phase conformation. Disulfide-intact BPTI cross sections measured by ion mobility methods²⁶³ (section IV.G.2) are $\sim 50\%$ larger than those measured by the triple quadrupole approach. This could arise from differences in collision energies of these experiments. However, comparison of both methods with cross sections calculated for the crystal conformation suggest that the model used to derive cross sections from the quadrupole scattering experiment systematically underestimates the actual value.

Another model that calculates the relative energies transferred during multiple collisions in dissociative processes has been developed and used to estimate the energies required to dissociate the heme from highly charged heme-myoglobin complexes.²³⁷ These studies suggest that the energetics of heme detachment is similar in highly charged ions (having open conformations) to values for low-charge state ions (having compact conformations) obtained by this and other methods: about 0.7 to 1.0 eV for the +8 to +20 charge states. These results suggest that the heme pocket may remain largely undisturbed, even in the highly charged open ion conformations. The authors noted that it is also possible that nonspecific interactions, which happen to give a similar binding

interaction, could account for the similar binding energies. Complementary measurements of the heme binding energies of higher charge states by other techniques will help corroborate the validity of the collision model as well as the proposed structural information.

A variation of the triple quadrupole approach has been presented by Javahery and Thomson who modified the gas-collision cell to consist of 10 short quadrupole rod segments that allow use of an axial drift field.²³⁸ In these experiments, ions are pulsed into the cell and cross sections are measured (as described in section IV.G.2.a) by determining the arrival time of ions at the detector. Cross sections for charge states of holo- and apo-myoglobin were found to agree with ion scattering measurements. This approach appears viable; however, the authors did not discuss any new structural information.

2. Ion Mobility Measurements

Ion mobility spectrometry methods (also called plasma or ion chromatography) have been used extensively for the analysis of small analytes,¹⁴ drugs, explosives, chemical warfare agents,¹⁵ and particle sizes^{239,240} and for studying ion molecule reactions. The ability of this method to discern different isomers, as shown by Hagen in 1979,²⁴¹ is currently evolving as an important complement for MS techniques. As noted above (section II.B), ion mobility spectrometry was applied early in the development of ESI in attempts to discern how ions were formed^{69–72} and as an alternative to MS for selective detection of charge states.⁷¹ In the 1990s, Jarrold's^{242,243} and Bowers'²⁴⁴ groups used these techniques to study atomic cluster ions (including carbon clusters) and developed relatively simple theoretical methods that allowed remarkably detailed structural information to be obtained.^{245–248}

In this section, we review the application of these experimental and theoretical methods to structural studies of biomolecular ions. These methods currently provide the most versatile and direct means of characterizing the shapes of macromolecular ions. The synergistic advances in experimental and theoretical methods have led to explosive growth in this field; most of the work that is described here was carried out during the last two years.

The basic idea behind structural determination based on mobilities is as follows. When a calculated mobility for a trial conformer is in good agreement with experiment, then this trial conformer becomes a candidate for the structure of the ion. A weakness of this approach is that many different conformations may have similar cross sections. However, it is straightforward to rule out many structures having cross sections that are in poor agreement with experiment. It is important to note that a breakthrough in the application of these methods came from studies of carbon clusters.^{245–248} Mobilities for different isomers (chains, rings, graphitic sheets, and fullerenes) of carbon clusters fell into families depending on cluster size.²⁴⁵ It was possible to unambiguously assign isomer structures by calculating mobilities as a function of cluster size. That is, the

changes in mobilities that occur with cluster size are very sensitive to the isomer structure. Even changes in the assignment of isomer structures involving the repositioning of a few atoms in the cluster significantly influence the ability to represent the family of clusters over the entire size distribution. Assignment of peaks of individual sizes are made based on the family of isomers observed over a range of sizes.

Although biological residues are more complex than atomic carbon, structural patterns in their growth should still occur at a unique rate depending on the type of structure that is formed. As one-dimensional chainlike or helical fragments become large enough to fold up, the growth rate will exhibit discontinuities; the larger fragments will grow as a higher-dimensional structure.

a. Experimental Mobilities and Cross Sections. When a pulse of ions is injected into a static buffer gas and subjected to a weak electric field, different conformations are separated due to differences in their mobilities through the gas. Drift velocities, v_D , are given by $v_D = KE$, where E is the strength of the applied electric field and K is the mobility constant. Under weak-field conditions in which E/N (where N is the number density of the buffer gas) is small, ions do not align as they drift through the instrument. Thus, the mobilities should correspond to an average of all orientations. Results are usually reported as reduced mobilities or collision cross sections as given by²⁴⁹

$$K_0 = \frac{L}{t_D E} \frac{P}{760} \frac{273.2}{T} \quad (5)$$

and

$$\Omega = \frac{(18\pi)^{1/2}}{16} \frac{ze}{(k_b T)^{1/2}} \left[\frac{1}{m_i} + \frac{1}{m_B} \right]^{1/2} \frac{t_D E}{L} \frac{760}{P} \frac{T}{273.2} \frac{1}{N} \quad (6)$$

respectively. In these expressions, the measured parameters t_D , L , P , and T correspond to the average drift time, the drift tube length, buffer gas pressure (in Torr), and temperature, respectively. The other terms are ze , the ion's charge; k_b , Boltzmann's constant; and m_i and m_B , the masses of the ion and buffer gas, respectively. Any two measurements of mobilities (or cross sections) recorded on the same instrument usually agree to within 1% (percent relative uncertainty). Measurements performed by different groups usually agree to within 2%.

b. Calculation of Mobilities and Cross Sections for Trial Geometric Structures. The theory of the mobility of ions in gases has a rich history that dates back to the work of Langevin in 1903.²⁵⁰ Information about the structures of different ions is obtained by comparing the experimental cross sections (or mobilities) with values that are calculated for trial conformations. Under weak-field conditions,²⁴⁹ ions do not align in the drift tube but rather sample all orientations as they travel through the gas. Therefore, calculations of cross sections for trial conformations must consider all possible orientations of the colliding pair. This orientationally averaged

collision cross section can be approximated by²⁵¹

$$\Omega_{\text{avg}}^{(1,1)} \approx \frac{1}{8\pi^2} \int_0^{2\pi} d\theta \int_0^\pi d\phi \sin \phi \int_0^{2\pi} d\gamma \pi b_{\text{min}}^2 \quad (7)$$

where b_{min} is the minimum impact parameter for a collision geometry that avoids a hard-sphere collision with any atom in the ion. Typical hard-sphere collision radii (in Å) for the individual atoms involved in collisions are H (2.2); C (3.1); N (2.8); O (2.7); S (3.6), and He (2.2). It has been previously noted¹⁶ that this calculational approach is remarkably similar to a "shadow-graphic" method described by Mack in 1925 in which he measured the shadows of beeswax models that were placed in different orientations with respect to a light source.^{252,253} Now known as the projection approximation, this approach appears to provide accurate cross sections for many different types of geometries of atomic clusters and is attractive because of its simplicity. However, this analysis ignores all of the interactions associated with the collision (e.g., potential interactions between the ion and the buffer gas, buffer gas scattering, and inelasticities of collisions) as well as changes in the conformation of the ion as it travels through the drift tube.

To address the former issue, Wyttenbach et al. have used a 12-6-4 potential to determine impact parameters, which are then used to calculate mobilities using the hard-sphere projection method.²⁵⁴ This approach is useful for estimating the mobilities for trial conformers as a function of temperature but does not rigorously include the dynamics of the collision. Shvartsburg and Jarrold have developed a method that includes the contribution of the scattering angle to the cross section which is referred to as the exact hard-sphere scattering (EHSS) method.²⁵⁵ Comparisons of cross sections calculated from the projection and EHSS approaches show that scattering is an important consideration, especially for accurate calculations of concave shapes.²⁵⁵

Recently, Mesleh et al. have developed a "trajectory method" for calculating the mobility.²⁵¹ In this approach, atoms (in the trial ion conformation) interact with the buffer gas atom along realistic potential surfaces and the dynamics of buffer gas scattering are rigorously included in the mobility calculation. This method is currently the most accurate means of evaluating the mobility of a trial conformation for large molecules.²⁵⁶ Shvartsburg et al. have recalculated the mobilities for carbon chains, rings, and graphitic sheets and find much better agreement with experiment than was reported previously.²⁵⁶ The computation of mobilities by Jarrold's trajectory approach is a significant achievement; although computationally demanding, the method has recently been applied to large ensembles of conformations such as those generated by molecular modeling strategies. A more sophisticated approach that takes into account rotational to translational energy exchange has been developed by Viehland and Dickinson;²⁵⁷ however, this method has only been applied to diatomics.

c. Separating Different Conformations within Individual ESI Charge States. In 1995, Clemmer,

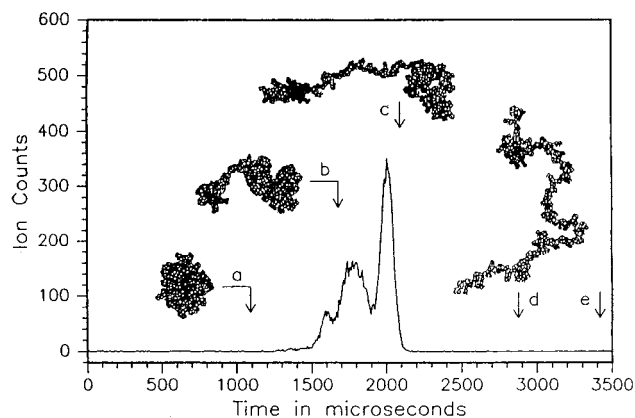


Figure 10. Drift time distribution recorded for the +7 charge state of bovine cytochrome *c* with a nominal injection voltage of 130 V. Arrows show the expected drift times for a variety of trial conformations of cytochrome *c*: (a) native crystal structure (~1100 μs); (b) partially unfolded structure with an open heme crevice (~1680 μs); (c) unfolded coil that retains the α -helices (~2070 μs); (d) typical random coil with no secondary or tertiary structure (~2880 μs); and (e) near-linear conformation (~3425 μs). It is important to note that structures b and c were chosen randomly and should be viewed as cartoons. (Reproduced with permission from ref 258. Copyright 1995 American Chemical Society.)

Hudgins, and Jarrold showed that multiple conformations of the +7 charge state of cytochrome *c* could be resolved based on differences in their mobilities.²⁵⁸ From comparisons with drift times calculated for trial conformers (section IV.G.2.b), the authors concluded that the peaks that were observed for the +7 ion corresponded to partially folded states and noted that these could be intermediates involved in folding. Drift times that were derived from the calculated projections of four trial conformations of cytochrome *c* are shown in Figure 10. The calculated drift time for the crystal conformation is substantially below that of the first peak observed experimentally, while the calculated value for the random string conformer is substantially longer than the experimental data. The poor agreement between these calculated values and the experiment indicates that neither extremely compact conformers nor extremely open string conformations are observed. Calculated drift times for two partially open conformations (cartoon structures that were chosen randomly) are in approximate agreement with the experimental peaks, indicating that the three features that are observed correspond to partially folded states of the protein ion. Clearly, many different partially unfolded trial conformers will have calculated drift times that are near the experimental features.

d. Studies as a Function of Injection Voltage. Instruments in which the ion source is decoupled from the drift tube allow mobilities to be studied as a function of the energy used to inject ions into the drift tube. As ions enter the drift tube, their kinetic energies are thermalized by collisions with the buffer gas. Further collisions cool the ions to the buffer gas temperature. The resulting heating/cooling cycle is varied by changing the injection energy of ions into the drift tube and provides an effective (and experimentally simple) means of inducing structural

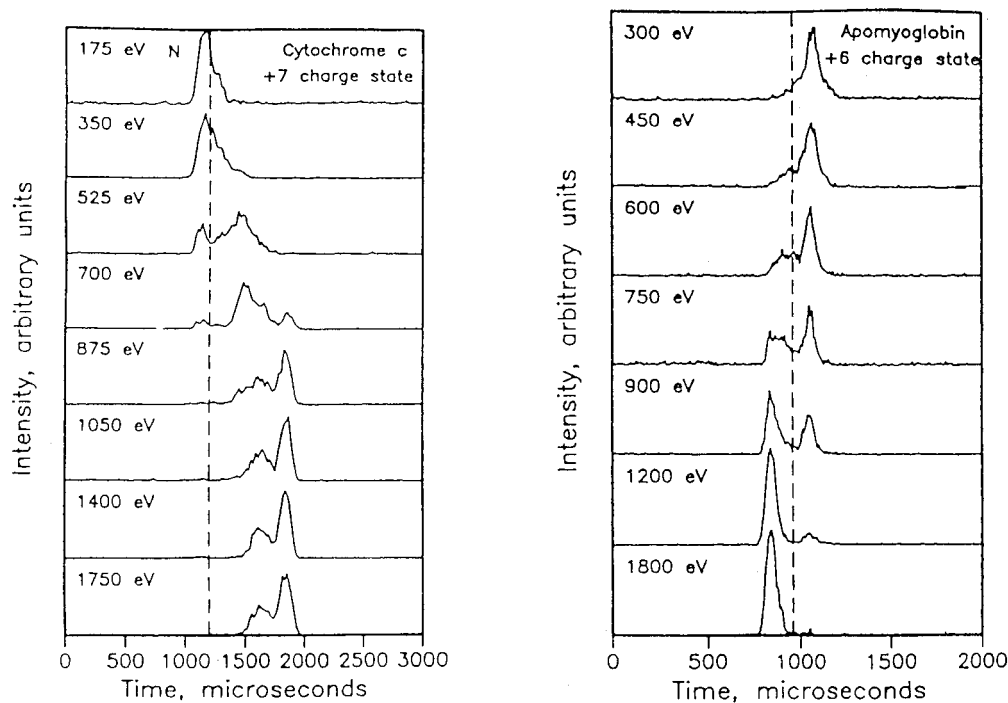


Figure 11. (a) Drift time distributions for the +7 charge state of bovine cytochrome *c* measured as a function of injection energy. The dashed line shows the drift time expected for the native crystal conformation of cytochrome *c*, as calculated by the EHSS method. (b) Drift time distributions recorded for the +6 charge state of apomyoglobin as a function of injection energy. The ions were produced by proton-stripping higher charge states with a base in the desolvation region. The dashed line shows the drift time expected for the native conformation of myoglobin, as calculated by the EHSS method. (Reproduced with permission from ref 16. Copyright 1997 John Wiley & Sons, Ltd.)

changes. This approach was originally used by Jarrold and co-workers in studies of silicon clusters.^{259,260} Liu et al. have shown that at very high injection energies it is possible to induce fragmentation and obtain sequence information.²⁶¹

Examples showing the changes in ion mobility distributions that occur with variations in injection energy are shown in Figure 11 for the +7 charge state of cytochrome *c* (part a) and the +6 charge state of apomyoglobin (part b), respectively.¹⁶ The calculated drift time for the crystal coordinates (EHSS method) is shown as a dashed line. At low injection voltages, the drift time of the +7 charge state of cytochrome *c* is slightly shorter than the calculated value, indicating that favored conformations are more compact than the crystal form. Apomyoglobin has a drift time that is longer than the calculated value, indicating that the anhydrous conformation is more open than the crystal conformation. As the injection energies for both systems are increased, the positions of drift time peaks shift. Cytochrome *c* (+7) favors more open conformations: a broad feature at $\sim 1500 \mu\text{s}$ at IE = 525 eV and a sharper feature at $\sim 1750 \mu\text{s}$ at 1050 eV. These results show that the compact +7 charge state of cytochrome *c* favored by ESI unfolds during the transient heating/cooling cycle associated with the injection process. The driving force for this transition is the relief of Coulombic repulsion between charged sites. The injection energy data for apomyoglobin show evidence for a folding transition at high injection energies, indicating the presence of a folding activation barrier. The new folded state is ~ 10 – 15% more compact than the crystal conformer and is substantially smaller than +6 ions formed

directly by ESI. Shelimov et al. proposed that a folding barrier arises because of Coulombic interactions.²⁶² As the protein folds, the Coulomb energy must increase; however, this is offset by attractive intramolecular interactions (in the compact state) which only become accessible at short range. Thus, folding of anhydrous proteins will involve surmounting barriers associated with long-range Coulomb interactions. In the case of atomic clusters, it appears that this heating/cooling cycle allows metastable structures to anneal into lower energy states. For multiply charged protein ions, this may not be the case. Here, open metastable states may be formed at high energies and may become trapped because of the long-range Coulomb barrier in these systems. To date, cross sections as a function of injection energy and charge state have been recorded for five proteins: several sequence variants of cytochrome *c*,²⁶² apo- and holo-myoglobin,²⁶² lysozyme,¹³⁸ BPTI,²⁶³ and ubiquitin.¹⁰¹

In later studies of cytochrome *c*, Mao et al. investigated the +7 state of cytochrome *c* as a function of buffer gas temperatures and injection energy.⁸¹ At high buffer gas temperatures, conformations having cross sections of $\sim 1760 \text{ \AA}^2$ are observed when both low and high injection energies are used. This state appears to be the thermodynamically most stable for the +7 charge state and is accessible by folding of the more elongated conformer (formed at high injection energy) or unfolding of the compact conformer (observed at low injection energy).

e. Collision Cross Section as a Function of Charge State. Ion mobility studies have provided a remarkably detailed view of the changes in collision

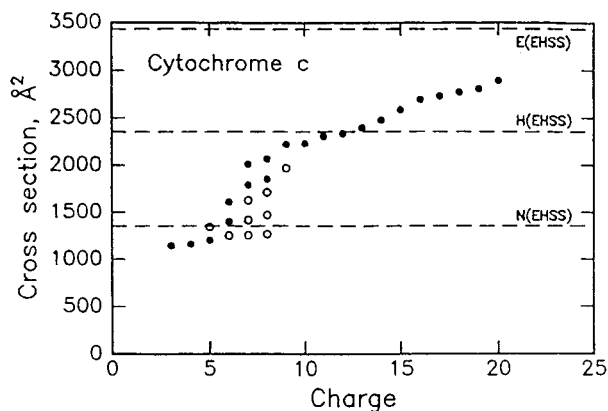


Figure 12. Plot of the cross sections determined for the main features resolved in the drift time distributions for the +3 to +20 charge states of cytochrome *c*. Cross sections for the features that dominate at high injection energies are shown by the filled points. The open points show the cross sections deduced for the conformations observed at lower injection energies. The dashed lines labeled N(EHSS), H(EHSS), and E(EHSS) show the cross sections determined using the exact hard spheres scattering model for the native crystal conformation, an α -helix, and an extended string, respectively. (Reproduced with permission from ref 263. Copyright 1997 American Chemical Society.)

cross sections that occur as a function of ion charge state. Clemmer, Hudgins, and Jarrold plotted cross sections for the +7 to +19 charge states of cytochrome *c* in their original report that different conformations could be resolved within an individual charge state.²⁵⁸ Shelimov et al. reexamined cytochrome *c* in more detail.²⁶² Figure 12 shows a plot of the +3 to +20 charge states of cytochrome *c*. This plot distinguishes between conformers favored at high and low injection energies and also includes states that were formed by addition of a base to the desolvation region in order to produce low charge states from proton stripping reactions. Thirty distinct ion forms (with different cross section or charge state) appear to be stabilized in the gas phase. These appear to fall into at least five different conformer families. When the different solution conditions (described in section II.E) are considered, at least eight additional conformers of cytochrome *c* are stable in the gas phase.

As originally considered by Smith and co-workers⁸⁰ and apparent in the early data from Douglas,²³⁵ it is clear that protein structure is mediated by the Coulomb repulsion energy between charges. Low-charge states have tightly folded conformations that can be more compact than the crystal form of the protein. Here, the intramolecular binding interactions are not mitigated by solvent-protein interactions. As the number of charges on the protein increases, more open conformations are favored. The injected-ion data for cytochrome *c* show multiple conformations for the +5 to +9 charge states. The +10 and higher charge states display single peaks in the ion mobility distributions corresponding to highly open conformations. The protein continues to expand with increasing charge state in order to relieve increasing Coulombic repulsion.

The trends observed in Figure 12 appear to be general for polypeptide chains that are free of disul-

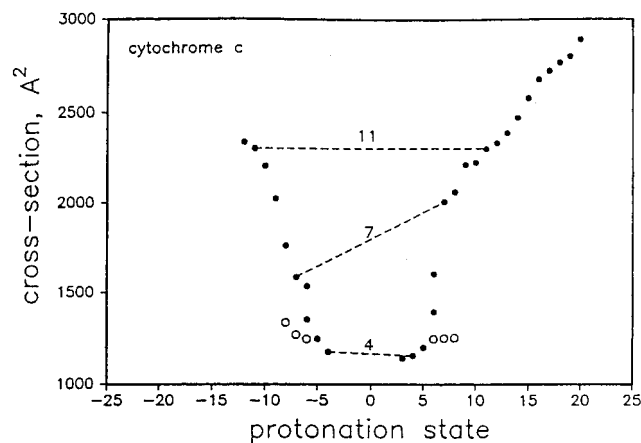


Figure 13. Cross sections measured for negatively charged (deprotonated) and positively charged (protonated) forms of cytochrome *c*. Only data for the most abundant feature in the drift time distributions recorded at high injection energies are plotted. The dashed lines show that low and high charge states have similar cross sections. Intermediate charge states such as the ± 7 ions have significantly different cross sections. (Reproduced with permission from ref 16. Copyright 1997 John Wiley & Sons, Ltd.)

fide bonds. For example, ubiquitin (76 amino acids)¹⁰¹ and apomyoglobin (129 amino acids)²⁶² show similar unfolding behavior as a function of charge state. Plots which account for the number of residues per charge show that different non-disulfide-bonded proteins unfold at similar rates.²⁶² Several studies have investigated the conformations of disulfide-bonded proteins such as insulin,²⁶⁴ BPTI,²⁶³ and lysozyme,¹³⁸ which contain two, three, and four disulfide bonds, respectively. The cross sections for these proteins also expand with increasing charge state; however, the degree of unfolding is restricted by the presence of disulfide bonds.

f. Influence of Charge Location upon Protein Cross Sections. Liu and Clemmer have examined how the positions of charged sites influence conformation by measuring cross sections for negatively charged (deprotonated) cytochrome *c* produced by ESI.¹⁶ Comparison of cross sections for positively and negatively charged protein ions can provide information about how the location of charge sites (determined by the numbers and positions of basic and acidic amino acids) and the nature of charge solvation affects the gas-phase conformations. The degree of charging associated with formation of positively and negatively charged ions can be understood by considering the numbers of basic and acidic residues, respectively. Cytochrome *c* has 22 basic Arg and Lys groups but only 12 acidic Asp and Glu residues. The highest charge state that was observed for positively charged ions was +20, whereas the highest charge state for negative ions was -12. Cross sections for the main features observed in the ion mobility distributions when ions are injected at high injection energies are shown in Figure 13. Cross sections for high and low charge states are nearly identical for protonated and deprotonated ions. However, large differences in cross section were observed for intermediate charge states, where repulsive Coulombic interactions are similar in magnitude to attractive forces that hold conformers in folded conformations.

For example, Figure 13 shows that the -7 charge state of cytochrome *c* is substantially more folded than the $+7$ state. At the high injection energies that were used for these studies, it is likely that this result reflects differences in the stabilities of negatively and positively charged gas-phase ions rather than differences in the antecedent solution structures.

g. Folding and Unfolding Transitions Induced by Gas-Phase Proton-Transfer Reactions. The influence upon structure that is induced by removal of protons can also be studied by ion mobility assessments. These types of experiments can be carried out by the addition of basic reagents to a gas cell that is either attached to or immediately follows the desolvation region, similar to the Y-tube proton-transfer studies discussed in section III.A.2. In the presence of a base, the charge state distribution shifts and new lower charge states are formed. Ion mobility distributions for different charge states are recorded before and after addition of proton-transfer reagents in order to monitor structural changes that occur. Shelimov et al. have investigated the structures of gas-phase cytochrome *c* and apomyoglobin ions that have undergone proton-transfer reactions.²⁶² These studies show that high charge states (with large collision cross sections) fold up into compact conformers when protons are removed. By considerations of the flow rates in the ESI source and gas cell, the authors estimated an upper limit to the folding time scale on the order of 50–100 ms.²⁶⁵

Valentine et al. have examined the gas-phase folding of disulfide-intact and reduced lysozyme ions¹³⁸ and have presented a detailed comparison of these results with the gas-phase basicity measurements on this system by Williams and co-workers.¹³⁷ Many similarities and some differences in interpretation of the gas-phase basicity and mobility studies were noted. Valentine assigned the cross sections for disulfide-intact ions to two families of conformations: a highly folded form observed for the $+5$ to $+10$ charge states having cross sections that were similar to values calculated for the crystal coordinates and a partially unfolded form, observed at high injection energies for the $+7$ to $+11$ charge states. When the disulfide bonds were reduced, only high charge states ($+10$ to $+18$) were observed; these ions had cross sections that were substantially larger than the partially unfolded state and were assigned as 'unfolded' conformers. As protons were removed from the disulfide-reduced ions, more compact conformations were generated. The authors noted the intriguing result that cross sections for compact conformations (and some partially folded states) formed by refolding disulfide-reduced ions in the gas phase were identical to those measured for disulfide-intact ions. This could indicate that when the disulfide-reduced ions fold up, the conformations that are formed are similar to disulfide-intact ions.

These ion mobility studies¹³⁸ can be combined with high-resolution FTICR results which show that disulfide bonds remain reduced during proton-transfer reactions.¹³⁷ If disulfide-reduced ions refold in the gas phase to similar conformations as disulfide-intact ions, then one would conclude that reformation of

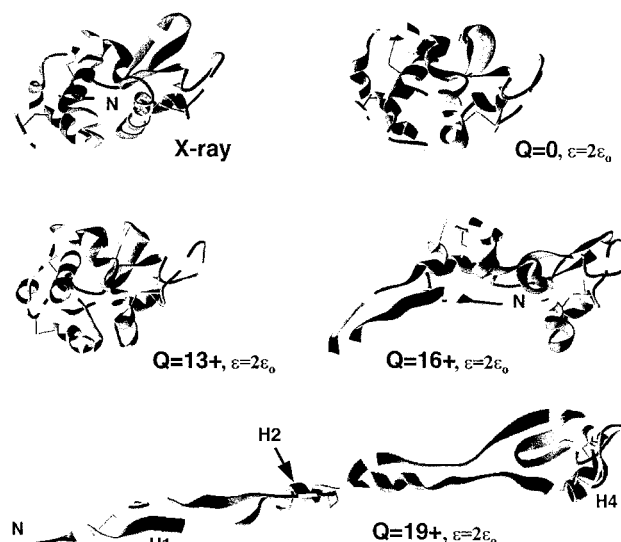


Figure 14. Structures of lysozyme visualized after ~ 1 ns of molecular dynamics simulation for the X-ray structure and for four different charge states. The N-terminus is labeled, and disulfide bridges are indicated. Charged residues are shown by darkened sections. Any helical or sheetlike structure is presented in ribbon form, even after denaturation, to aid in identification of formerly intact secondary structural elements. (Reproduced with permission from ref 271. Copyright 1998 American Chemical Society.)

disulfide bonds is not a key factor in the gas-phase folding of lysozyme. The importance of disulfide bonds in the refolding of proteins in solution is currently an active research area and has been explored in detail for lysozyme.^{266–269} In solution, heterogeneities associated with the kinetics of refolding of disulfide-reduced lysozyme suggest that kinetically trapped states are present, and several origins, including misformation of disulfide bonds (which results in knotting of the protein), have been proposed.^{266,268}

Recently, Reimann et al. have presented results from molecular dynamics studies of lysozyme in vacuo.^{270,271} Qualitatively, differences between results for disulfide-intact and disulfide-reduced lysozyme are consistent with experimental measurements of collision cross sections (section IV.G.2.g),¹³⁸ gas-phase basicities (section III.A.3),¹³⁷ as well as surface impact studies (described in section IV.H).¹⁴⁰ Several example conformations that are found from molecular modeling of four disulfide-bonded charge states and the X-ray crystal structure are shown in Figure 14. Here, the overall shapes of neutral and $+13$ lysozyme (disulfide intact) are similar to the crystal structure; additionally, a substantial fraction of the α -helical structure is retained. Molecular modeling results for the $+16$ and $+19$ ions show a substantial loss of tertiary structure. The $+19$ ion adopts an extremely elongated conformation that is limited by disulfide bonds that link the polypeptide chain, as shown. In other studies,¹⁴⁰ this group has shown that when the disulfide bonds are removed, the ion can adopt highly extended conformations as indicated by the ion mobility and proton-transfer results.

Very recent molecular modeling studies by Arteca et al. indicate that the relaxation dynamics of un-

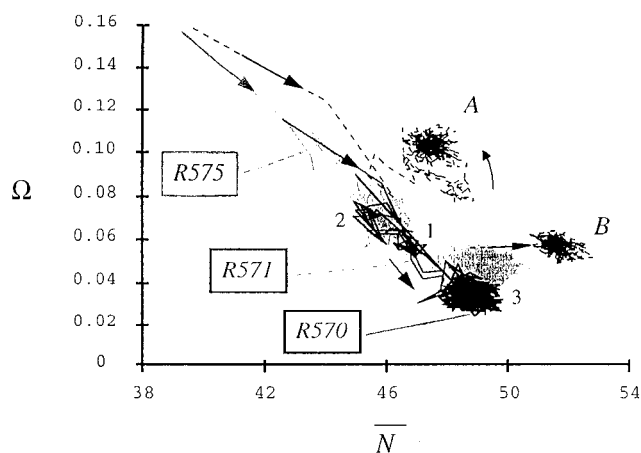


Figure 15. Anisometry-and-entanglement map (\bar{N} , Ω) showing the effect of pair interactions over the refolding trajectories leading to quasi-native folds of lysozyme. The arrows indicate the time evolution along the trajectories. The R570, R571, and R575 trajectories lead to quasi-native conformers by using none, one, or two intermediate “states,” respectively. (In the case of R571, the final structures after 2 ns are indistinguishable from fluctuations of the native state in vacuo. The three “states” in the R571 trajectory are labeled 1, 2, 3.) The trajectories labeled A and B are recomputations of the R575 trajectory in which the C_6 coefficients of the Lennard–Jones pair potential are increased by 50% (the attraction has been made more dominant). In case A, the changes in the force field derail the prior refolding pattern. In case B, a stronger attraction does not make the conformers more globular. (Reproduced with permission from ref 272. Copyright 1999 The American Physical Society.)

folded lysozyme is not random.²⁷² The authors followed unfolded structures of neutral lysozyme and found evidence that the system spontaneously folds into preferential native, quasi-native, and compact structures. Figure 15 shows a plot of molecular asphericity (Ω) as a function of an average entanglement parameter (\bar{N}) for molecular modeling trajectories associated with folding. In this plot an $\Omega = 0$ corresponds to a spherical conformer. The entanglement parameter \bar{N} reflects the number of projected crossings between the backbone bonds averaged over all orientations. The combined parameters provide insight about tertiary (Ω) and secondary (\bar{N}) structures. That is, conformers with large Ω and small \bar{N} have rather open structures with little secondary helical content. Structures having $\Omega \approx 0$ and large \bar{N} must be highly folded with significant helical content. The dashed, solid, and gray lines in Figure 15 show trajectories that have folded to different (Ω, \bar{N}) positions. Of particular interest is the cluster of conformers labeled (3) found at $\Omega = 0.02$, $\bar{N} = 48.5$. These are within the range of those that are expected for reformation of the native structure (in this case, the solution structure that has been allowed to relax in vacuo).

The combined experimental and theoretical results for lysozyme are very intriguing. Not only do elongated lysozyme conformers collapse in the absence of solvent, but there is also evidence for preferential pathways for this collapse. As a result, it appears that preferred conformations are formed. The observation that some of these structures resemble the native structure suggests that solvent may be relatively

unimportant in the folding of this protein. If true, these results have implications regarding the evolutionary role of water in folding, suggesting that the polypeptide chain alone contains the information necessary for formation of the native fold. While clearly exciting, it is important that future studies are undertaken to test the similarities of these systems. Valentine and Clemmer are currently working on H/D exchange studies (section IV.G.2.h) of disulfide-intact lysozyme and reduced (gas-phase folded) states to provide future experimental characterization of this system.

Valentine, Counterman, and Clemmer¹⁰¹ have investigated the influence of removing protons on the conformations of ubiquitin ions when ions were exposed to different proton-transfer reagents: acetone, acetophenone, *n*-butylamine, and 7-methyl-1,5,7-triaxabicyclo[4.4.0]dec-5-ene, having gas-phase basicity values (all in kcal mol⁻¹) of 188.9, 197.4, 210.6, and 243.3, respectively.²⁷³ This work showed that for a given charge state the apparent gas-phase basicities (reported as gas-phase acidities in order to be consistent with Cassady’s previous work)¹⁴² of the different conformations are ordered as compact < partially folded < elongated, as would be expected by Williams’ model.⁸³ The authors also concluded that there was no evidence that ubiquitin ions refold upon removal of charges, suggesting either that the system cannot overcome the Coulomb barrier associated with refolding or that repulsive Coulombic interactions outweigh attractive intramolecular interactions, even for low charge states. Further measurements by Li and Clemmer using high-pressure ion mobility corroborated this finding.²⁷⁴ It appears that solvent stabilization is vitally important for refolding of ubiquitin (section II.E). A natural question that arises is what critical level of solvent is required? Jarrold and co-workers have begun such studies for cytochrome *c* (section IV.G.2.k).

h. Combined Ion Mobility/H–D Exchange Methods. By doping the drift tube with deuterated solvents, it is possible to monitor H–D exchange reactions for shape-resolved conformations. Valentine and Clemmer have examined the H–D exchange reactivity of compact and elongated forms of horse cytochrome *c* (which has a total of 198 exchangeable sites) with D₂O vapor.¹⁷⁴ The result of combined ion mobility and H–D exchange studies of different conformation types of the +8 charge state of cytochrome *c* were studied in detail. At low injection energies, compact conformers are favored. The corresponding H–D exchange levels (obtained under saturation conditions for the rapidly exchanging sites) shows a broad distribution centered around exchange of 45 sites. Injection of the +8 charge state at high injection voltages favors elongated states (as shown by the ion mobility distribution); the corresponding mass spectral peak for these ions shows that ~60 sites exchange. The higher level of exchange observed for the more elongated states is in line with the expectation that more sites should be exposed in this more open conformation. Higher charge states (which favor increasingly more open conformations)

show a similar level of ~ 60 rapidly reacting exchange sites.

The observation that higher charge states have a constant exchange level is in agreement with previous H–D exchange studies performed by McLafferty and co-workers using FTICR (section III.B.2).^{99,175} However, the exchange levels in drift tube experiments are substantially below those observed in FTICR studies, even though the mobility measurements indicate that these conformations must be extremely elongated. Valentine noted that complete saturation of rapidly exchanging sites in the FTICR requires long (minutes) time scales (using D_2O exposure levels of $\sim 10^{-7}$ Torr) whereas in a drift tube exchange occurs over millisecond time scales (using D_2O exposure levels of ~ 0.1 to 0.5 Torr). Because the total number of ion– D_2O collisions are similar, it appears that the differences must be related to different conformations or differences associated with exchange processes that occur over short (ms) and long (minutes) time scales. It is possible that exchange over longer time scales allows conformations to fluctuate, exposing regions that were protected and providing more extensive exchange. In this case, during the short time scales of the drift tube experiments, conformations may not undergo substantial fluctuations; thus, the drift tube experiment may provide what is effectively a “snapshot” of the most rapidly exchanging sites.

i. High-Pressure Ion Mobility Studies. Substantially higher ion mobility resolving powers can be obtained by operating the ion mobility spectrometers using higher drift fields (e.g., $E = 200\text{--}300$ V cm^{-1}). These instruments are operated at high buffer gas pressures and are naturally suited for studies of ion conformation under different ESI and solution conditions because ions are not exposed to violent collisions in interfacial pressure regions. Hudgins, Woenckhaus, and Jarrold have recorded ion mobility distributions for cytochrome *c* and BPTI using their high-resolution apparatus.⁹⁸ Although the higher resolving power allowed more conformations to be discerned, the resolved features were much broader than expected for single rigid conformations. Figure 16 shows examples of the influence of solution composition upon ion mobility distributions for the +12, +13, and +14 charge states of bovine cytochrome *c* that were electrosprayed from solutions containing variable concentrations of acetic acid (1% or 10%). Differences in the abundances and positions of peaks are clear for all three charge states. Studies in which the fraction of methanol was varied show similar trends, indicating that even mildly denaturing conditions are discernible by this approach. Several of the features that were observed could be directly correlated with solution states in the acid denaturation process (state III \leftrightarrow state IIIa \leftrightarrow state II \leftrightarrow state I; state III is the native state and state I is a denatured form in which the Met⁸⁰ heme linkage has been broken) that are known to exist under the various experimental conditions that were employed.

Li et al. have used high-pressure high-resolution ion mobility techniques to examine the conformations of electrosprayed ubiquitin ions as a function of

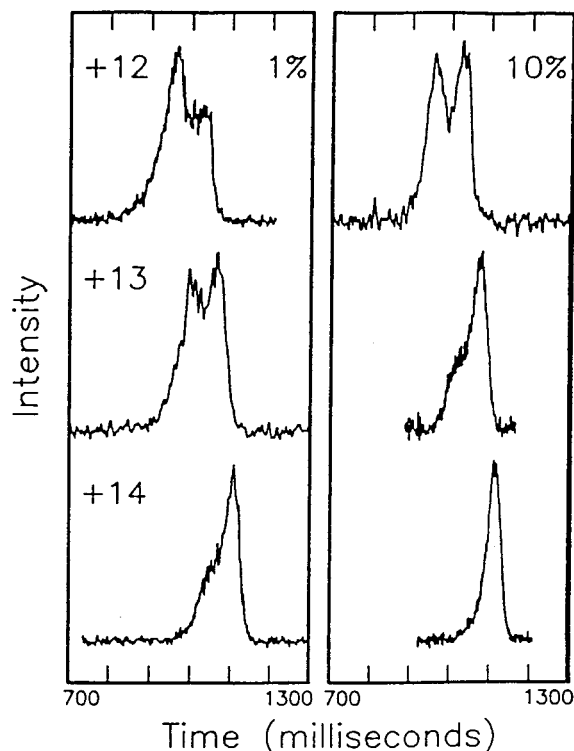


Figure 16. Drift time distributions recorded for the +12, +13, and +14 charge states of bovine cytochrome *c* with solutions of 3:1 water and acetonitrile with 1% and 10% acetic acid. All distributions were obtained using a $750 \mu s$ pulse of ions. (Reproduced with permission from ref 98. Copyright 1997 Elsevier.)

solution composition and ESI capillary temperature.¹⁰⁰ This work also shows that the conformations of gas-phase ions are highly sensitive to ESI solution conditions. In addition, studies as a function of temperature show differences in the stabilities of the gas-phase ion conformations. All of the charge states for different solutions were observed to undergo unfolding transitions at elevated capillary temperatures; however, unfolding transitions for ions formed from ‘pseudo-native’ solution conditions (89:9:2 water:acetonitrile:acetic acid) occurred at higher temperatures than those observed for denaturing solutions (49:49:2 water:acetonitrile:acetic acid).

An example is shown for the +7 charge state in Figure 17. At $25^\circ C$, ions from the pseudo-native solution favor a narrow distribution of compact conformers (centered near $\Omega \approx 1000 \text{ \AA}^2$); ions from the denatured solution display a bimodal distribution with features at ~ 1050 and 1230 \AA^2 . At $76^\circ C$, a new feature at $\sim 1230 \text{ \AA}^2$ is observed in the distribution of ions from the pseudo-native solution, near the feature observed from the denatured solution. At $97^\circ C$, most of the compact form has unfolded to the 1230 \AA^2 state. Ions from the denatured solution unfold to a more extended form centered near 1400 \AA^2 . These data indicate that the different initial precursor conformations may unfold to similar favorable gas-phase conformer states. The results also demonstrate that when comparisons are made between laboratories, special attention should be given to the differences in conditions used to form ions.

j. Thermally Driven Transitions. Mao et al. have recorded mobilities for the +5 and +7 ions of

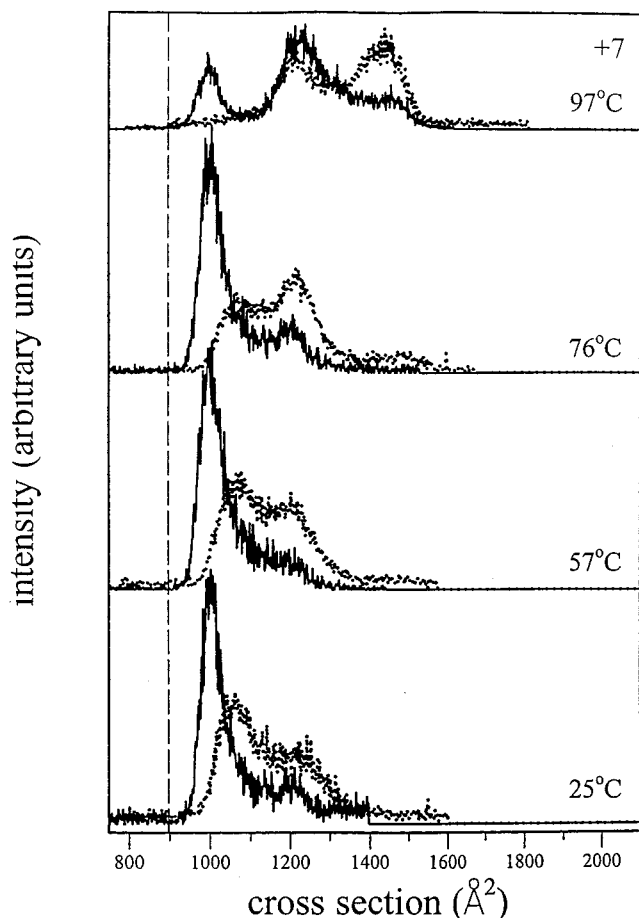


Figure 17. Cross section distributions for the +7 charge state of ubiquitin at capillary temperatures of 25, 57, 76, and 97 °C. The dotted lines represent data obtained by electro spraying a 49:49:2 water:acetonitrile:acetic acid solution (denatured). The solid lines correspond to the pseudo-native 89:9:2 water:acetonitrile:acetic acid solution. The dashed line shows the calculated cross section from the projection method for the crystal coordinates of ubiquitin. (Reproduced with permission from ref 100. Copyright 1999 Elsevier.)

cytochrome *c* as a function of buffer gas temperature up to 300 °C.⁸¹ Although slight shifts in the cross section are observed for the +5 ion, this state retains a compact structure at all temperatures, demonstrating compact conformations are extremely stable for the +5 charge states. A fascinating result is obtained for the +7 ion. Compact structures (favored at low injection voltages in 25 °C buffer gas) unfold to a state with $\Omega \approx 1760 \text{ \AA}^2$ when the temperature of the buffer gas is increased to $\sim 150\text{--}200 \text{ }^\circ\text{C}$. Additionally, elongated ($\Omega \approx 2050 \text{ \AA}^2$) conformers of the +7 state (present at high injection energies and 25 °C buffer gas) are observed to fold up to a state having $\Omega \approx 1760 \text{ \AA}^2$ at buffer gas temperatures of $\sim 150 \text{ }^\circ\text{C}$. These results suggest that the $\Omega \approx 1760 \text{ \AA}^2$ state is thermodynamically stable and accessible from drastically different pathways (i.e., compact conformers may unfold to this state and elongated conformers fold up to this state). The observation that favored conformers are formed from different precursor states is consistent with current funneling mechanisms of folding for proteins in solution.³² The importance of the folding funnel mechanism is that it explains the ability of many different thermodynamically unfavor-

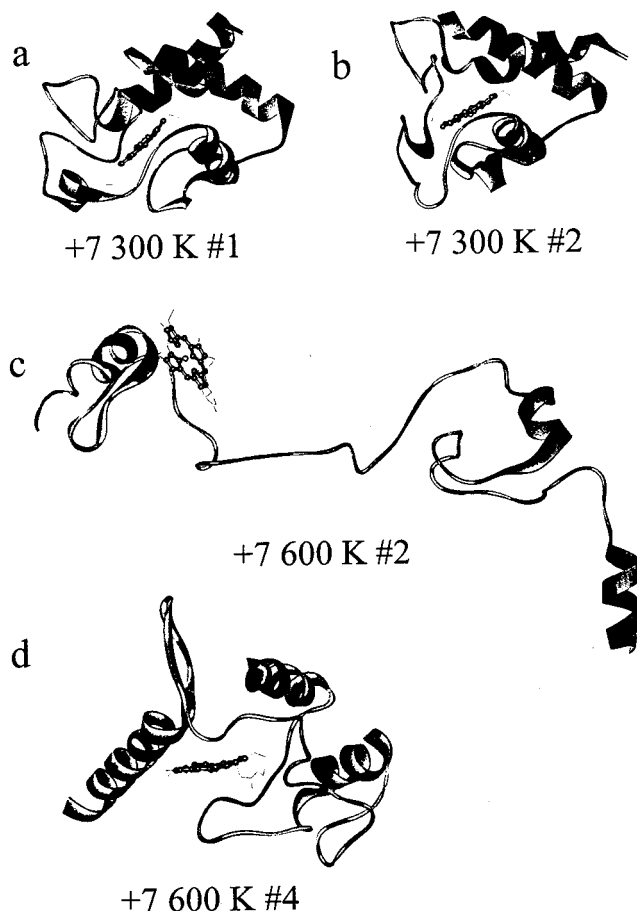


Figure 18. (a and b) Representative structures for the two lowest energy molecular dynamics simulations for the +7 charge state of cytochrome *c* at 300 K. The structures shown are for charge permutations K13 K27 R38 K55 K72 R91 K100 (a) and K13 K27 R38 K55 K79 R91 K100 (b). (c and d) Representative structures for the two lowest energy molecular dynamics simulations for the +7 charge state at 600 K. The structures shown are for charge permutations K13 K27 R38 K39 K55 R91 K100 (c) and K13 K27 R38 K55 K79 R91 K100 (d). (Reproduced with permission from ref 81. Copyright 1999 American Chemical Society.)

able “random coil” states to rapidly fold into energetically favored states. With this type of mechanism, all states are funneled down to a few low-lying conformations.

In the case of the +7 charge state of cytochrome *c*, it appears that a relatively open conformation can be formed from tightly folded or highly elongated precursor states. Mao et al. presented molecular modeling studies of the +5 and +7 cytochrome *c* at 300 and 600 K.⁸¹ A substantial fraction of the modeling work was the development of a scheme for assigning charged site locations. The +5 ions retain a compact conformation, even at 600 K. Figure 18 shows two structures obtained for the +7 charge states at both 300 (a and b) and 600 K (c and d). A compact state was favored for all of the 300 K simulations. At 600 K, some low-energy structures with more open conformations were observed. It appears that a key step in thermal unfolding is the separation of the terminal helices. While these results are in qualitative agreement with experiment, only modest quantitative agreement of model and experimental cross sections is obtained. Calculated

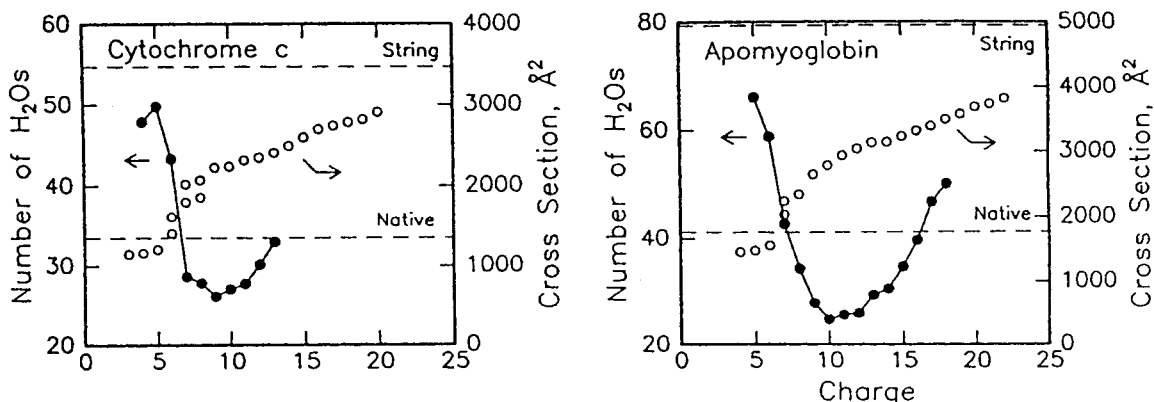


Figure 19. Average number of water molecules adsorbed on cytochrome *c* +4 to +13 charge states and apomyoglobin +5 to +18 charge states in a drift tube doped with 0.73 Torr of water vapor at $-20\text{ }^{\circ}\text{C}$ (●, left-hand scale). Also shown are collision cross sections (○, right-hand scale) determined from separate ion mobility experiments (reported in refs 262 and 263). Dashed lines represent cross sections calculated for the native structure (from crystal coordinates) and extended string structures. (Reproduced with permission from ref 278. Copyright 1998 American Chemical Society.)

cross sections for folded +5 states are larger than that observed experimentally, while the unfolded +7 model conformations have calculated cross sections that are smaller than experiment.

Perhaps as interesting as the observation of thermal transitions and the qualitative agreement of unfolding in this study is the fact that such poor quantitative agreement between experimental and molecular modeling results is obtained. This underscores the tremendous complexity of molecular modeling and cross-section calculations. It is possible that the available state-of-the-art force fields and sampling methods simply cannot handle such large systems. Alternatively, the +7 and +5 states formed during ESI may have protons placed at strategic locations that were not found in the calculations. Fundamental studies that address issues associated with the reliability of modeling in vacuo should help refine theoretical structures. Issues associated with charged site assignment are also clearly important and remain largely unsolved.

k. Rehydration of Naked Proteins. Once naked biomolecular ions are formed, it is possible to select different ions by their m/z ratios, expose these ions to solvent vapor, and investigate the formation of hydration shells. Kebarle and co-workers have investigated the hydration equilibrium for a series of small ions including some polyglycines, $[\text{Gly-Lys} + \text{H}]^+$, and $[\text{Lys-Tyr-Lys} + \text{H}]^+$, and reported the free energy changes at 293 K and 1 atm for addition of initial water molecules.^{275,276} Free energies of hydration are used to determine whether the naked ions undergo proton-induced cyclization.

Jarrod and co-workers have used ion mobility techniques to measure equilibrium binding of the first few water molecules that associate with BPTI,²⁷⁷ cytochrome *c*, and apomyoglobin.²⁷⁸ In these studies the He buffer gas is doped with low pressures (~ 0.005 to 0.8 Torr) of water vapor. At room temperature, Valentine and Clemmer reported that water does not bind significantly to elongated states of cytochrome *c*,¹⁷⁴ the authors noted that a small degree of clustering could explain some shifts in mass spectral peaks for compact conformers. At 271 K, Woenckhaus et al. observed addition of up to nine water molecules for

the compact conformer of the +5 charge state and five water molecules to unfolded forms of the +7 charge state of cytochrome *c*. With increasing water adsorption, $\Delta G_{271\text{K}}$ for the unfolded (+7) and folded (+5) conformers increased from -15 to -14 and -19 to -15 kJ mol^{-1} , respectively. These changes are substantially smaller than changes observed upon adduction of water to protonated glycine (ΔG_{271} ranges from -42 to 24 kJ mol^{-1}) and hydronium ion (ΔG_{271} ranges from -57 to -16 kJ mol^{-1}). The large differences in the magnitudes of ΔG for proton-bound water clusters with size arises from differences in the accessibility of the charge. The authors interpreted the much smaller values of ΔG as an indication that the charges for the +5 and +7 charge states were effectively shielded in both conformations. The larger magnitude of ΔG for the compact (+5) conformer could be due to incorporation of some structural waters.

Fye et al. examined the rehydration of folded and unfolded cytochrome *c* and apomyoglobin as a function of charge state at 253 K under saturating conditions [0.73 Torr, near the equilibrium vapor pressure of water (ice), 0.776 Torr].²⁷⁸ The average number of water molecules adsorbed as a function of charge state is shown in Figure 19. Unfolded conformations adsorb substantially less water than folded conformers for both proteins. The ability of compact conformers to retain substantially more solvent than elongated states demonstrates the importance of cooperative effects, where water molecules are associated with multiple sites of a protein. Additional studies of BPTI have shown evidence for structural waters.²⁷⁷ Woenckhaus, Hudgins, and Jarrod measured enthalpy and entropy changes for addition of the first few waters to the +6 state of BPTI. Molecular mechanics studies of BPTI (which contains three disulfide bonds and is relatively small in size) show that its gas-phase structure retains much of the solution phase structure.^{279,280} Addition of the first water molecule had a dramatic effect on the entropy, a result which indicated that the first water serves as a means of locking together two parts of a peptide chain. The experimental observation of a dramatic change in structure of an isolated mol-

ecule induced by a single water is an important achievement. This type of behavior has been noted previously in crystallographic^{281–283} and solution studies.²⁸⁴

l. Peptides. The first ion mobility studies of peptide ions were reported by Bowers and co-workers for protonated and sodiated bradykinin ions produced by MALDI.¹⁵² The ion mobility data revealed a single peak for each ion, and cross sections of $[M + H]^+ = 242 \pm 5$, $[M + Na]^+ = 245 \pm 5$, and $[M + 2Na]^+ = 247 \pm 5 \text{ \AA}^2$ were reported for these ions at 300 K. Studies over a 300–600 K temperature range showed no evidence for structural changes. The authors interpreted this as an indication that gas-phase conformations of bradykinin are held in place by strong intramolecular interactions between the electronegative carbonyl groups and the charge site. An important aspect of this work (and a previous preliminary report)²⁸⁵ was the application of molecular modeling techniques to simulate the conformations of the ions. One hundred trial conformations of ions were created using the AMBER 4.0 programs²⁸⁶ and a simulated annealing approach in which trial conformers were heated to 800 K over 30 ps, gradually cooled to 100 K over 10 ps, and then energy minimized to 0 K. From a detailed analysis of the molecular modeling results, the authors concluded that preferred interactions between the charged site and the backbone carbonyl residues were responsible for formation of a relatively compact conformation. Figure 20 shows a summary of some of the preferred interactions (for three different charge assignments) that were found. It is notable that isomer C corresponds to the protonation of both the Arg¹ and Arg⁹ residues and deprotonation of the C-terminal carboxylic acid (a salt-bridged form as proposed by Williams, section IV.D). Calculations of cross sections for all three isomers in Figure 20 were consistent with the measured cross sections.

Counterman et al. used high-resolution ion mobility techniques to examine electrosprayed bradykinin ions.¹⁹⁰ The principal focus of this study was the observation of peptide aggregates ($[M_n + nH]^{n+}$ ions) that were revealed in the ion mobility data but hidden in the mass spectra. The authors also reported cross sections of 239, 240, and 284 \AA^2 for the +1, +2, and +3 charge states. The 239 and 240 \AA^2 values for $[M + H]^+$ and $[M + 2H]^{2+}$ are in agreement with the 242 ± 5 value reported by Wyttenbach et al.¹⁵² It was noted that the large cross section for the +3 charge state arises because of the substantial Coulomb repulsion associated with this charge state; the authors noted that the +3 ion cannot be stabilized by intramolecular charge exchange because the three most basic sites (proton acceptors) are already protonated during ESI.

m. Polyamino Acids. Recently, several groups have investigated the structures of polyamino acids. Wyttenbach, Bushnell, and Bowers have measured cross sections for $[\text{Gly}_n + H]^+$ and $[\text{Gly}_n + Na]^+$, where $n = 1–6$.²⁸⁷ In both cases, cross sections increased in a linear fashion with increasing chain length. Both theory and experiment indicate that sodiated glycine ions do not form salt-bridge struc-

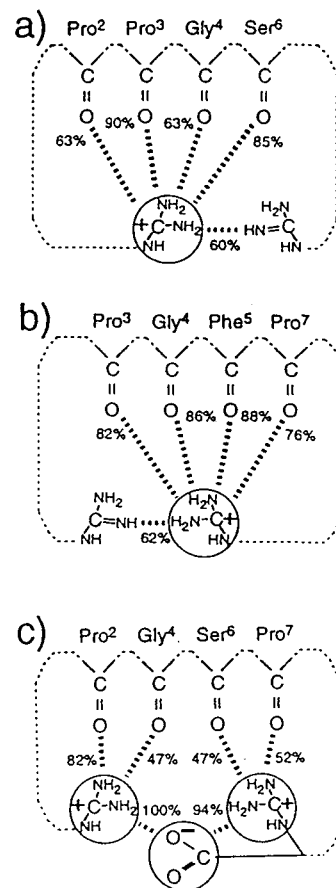


Figure 20. Schematic showing the most common electrostatic interactions found for $[BK + H]^+$ (parts a, b, and c; BK = bradykinin.) (a) Charge is localized on the Arg¹ residue; (b) charge localized on the Arg⁹ residue; and (c) salt-bridged structure. (Adapted with permission from ref 152 Copyright 1996 American Chemical Society.)

tures in the gas phase. Jarrold and co-workers have measured cross sections for larger glycine chains (with n as high as 20) and find that these ions form roughly globular conformations in the gas phase.¹⁵⁴ The primary structural feature is that the charged amino terminus is solvated by interactions with electronegative groups. This type of structure is consistent with the observation that the gas-phase basicities of polyglycines increase with chain length.^{123,126,127}

Hudgins, Ratner, and Jarrold have also reported collision cross sections for $[\text{Ala}_n + H]^+$, where $n = 5–20$, and reported that these ions form globular structures in which the protonated amino terminus is solvated by the electronegative carbonyl groups.^{153,154} Samuelson and Martyna¹⁵⁵ have considered the distributions of conformations of protonated $[\text{Ala}_8 + H]^+$ and $[\text{Ala}_{16} + H]^+$ in the gas phase using molecular dynamics and sampling methodology. The average cross sections for distributions of model conformers were compared to cross sections measured by Li and Clemmer.²⁸⁸ An α -helix is stabilized by hydrogen bonding between each i carbonyl and the backbone N–H of the group that is 4 residues beyond the carbonyl (this is called $i \rightarrow i + 4$ hydrogen bonding). Figure 21 shows plots of the probability distributions associated with the distance of each i carbonyl to its corresponding $i + 4$ N–H backbone in solution

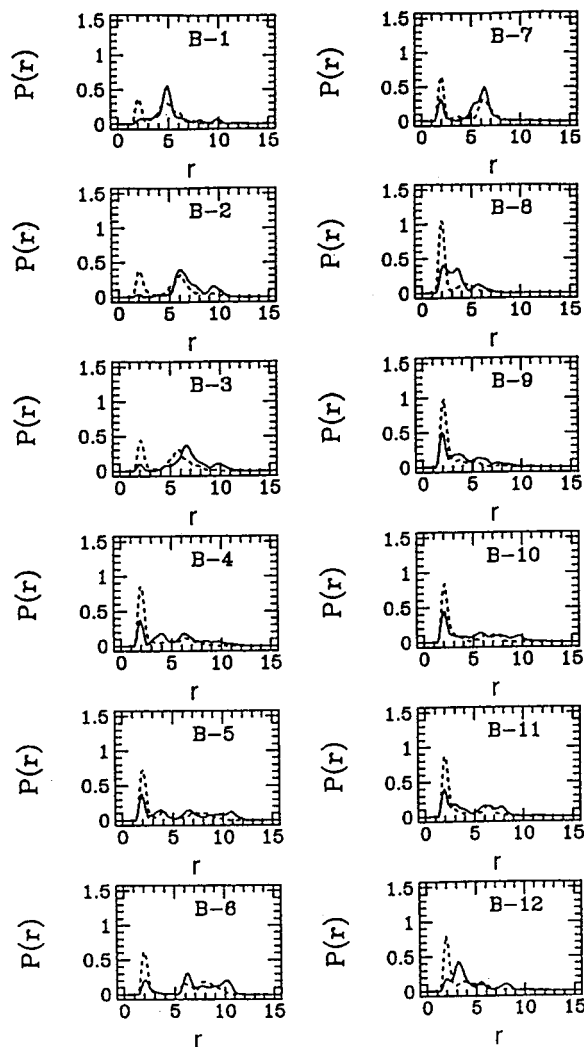


Figure 21. Probability distributions of each of the 14 hydrogen-bonding distances in $\text{Ala}_{16}\text{H}^+$ in vacuo at 300 K (—) and in water (solution contains neutralizing chloride anions) at 300 K and 1 atm (---). Calculations were performed using the CHARMM22 force field. (Reproduced with permission from ref 154. Copyright 1999 American Institute of Physics.)

(dashed lines) and in the gas phase (solid lines). A maximum in the gas-phase probability distribution at ~ 2 Å indicates that the residues between i and $i + 4$ are involved in a helical turn. The results show that residues 4–12 show a slight propensity for helix formation (~ 1.5 helical turns over the entire peptide are typical); however, in general, other backbone torsion angles are favored. A plot of a typical conformation found in this work shows that the protonated N-terminal amino group is solvated by backbone carbonyl groups. Calculations for the ions in solution¹⁵⁴ show that the probability of helix formation is substantially enhanced (~ 3 turns in each peptide). In this case, the high dielectric of the solvent effectively shields the charge site and the system is stabilized by formation of $i \rightarrow i + 4$ hydrogen bonds.

The development of ion mobility/time-of-flight techniques (discussed in section IV.G.2.o) have simplified cross-section measurements of polyamino acids, since it is possible to record ion mobilities and m/z ratios for all ESI generated ions simultaneously. An example data set that has been recorded for polyalanine

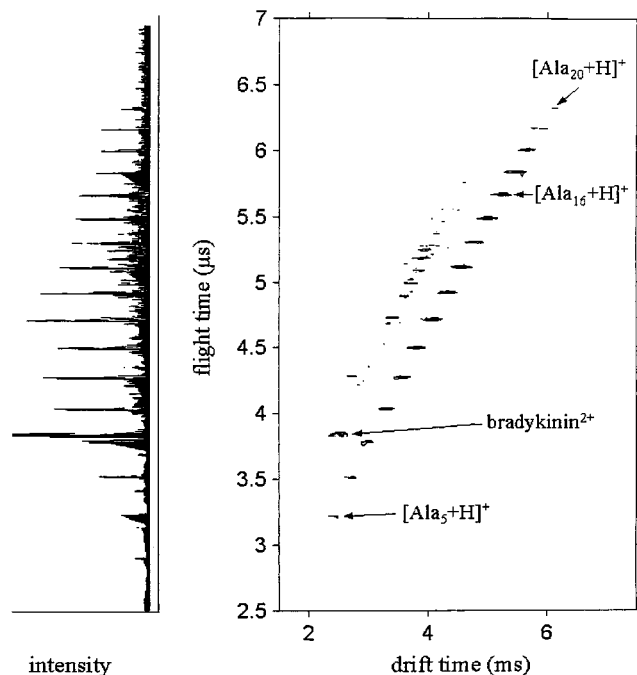


Figure 22. Contour plot of drift and flight times obtained for $[\text{Ala}_n + \text{H}]^+$ ions ($n = 3-20$) using ion mobility/time-of-flight methods. The plot on the left shows the distribution of flight times obtained by compression of the drift time axis.

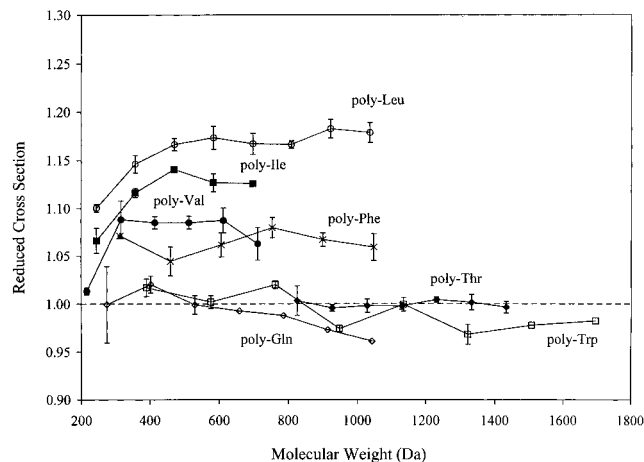


Figure 23. Reduced collision cross sections [experimental cross section divided by the value determined from a fit to measured polyalanine cross sections (at the same molecular weight)] for singly protonated polymers of Leu, Ile, Val, Phe, Thr, Trp, and Gln.

is shown in Figure 22.²⁸⁹ Here, drift times for the $[\text{Ala}_n + \text{H}]^+$ ($n = 3-20$) ions, assigned by m/z ratios, can be used to determine collision cross sections. Similar results have been obtained for $[\text{Val}_n + \text{H}]^+$ ($n = 2-7$), $[\text{Ile}_n + \text{H}]^+$ ($n = 2-6$), $[\text{Leu}_n + \text{H}]^+$ ($n = 4-9$), $[\text{Phe}_n + \text{H}]^+$ ($n = 2-7$), $[\text{Thr}_n + \text{H}]^+$ ($n = 8-14$), $[\text{Trp}_n + \text{H}]^+$ ($n = 2-9$), and $[\text{Gln}_n + \text{H}]^+$ ($n = 2-8$). Figure 23 shows a plot of the cross section for each ion divided by the cross section of a fit to the polyalanine (at an identical molecular weight). This provides information about the relative sizes of each polymer. The results show that after molecular weights have been accounted for, Leu, Ile, Val, and Phe polymers are substantially larger than Thr, Trp, Gln, and Ala polymers. The ordering of the different

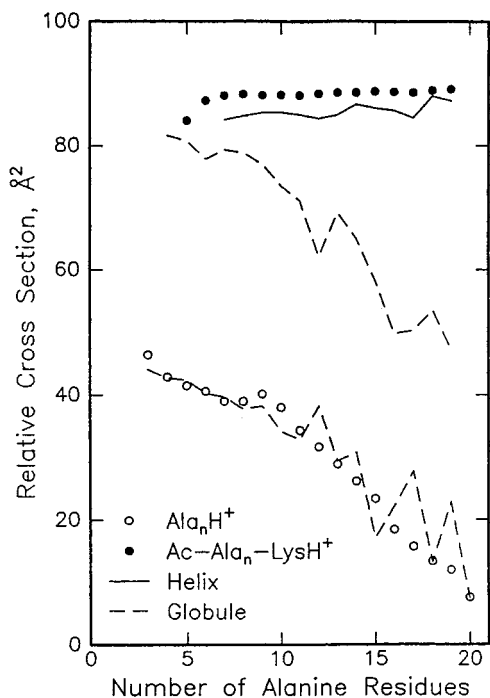


Figure 24. Relative cross sections of Ala_nH^+ (●) and $\text{Ac-Ala}_n\text{-LysH}^+$ (○) as a function of the number of alanine residues (n). Relative cross section is defined as $\Omega_{\text{av}} = 14.50n$, where Ω_{av} is the measured cross section and 14.50 \AA^2 is the average cross section per residue calculated for an ideal polyalanine α -helix (torsion angles set to $\phi = -57^\circ$ and $\psi = -47^\circ$). Reproduced with permission from ref 153. Copyright 1998 American Chemical Society.

sizes of these polymers (e.g., at molecular weight $\sim 600 \text{ Da}$, $\Omega(\text{Gln}_n) < \Omega(\text{Trp}_n) < \Omega(\text{Phe}_n) < \Omega(\text{Val}_n) < \Omega(\text{Ile}_n) < \Omega(\text{Leu}_n)$) is very similar to intrinsic size parameters for different amino acid residues derived from a database of tryptic peptide cross sections (described in section IV.G.2.p).

n. Design of a Stable Helix in Vacuo. The ubiquitous nature of the α -helix in solution, originally predicted by Pauling based on considerations in which solvent was neglected,²⁹⁰ makes this motif an important target for observation in the gas phase (as noted in section IV.F.1). Hudgins, Ratner, and Jarrold have investigated the stability of alanine-based helices in the gas phase.¹⁵³ In solution, the alanine residue is known to have one of the highest helix-forming propensities.^{291–293} The solvation of the N-terminal amino group by electronegative carbonyl backbone moieties in pure $[\text{Ala}_n + \text{H}]^+$ ions disrupts helix formation and globular forms are favored. Hudgins et al. synthesized a series of Ala_nLys peptides (where $n = 5–19$) in which the N-terminal amino group was acetylated; this forces the proton to reside on the basic lysine group located at the C-terminal end of the peptide. A plot of relative collision cross sections against the number of alanine residues is shown in Figure 24 for both $[\text{Ala}_n + \text{H}]^+$ ($n = 3–20$) and $[\text{Ac-Ala}_n\text{Lys} + \text{H}]^+$ ($n = 5–19$). Also shown are cross sections for helical structures and globular conformations of these ions that were generated by molecular dynamics. Calculated cross sections for $[\text{Ac-Ala}_n\text{Lys} + \text{H}]^+$ ($n = 5–19$) helices (such as the structure shown in Figure 25) are in excellent agreement with the experimental results, while

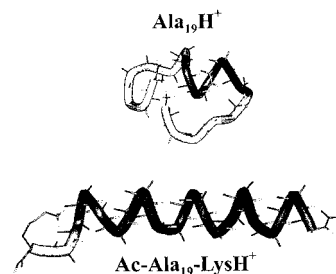


Figure 25. Conformations of $\text{Ala}_{19}\text{H}^+$ (top) and $\text{Ac-Ala}_{19}\text{-LysH}^+$ (bottom) generated by molecular dynamics simulations. (Reproduced with permission from ref 153. Copyright 1998 American Chemical Society.)

globular conformations (such as that shown for $\text{Ala}_{19}\text{H}^+$ in Figure 25) are in poor agreement with experiment. A remarkable result of this study was the tremendous helix stability which arises because of optimal hydrogen bonding of the charged lysine with the C-terminal carbonyl backbone groups and the favorable location of the charge with respect to the helix dipole. Helices persist in sequences containing as few as eight residues, significantly shorter than in solution.^{294,295} In a subsequent study, Hudgins and Jarrold investigated $[\text{Gly}_n\text{-Lys} + \text{H}]^+$ peptides and found that helical conformations are not stabilized, even though the charged residue would be oriented along the helix dipole.²⁹⁶ The authors concluded that entropy is an important factor in the loss of helicity in Gly_n peptides. The absence of a formidable steric group on the Gly residue allows free rotation of this residue about the backbone. This result establishes that the ordering of helix propensities ($\text{Ala} > \text{Gly}$) is analogous to that found in solution. This work is the first clear demonstration of the ability to control structural motifs in vacuo.

Samuelson and Martyna²⁹⁷ have investigated the 16 residue alanine-based $\text{Ac-(AAAAK)}_3\text{A-NH}_2$ peptide which has been studied extensively in solution by NMR and ESR methods^{298–302} and has recently been investigated in the gas phase using ion mobility techniques.³⁰³ Figure 26 shows a comparison of the typical solution and gas-phase ion structures (+3) that were determined. Calculated cross sections for distributions of conformations that were obtained are in good agreement with the experimental results. In solution, the charged lysine side chains are extended because solvent can stabilize charges. However, in the gas phase, the protonated side chains wrap back toward the helix in order to hydrogen bond with backbone carbonyl groups. The net effect of these charged residues in the gas phase relative to solution is slight disruption of the helix at the termini.

o. Development of Ion Trap/Ion Mobility/Time-of-Flight Mass Spectrometry Techniques for the Generation of Gas-Phase Sequence-Structure Databases. A limitation of the ESI-ion mobility combination is that ESI is a continuous ion source while pulses are required for mobility measurements. It is typical to discard 99–99.9% of the ion signal during the mobility experiment. Hoaglund, Valentine, and Clemmer have developed an ion trap interface between the ESI source and the mobility experiment that effectively solves this problem.³⁰⁴ A

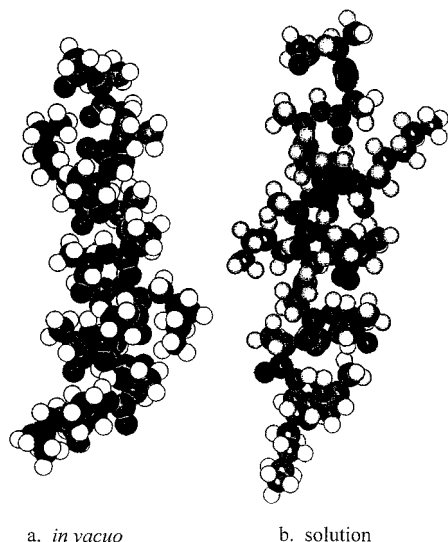


Figure 26. Representative calculated conformations of $[\text{Ac}-(\text{AAA}\text{AK})_3\text{A}-\text{NH}_2 + 3\text{H}]^{3+}$ in (a) water solution and (b) the gas phase. For a complete discussion see ref 297.

second source of experimental inefficiency is associated with the scanning nature of a quadrupole mass filter, which requires that ion mobilities and mass spectra be measured independently. For systems in which multiple ions are present, such as the charge state distributions formed by ESI, separate ion mobility distributions must be recorded for each m/z ion. Guevremont et al. have reported essentially the reverse approach: ions are selected by differences in their mobilities in a drift tube and mass spectra are subsequently recorded using a time-of-flight (TOF) mass spectrometer.⁷² This approach requires that separate mass spectra be recorded for ions with different mobilities. In both approaches, ions that are not selected are discarded during experiments. Hoaglund et al. have developed an injected ion mobility/TOF mass spectrometer that records ion mobility distributions and m/z ratios for multiple ions simultaneously,³⁰⁵ which has recently been extended to include an ESI-ion trap interface.³⁰⁶ This method takes advantage of the fact that flight times in the evacuated flight tube are much shorter than drift times through the buffer gas, making it possible to record hundreds of mass spectra with respect to each packet of ions that is injected into the drift tube. Figure 27 shows an example distribution for ESI of a mixture of tryptic digest peptides from sheep albumin. Here, the drift time axis provides information about the cross section (or conformation) of each ion and the flight time axis distinguishes the m/z ratios. With this approach, it is possible to derive cross sections for hundreds of ions from a single data set.

p. Prediction of Cross Sections from Intrinsic Size Parameters that Are Derived from a Database of Tryptic Digest Peptides. Valentine has recently recorded cross sections for peptides formed from tryptic digestion of 34 common proteins. A database which contains information about the digested protein, peptide sequence, molecular weight, and cross section for 660 different ions, including 420 singly protonated peptides ranging in size from 2 to

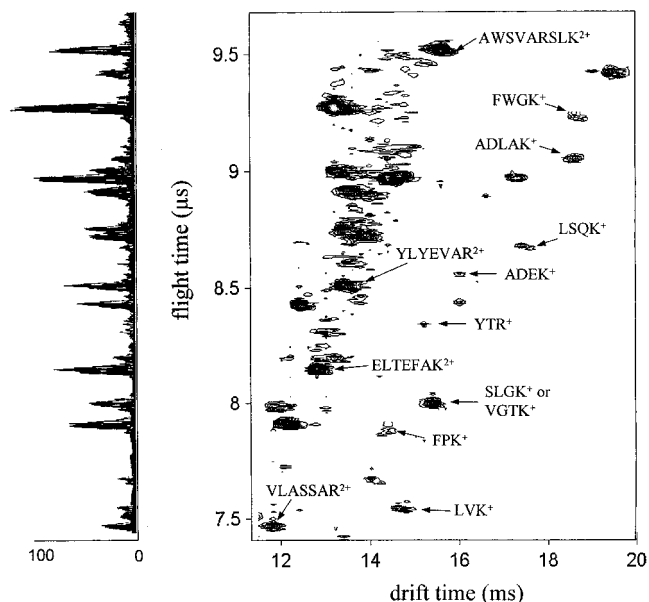


Figure 27. Contour plots of nested drift time (bottom axis) and flight time (left axis) data for a mixture of peptide ions that were formed by electrospray ionization of a tryptic digest of sheep albumin. Representative peaks are labeled with sequences determined by comparison of the flight times of each peak maxima with those expected from digest peptides. Projection of the data along the left axis shows the intensity distribution collapsed to the time-of-flight axis.

15 residues and 240 doubly protonated peptides with 4–24 residues, has been reported.³⁰⁷ It is noteworthy that because trypsin cleaves at basic Arg and Lys residues, most peptides have basic sites at each end—the N-terminal amino group and the basic Arg or Lys as the C-terminal residue.

Intrinsic properties of amino acid residues can be obtained by considering subsets of the database. Valentine considered cross sections for 113 peptides containing 5–10 residues and having a single lysine group located at the C-terminal end.³⁰⁸ These peptides are expected to have compact conformations where the charged group is solvated by electronegative backbone and side chain groups. It is possible to derive the average intrinsic contributions to size of each amino acid by solving a system of equations that relates the unknown size parameter p_i to a series of reduced cross sections $\Omega_j(\text{exp})/\Omega_j(\text{PA})$ by

$$\frac{\sum_i n_{ij} p_i}{\sum_i n_{ij}} = \frac{\Omega_j(\text{exp})}{\Omega_j(\text{PA})} \quad (8)$$

where n_{ij} corresponds to the number of times an amino acid i occurs in each sequence j . $\Omega_j(\text{exp})$ is the measured cross section for each j peptide, and $\Omega_j(\text{PA})$ is the value of a fit to the polyaniline cross sections at the molecular weight of each j peptide. The system of equations has been solved for 17 p_i parameters (amino acids except for Cys, Arg, and His) by a linear algebra regression method.³⁰⁹ The resulting best fit average size parameters for each amino acid in the 5–10 residue Lys-terminated peptides are displayed

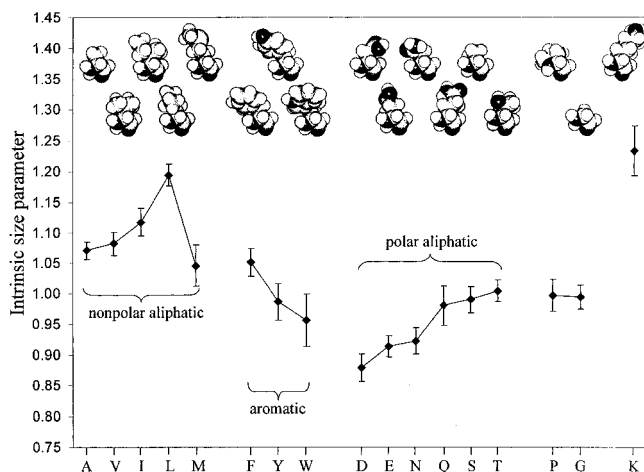


Figure 28. Intrinsic size parameters extracted for individual amino acids from a database of ion mobility collision cross sections for 113 Lys-terminated tryptic digest peptides. Uncertainties correspond to one standard deviation about the mean values that are determined by solving the system of reduced cross section equations. (See text for discussion.) Atomic structures for amino acids including the peptide backbone are also shown. (Reproduced with permission from ref 307. Copyright 1999 American Chemical Society.)

in Figure 28. It is interesting to note that magnitudes of the relative cross sections discussed above (section IV.G.2.m) for the polyamino acids vary as $\text{Gln} < \text{Ala} < \text{Trp} < \text{Thr} < \text{Phe} < \text{Val} < \text{Ile} < \text{Leu}$. With the exception of tryptophan, the ordering of the intrinsic residue size contributions is derived for individual amino acids from the tryptic digest peptides. The largest contributions to cross section come from the nonpolar Ala (1.07 ± 0.01), Val (1.08 ± 0.02), Ile (1.12 ± 0.02), and Leu (1.19 ± 0.02) residues. Contributions from polar groups such as Asp (0.88 ± 0.02), Glu (0.91 ± 0.02), and Asn (0.92 ± 0.02) are much smaller. It was suggested that the different behaviors of these residues could be ascribed to differences in long-range interactions of the different residue types with other residues and the charge site. The authors also noted that Met was grouped as a nonpolar aliphatic residue because it is normally characterized as such in solution even though the side chain contains a sulfur atom.³¹⁰ The intrinsic size parameter obtained from these studies suggests that in the gas-phase Met should be grouped as a large polar residue.

An important outcome of this analysis is the possibility of predicting cross section from sequence. This was tested by combining parameter values with peptide sequences to calculate cross sections. The comparison of the calculated reduced cross sections with the reduced experimental results for all 113 of the 5–10 residue C-terminal lysine peptides are shown in Figure 29. Ninety-eight (~90%) of the 113 calculated values fall within 2.0% of the corresponding experimental value. This result shows that amino acid composition is an important factor in establishing cross section. The accumulation of a large database is a first step toward a general sequence–structure prediction in the gas phase, an area that has received tremendous attention in condensed phase work.^{34,311} Sequence–structure predictions for

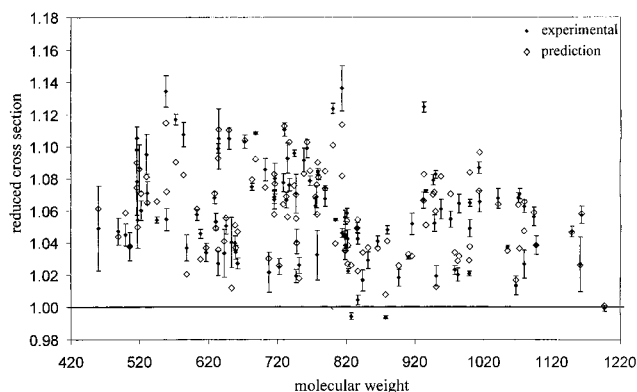


Figure 29. Comparison of experimental reduced cross sections (solid diamonds) and values that have been calculated (\diamond) from sequences using the intrinsic amino acid size parameters shown in Figure 28 for a database of 113 $[(\text{Xxx})_n\text{Lys} + \text{H}]^+$ tryptic digest peptides. See text for discussion. (Reproduced with permission from ref 307. Copyright 1999 American Chemical Society.)

molecules in the gas phase should be especially attractive for theoretical methods because of the simplicity of this environment.

q. Average Amino Acid Volumes in Peptides. Counterman and Clemmer³¹² have used measurements of 103 cross sections for 5–9 residue $[(\text{Xxx})_n\text{Lys} + \text{H}]^+$ ions to select model conformers for calculation of volumes based on a method developed by Connolly.³¹³ The 103 average volumes for conformers with cross sections that agreed with experiment were used to elucidate the volumes of individual residues by a method that is analogous to that discussed for eq 8. A summary of amino acid volumes in solution, residue volumes in protein cores,³¹⁴ residue volumes for peptide ions, and intrinsic volumes of amino acids determined by Counterman is given in Table 5. Several studies have reported average amino acid volumes from crystal coordinates using Richards' modification³¹⁵ of the Voronoi polyhedra approach.³¹⁶ Molecular modeling studies have shown that the volumes associated with surface residues are typically greater than those found in protein core regions because of a solvent ordering effect.³¹⁴ Counterman found that residue volumes were smaller in gas-phase peptide ions than in the corresponding sequence in protein cores. Figure 30 shows a comparison of structures obtained for the VDPVNFK sequence when the sequence exists in the core of human hemoglobin and as a protonated gas-phase ion. In the core, the volume associated with this sequence is restricted by constraints imposed by structural qualities of the protein. Thus, the gas-phase ion appears significantly smaller. Figure 31 compares the volumes of individual amino acid residues in gas-phase peptide ions with those found in protein cores. The average volumes are smaller in the gas-phase peptide than in protein cores, a result that the authors rationalized by noting that in such small systems, few gaps or crevices exist. Additionally, electroconstriction (constriction around a charge, including charge solvation by electronegative groups) appears to decrease the sizes of amino acid volumes in the gas phase. This phenomenon appears to significantly reduce the volume associated

Table 4. Collision Cross Sections (in Å²) of Individual Protein Charge States Measured by Ion Mobility Techniques^a

z ^b	Ubiquitin (bovine) ^d		cytochrome <i>c</i> (horse) ^e		lysozyme ^f	apomyoglobin (sperm whale) ^g	
	pro-tonated	pro-tonated	pro-tonated	depro-tonated	pro-tonated	pro-tonated	depro-tonated
3			1139				
4	775	1004	1153	1174		1459	
		1059					
5	810	1027	1196	1246	1313	1484	1433
		1137	1340				
		1239					
6	875	1041	1393	1351	1355	1562	1539
		1220	1244	1535		1959	1795
		1525	1602	1244			
7	960	1317	1785	1267	1364	2250	1743
		1580	1247	1586	1674		2025
			2007		2057		1581
			1620				
8		1442	1845	1334	1363	1673	2203
		1622	1250	1760	1781	2352	1624
			2061		2203		
			1702				
9		1649	2215	1707	1407	1758	2532
			1964	2024	1899	2659	1717
					2384	2704	
10		1732	2226	2207	1446	1897	2656
					1961	2796	
					2390		
11		1802	2303	2305	2459	2942	2879
12			2335	2340	2525	3044	2968
13			2391		2598	3136	3057
14			2473		2672	3143	3136
15			2579		2733	3230	3226
16			2679		2823	3313	3281
17			2723		2894	3384	3395
18			2766		2989	3489	
19			2800			3570	
20			2889			3682	
21						3792	
22						3815	

^a All values correspond to data obtained in He buffer gas at 298 K. Multiple values for a single protein charge state indicate the observation of multiple resolvable peak maxima in the ion mobility distributions. ^b Ion charge state (absolute value). ^c Values are taken from ref 263. ^d Values are taken from ref 101. ^e Values for protonated ions reported in ref 174. Values for deprotonated ions reported in ref 16. (See Figure 13.) ^f Values are taken from ref 138. ^g Liu, Y.; Valentine, S. J.; Clemmer, D. E. Unpublished results.

with the Lys residue, which is expected to carry the charge in these peptides.

H. Microscopy Studies of Surface Imprints

An extremely innovative approach that uses microscopy methods to image surfaces that have been exposed to high-energy ion impacts has recently been applied to studies of biomolecular ion conformation. This method is adapted from studies that are aimed at investigating the damage imparted to objects in space upon impact by energetic cosmic dust particles.³¹⁷

In these studies, ions are formed by ESI and extracted into a vacuum chamber. A specific *m/z* ratio is selected in a quadrupole mass filter, accelerated to high energies (~150 keV), and focused to a spot area of ~2 mm² onto a known surface (e.g., highly

Table 5. Volumes of Amino Acids in Solution and Residues in Protein Crystals and Gas-Phase Peptide Ions^a

residue	protein core ^b (Å ³)	solution ^c (Å ³)	peptide ions ^d (Å ³)	extended ^e (Å ³)
Gly	63.8(2.9)	71.7	56.5(2.3)	52.7(1.2)
Ala	90.1(4.2)	100.3	81.8(1.1)	72.1(0.6)
Val	139.1(4.7)	150.6	122.7(1.7)	106.9(0.9)
Ile	164.9(6.2)	175.4	144.1(3.0)	128.1(1.6)
Leu	164.6(5.9)	178.7	142.8(1.5)	127.5(0.7)
Met	167.7(6.7)	174.9	148.3(8.2)	134.1(3.5)
Phe	193.5(5.9)	202.3	171.7(3.1)	154.4(1.3)
Tyr	197.1(6.5)	205.3	183.5(5.1)	167.7(3.0)
Trp	231.7(5.6)	239.0	210.7(11.1)	188.2(5.3)
Ser	94.2(3.7)	100.7	89.4(3.2)	83.9(1.4)
Thr	120.0(4.8)	127.6	111.5(2.1)	99.8(0.9)
Asn	127.5(4.2)	128.4	115.9(3.3)	106.0(1.7)
Asp	117.1(4.0)	113.1	111.0(2.3)	104.3(1.2)
Gln	149.4(4.9)	156.0	134.7(8.5)	122.8(2.8)
Glu	140.8(5.3)	140.2	131.4(1.7)	124.8(0.8)
Pro	123.1(5.9)	137.2	106.4(5.3)	98.1(2.2)
Lys	170.0(5.1)	170.3	131.0(3.7)	156.5(1.8)

^a Unless otherwise noted, values correspond to volumes for residues. ^b Values are taken from ref 314. ^c Values correspond to individual amino acids, as taken from ref 314. ^d Values correspond to the average Connolly volumes determined from trial conformers obtained from molecular modeling of 103 [Xxx_{*n*}Lys + H]⁺ peptides (*n* = 4–8). See text for discussion. ^e Values were determined from Connolly volumes for fully extended forms of the [Xxx_{*n*}Lys + H]⁺ peptides (*n* = 4–8).

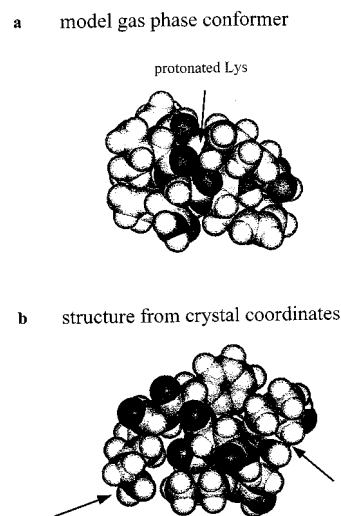


Figure 30. (a) Representative compact trial conformer of [VDPVNFK+H]⁺ having calculated cross sections of $\Omega(\text{EHSS}) = 212.4 \text{ \AA}^2$ and $\Omega(\text{projection}) = 209.2 \text{ \AA}^2$ (in good agreement with the experimental value of $208.7 \pm 0.9 \text{ \AA}^2$) is shown. The arrow indicates the protonation site on the C-terminal Lys residue, which is solvated by electronegative carbonyls of the peptide backbone. (b) Conformation of the VDPVNFK sequence in the folded structure of human hemoglobin (Protein Data Bank accession number 1A3N). The arrows on the left and right indicate the terminal Lys residue and starting Val residues, respectively, by which the sequence is connected in the protein.

oriented pyrolytic graphite (HOPG), mica, SiO₂ and L-valine amino acid crystals). The experimental apparatus is termed a multiply charged macromolecular accelerator (MUMMA). Impact rates are typically 10³–10⁵ ions s⁻¹; surfaces are irradiated with the beam for several hours to produce ~10 impacts μm^{-2} . After ion beam irradiation, the surfaces are removed from the vacuum chamber and imaged in

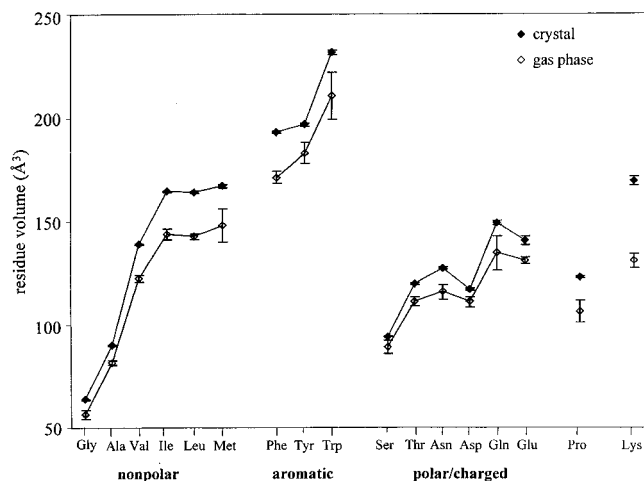


Figure 31. Average volumes and uncertainties for individual amino acid residues found in gas-phase peptide ions (\diamond) and for residues in protein cores (\blacklozenge), which are taken from ref 314. Volumes for gas-phase residues were derived from Connolly volumes for trial conformations of 103 tryptic digest peptides having a C-terminal Lys. Peptide volumes were an average of volumes for many conformations having calculated cross sections in agreement with the experimental value.

ambient air using scanning force microscopy (SFM) or scanning tunneling microscopy (STM).

The hillock formation is explained by analogy to latent track formation in ordered magnetic insulators bombarded by MeV atomic ions.³¹⁸ In the MUMMA experiments, the impact of highly charged biomolecules with a smooth graphitic surface is sufficiently energetic that the graphite surface melts and is immediately quenched into an amorphous, lower density state. The resolidified area of impact appears as a hillock in microscopy analysis. The dimensions of the hillock are broadened relative to the projectile size due to energy diffusion. To model this broadening and extract a measure of projectile size, Sullivan and co-workers¹³⁹ presented a modified version of the thermal spike model originally proposed by Szenes.³¹⁸ Figure 32 illustrates the creation of a hillock from an impact of an extended structure. Here, the impact of the molecule with the surface is assumed to deposit energy along a line of length l , which is determined from a fit to the energy density (a function which accounts for the thermal diffusivity of the surface, the amount of energy deposited per monolayer, and the lattice spacing of the graphite). As shown, the length l is taken to be the projection of the length of the molecule, L , on the surface ($l = L \sin(\theta)$). Differences in orientation of the molecule with respect to the surface will be reflected in the distribution of hillock sizes. A two-dimensional representation of the energy diffusion process is shown in Figure 32b. The molecular length (L) is found from the length of the largest defect (l). The observed dimensions of surface features are also influenced by the size of the probe tip.

In the first study of biomolecular ions using this method, Reimann and collaborators examined the +41 charge state of disulfide-intact and +47 charge state of disulfide-reduced bovine albumin.³¹⁹ The elliptical defects observed for the disulfide-intact ions

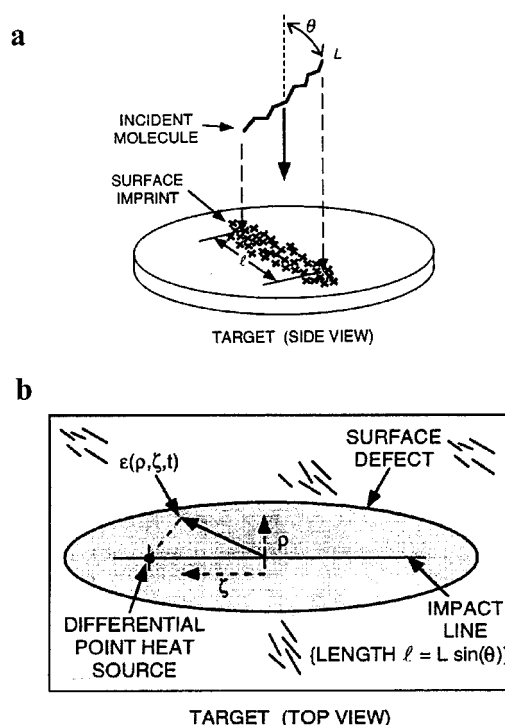


Figure 32. (a) Schematic diagram of an extended, narrow stick-like protein ion creating a surface imprint on impact. L is the length of the protein, and θ is the polar orientation angle. The projected length of the protein on the surface is $l = L \sin(\theta)$. The actual length of the surface imprint (x 's) exceeds $L \sin(\theta)$ because of the transport of deposited energy. (b) Energy transport from the impact line given by the projected length $l = L \sin(\theta)$ of the incident molecule creates a melted and resolidified region which is visualized by scanning force microscopy. ρ and ζ are the spatial coordinates, and $\epsilon(\rho, \zeta, t)$ is the time-dependent radial profile of the energy density. $\epsilon(\rho, \zeta, t)$ is found by solving the two-dimensional heat-diffusion equation (discussed in ref 139) for a set of differential point heat sources along the impact line of length l . (Reproduced with permission from ref 140. Copyright 1998 American Chemical Society.)

were larger than would be expected if albumin retained its native shape; the expansion of these ions was attributed to Coulombic repulsion. The disulfide-reduced ions yielded hillocks having a wide range of sizes; large defects were assigned to the impact of the denatured ion, and smaller features were attributed to fragmentation of the ion with residual gas. The hillock dimensions observed by Quist et al. for bovine insulin (+5), bovine trypsin (+15), horse heart cytochrome *c* (+10), and bovine albumin (+42) are shown in Figure 33.³²⁰ A current limitation of this method is that exactly what factors are responsible for hillock dimensions are not entirely understood. The lateral axes of surface defects created by impact of the multiply charged biomolecules is much larger than the diameters of the native biomolecules (by factors of 5–15 for the ~ 100 –800 keV energies studied); however, the differences in defect size suggest that information about the ion conformations are retained. The narrow hillocks formed by impact of insulin and trypsin are consistent with restriction of the conformations of these proteins by disulfide bonds, as in the native state. The feature observed for cytochrome *c* has a substantially wider lateral axis; this is consistent with unfolding due to Coulomb

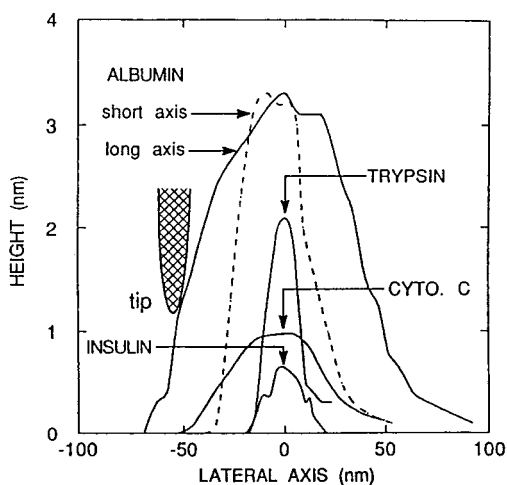


Figure 33. Cross-sectional profiles of typical polyatomic impact-induced features imaged in the contact SFM mode. For comparison, the profile of the SFM tip is included. The height and lateral axes are not on the same scale, the hillocks are actually very shallow, and the tip end is approximately spherical. (Reproduced with permission from ref 320. Copyright 1994 Elsevier.)

repulsion, as previously noted for albumin. No attempts to account for hillock broadening due to energy transfer processes were made in these studies.

In later studies, Reimann and co-workers examined surface impact sites formed by apomyoglobin and disulfide-intact and -reduced lysozyme.^{139,140} The studies of lysozyme showed that the distributions of hillock lengths produced from disulfide-reduced +10 ions shifted to higher values and were twice as broad as those observed for disulfide-intact +9 ions. This is shown in Figure 34 parts a and b. Further elongation of the observed features was noted for the +14 state (Figure 34c) and ascribed to Coulombic repulsion.

The qualitative changes observed from microscopy studies for different charge states in the apo-myoglobin and lysozyme systems are in good agreement with the conclusions drawn from ion mobility^{138,262} and gas-phase basicity¹³⁷ studies. That is, low charge states of disulfide-intact ions favor compact conformations, and in the absence of disulfide bonding, the proteins adopt more extended structures in order to reduce Coulomb repulsion. Although the details of hillock formation are unresolved, the potential ability of this method to provide direct information about ion shape (i.e., typical aspect ratios of conformations) appears promising.

V. Other Biopolymers: DNA and Oligosaccharides

A few studies of the structures of DNA and oligosaccharides have been carried out. Studies of DNA are likely to be particularly important in understanding the relationship of solution-to-gas-phase hydrogen bonding interactions. Unlike the limited understanding of sequence-to-structure that exists for peptides and proteins in solution, the strong tendencies for base pairing interactions in oligonucleotides allow structures to be largely predicted from sequence. This could provide an important link in understanding

what aspects of solution structure are preserved in the gas phase. Numerous studies have now shown that complementary solution duplexes can be observed by ESI-MS.^{321–327} Recently, BIRD measurements of complementary, partially complementary, and noncomplementary duplexes have provided evidence for Watson–Crick base pairing in the gas phase.^{322,327} Ion mobility³²⁸ and H/D exchange methods^{329,330} have provided insight into the structures of single strands. In addition to studies of DNA, ion mobility^{261,331} and H/D exchange³³² measurements of oligosaccharides have also been made. The ability of ion mobility methods to distinguish between different isomer forms should be an important complement to MS-based analyses of these molecules. These techniques are likely to evolve as a means of studying protein glycosylation.³³³

VI. New Analytical Methods that Are Based on Gas-Phase Ion Properties

The understanding of the properties of gas-phase ion conformation has led to the development of several new analytical methods. The observation that ESI charge state distributions reflect solution conformation^{85–87,92–94} provides a simple means of monitoring solution conformation. Ion scattering and ion mobility measurements of cross section can be used to complement the ESI–MS data by providing information about the ion shape. With this approach, it seems possible to discern solution structure that is not apparent in the MS data alone. Gas-phase H–D exchange and solvent adduction,^{43,100,153,277} may also prove useful. However, current methods to study proton-transfer reactions are not sensitive to subtle changes in noncovalent structure from solution.⁶³

Differences in gas-phase ion conformations and chemical reactivities provide many new options for analysis of mixtures. Biomolecular mixtures are traditionally difficult to analyze, and new combinatorial strategies have created tremendous challenges for mass spectrometrists.³³⁴ One of the complications associated with ESI of macromolecular mixtures is that mass spectra rapidly become congested due to the multiple charging phenomenon. Algorithms for obtaining mass information directly from MS data for electrosprayed mixtures have been devised.^{335,336} However, for large mixtures, new strategies are necessary. A number of groups have noted that reactions of ions in a distribution of charge states with bases can be used to concentrate distributions into a few higher intensity peaks corresponding to lower charge state ions.^{134,135,337–339} Distributions of highly charged ions can also be exposed to oppositely charged species in order to generate lower-charge states. Rates of charge transfer between negatively and positively charged ions are controlled by the long-range attractive potentials; high charge states react more rapidly than low charge states. This allows analytes which favor low charge states upon ESI to be analyzed simultaneously with those produced as high charge states without deleterious discrimination between components due to losses associated with preferential neutralization.^{340–342} This method has been used extensively in ion traps,^{340,341} in differential

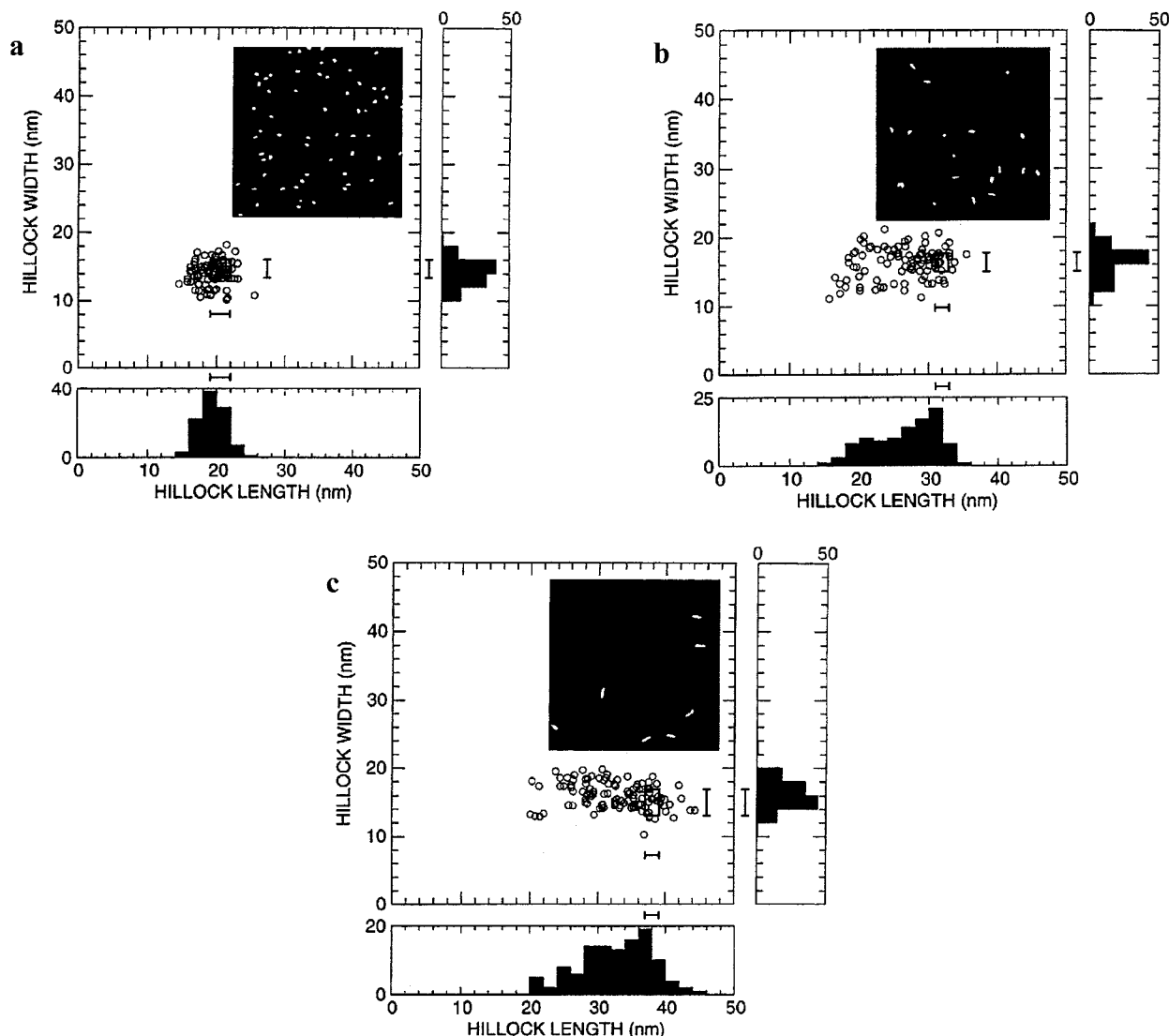


Figure 34. (a) Image ($500 \times 500 \text{ nm}^2$) of highly elongated surface defects created by incident energetic disulfide-intact lysozyme ions (+9), corresponding length and width histograms, and plot of width versus length. One hundred surface defects were measured. A box and range bars show the characteristic points taken to be representative of the longest defects. The height and gray scales were chosen to highlight the lateral extent of the surface defects. (b) Image ($500 \times 500 \text{ nm}^2$) of generally oblong surface defects created by incident energetic disulfide-reduced lysozyme ions (+10), corresponding length and width histograms, and plot of width versus length. One hundred two surface defects were measured. (c) Image ($500 \times 500 \text{ nm}^2$) of slightly oblong surface defects created by incident energetic disulfide-reduced lysozyme ions (+14), corresponding length and width histograms and a plot of width versus length. One hundred fourteen surface defects were measured. (Reprinted with permission from ref 140. Copyright 1998 American Chemical Society.)

mobility analysis of particle sizes,³⁴³ and recently extended for use in TOF mass spectrometry.³⁴²

Measurements of collision cross sections by triple quadrupole and ion mobility methods make it possible to distinguish between many types of ions with identical m/z ratios, such as isomers, conformers, and multiply charged multimers (section IV.G). A number of other methods are also evolving for this purpose. Schnier and Williams have shown that BIRD can also be used to distinguish between peptides with identical compositions but different sequences.³⁴⁴ The des- R^1 and des- R^9 isomers of bradykinin were distinguished based on differences in the dissociation kinetics. Cooks and co-workers have shown that the ion–buffer gas collisions in an ion trap can be used to distinguish different isomers;^{345,346} in this approach, the background buffer gas and asymmetries associated with the trapping field produce “chemical

shifts” in the mass measurement which depend on ion structure. Very recently, a pulsed-field differential mobility technique, which separates ions based on differences in their mobilities in high and low drift fields, has been developed.^{347–349} Guevremont and co-workers have coupled this method with a quadrupole mass filter³⁵⁰ and an ESI source such that it is capable of analysis of biomolecular ions.³⁵¹ Both of these approaches have exciting potential as complements to MS measurements of conformation. Ion mobility/time-of-flight methods appear to be especially well-suited for analysis of biological mixtures. Here, ions having identical m/z ratios can be discerned based on differences in mobility. Valentine et al. have shown that mixtures of peptides from tryptic digestion separate into charge state families based on differences in their mobilities.³⁰⁷ This significantly reduces spectral congestion, and the charge assign-

ment can be made based on the position of the peak in a charge state family. The example spectrum obtained by ion mobility/TOF analysis of a mixture of peptides from tryptic digestion of sheep albumin was shown in Figure 27. These data are beginning to resemble those obtained with two-dimensional gel separation methods; however, the mass and mobility axes are powerful delineators for assessing components. The high resolution of the ion mobility axis significantly reduces spectral congestion and allows many new features to be easily resolved.

VII. Summary and Future Prospects

Isolation of protein molecules in vacuo provides a means of differentiating intramolecular and solvent–molecule interactions. Although this is a relatively new field, a number of thought-provoking results have been obtained. The ability to induce folding and unfolding by highly controlled collisional or laser excitations or the manipulation of protonation states is unique to the gas-phase experiment. A traditional difference between chemistry in the gas phase and that in solution is that intermediates are routinely trapped and characterized in solution while intermediates in the gas phase are elusive and difficult to study because of their relatively short lifetimes. It appears that for macromolecules this situation is reversed. Isolating folding intermediates in solution is challenging because of the large sizes and dynamic natures of these molecules. Distinct conformations are stable in the gas phase over longer time periods because of a balance of long-range electrostatic interactions, shorter-range hydrogen bonding, and van der Waals interactions in a uniquely homogeneous environment.

Currently, the degree of similarity between structures of protein ions in vacuo and in solution remains largely unknown; however, substantial progress in addressing this question has been made. Evidence for stable α -helices and β -sheet structures in the gas phase has been presented. It is now apparent that electrosprayed protein ions can retain a degree of memory of their solution structures; whether these are the kinetically and thermodynamically favored 'folded' states of the gas-phase ions needs to be assessed on a case-by-case basis. From molecular modeling studies, it appears that many structural details within large proteins in solution (such as the basic elements of the fold that lead to the tertiary conformation and many regions of secondary structure) are conserved in the gas phase, especially in low charge state ions. Higher charge states may retain solution-like structure in metastable states but often unfold when heated or exposed to energizing collisions or laser radiation. These unfolded states may not refold because of long-range Coulomb barriers that arise in the gas phase.

The ultimate test of the similarity of gas-phase ions to native solution conformations is function. So far, no results indicating that the gas-phase ion is capable of enzymatic action have been presented. It may be the case that few (or even none) of the naturally occurring polypeptide sequences will be active in the gas phase. However, heavily solvated ions or se-

quences that are designed to fold in vacuo should be capable of enzymatic action. The long-range attractive nature of ion–molecule interactions may lower reaction barriers, making the gas phase an exciting venue in which to study reactivity.

It was expected that the influence of charged sites upon structure in the low-dielectric gas-phase environment would be substantial. Many experimental findings indicate that this is indeed the case. Intramolecular solvation of charged moieties is an important structural feature of gas-phase protein ions that may disrupt local regions of secondary structure. As the level of charging increases in the gas phase, substantial loss of tertiary structure occurs; the correlation of structures for high charge state ions with those that exist in extreme pH environments in solution is difficult to assess, in part because only the general shapes of the ions in the gas phase are known; additionally, little is known about the structures of denatured states in solution. The ability to study partially solvated ions is particularly exciting as it offers the potential of elucidating the influence of solvation shells upon conformation. In the gas phase, it appears possible to explore solvation shells associated with different folded domains of the protein.

An advantage of structural studies in the gas phase is the intrinsically rapid and sensitive nature of mass spectrometry. It is likely that the physical properties of biomolecular ions will provide the basis for new analytical techniques. Large sequence–structure databases have already been compiled. For groups of lysine-terminated peptides, progress in the prediction of cross sections from amino acid composition has been made. Work involving the incorporation of sequence parameters such that gas-phase conformations can be predicted from sequences is underway. It is not yet clear how to relate structural predictions from gas-phase considerations to prediction of structure in solution; work in this area will be required to address this problem.

Answers to a number of important fundamental questions about ions remain elusive. Definitively determining the positions of protonated sites for specific gas-phase ion charge states and conformations would have a tremendous impact on the ability to model conformations. Likewise, the use of chemical reactivity information as a probe of structure is intimately linked to the gas-phase reaction mechanisms, which are not fully understood in macromolecular ion systems. These two problems are closely related, as can be seen by considering the isotopic H–D exchange probe, where simple mechanisms for exchange depend on the relative proton affinities of the reactants. An understanding of charge site distributions would allow estimates of the gas-phase basicities for specific sites in specific conformations to be made. Progress in these fundamental areas could allow substantially more detailed characterization of the conformations and properties of larger ions to be obtained. Development of new techniques that allow multiple structural probes to be applied simultaneously (such as the combination of H–D exchange, ion mobility, and perhaps other

spectroscopic and chemical probes) will also be important for refining experimental structures.

VIII. Acknowledgment

We gratefully acknowledge support of our work by the NSF (CAREER, Grant No. CHE-9625199) and NIH (Grant No. 1R01GM55647-01), with additional support from the ACS (Grant No. ACS-PRF 31859-G4), the Alfred P. Sloan Foundation, and an ASMS Research Award from Finnegan MAT. The authors thank their colleagues Steve Valentine, Cathy Srebalus, John Taraszka, Sheila Henderson, Dr. Yansheng Liu, Dr. Jianwei Li, Dr. Marty Pagel, and Professors Glenn Martyna and Martin Stone for their many stimulating discussions regarding these problems. The methods developed at Indiana University have benefited from the tremendous skills of John Dorsett, Kenny Bastin, and C. Ray Sporleder. Finally, we acknowledge the valuable comments of the reviewers of our manuscripts.

IX. References

- Fenn, J. B.; Mann, M.; Meng, C. K.; Wong, S. F.; Whitehouse, C. M. *Science* **1989**, *246*, 64.
- Karas, M.; Hillenkamp, F. *Anal. Chem.* **1988**, *60*, 2299-2301.
- Miller, P. E.; Denton, M. B. *J. Chem. Ed.* **1986**, *63*, 617.
- Quadrupole Mass Spectrometry and its Applications*; Dawson, P. H., Ed.; AIP Press: Woodbury, 1995.
- Konenkov, N. V.; Kratenko, V. I. *Int. J. Mass Spectrom. Ion Processes* **1991**, *108*, 115.
- March, R.; Huges, R. *Quadrupole Storage Mass Spectrometry*; Wiley: New York, 1989.
- Cooks, R. G.; Kaiser, R. E., Jr. *Acc. Chem. Res.* **1990**, *23*, 213.
- Glish, G. L.; McLuckey, S. A. *Int. J. Mass Spectrom. Ion Processes* **1991**, *106*, 1.
- March, R. E. *J. Mass Spectrom.* **1997**, *32*, 351.
- Marshall, A. G.; Grosshans, P. B. *Anal. Chem.* **1991**, *63*, 215A.
- Anderson, J. S.; Vartanian, V. H.; Laude, D. A., Jr. *Trends Anal. Chem.* **1994**, *13*, 234.
- Guan, S.; Kim, H. S.; Marshall, A. G.; Wahl, M. C.; Wood, T. D.; Xiang, X. *Chem. Rev.* **1994**, *94*, 2161.
- Marshall, A. G. *Acc. Chem. Res.* **1996**, *29*, 307.
- St. Louis, R. H.; Hill, H. H. *Crit. Rev. Anal. Chem.* **1990**, *21*, 321.
- Hill, H. H.; Siems, W. F.; St. Louis, R. H.; McMinn, D. G. *Anal. Chem.* **1990**, *62*, 1201A.
- Clemmer, D. E.; Jarrold, M. F. *J. Mass Spectrom.* **1997**, *32*, 577.
- McLuckey, S. A.; Goeringer, D. E. *J. Mass Spectrom.* **1997**, *32*, 461.
- Scanning Tunneling Microscopy and Spectroscopy*; Bonnelli, D. A., Ed.; VCH Publishers: New York, 1993.
- Magonov, S. N.; Whangbo, M.-H. *Surface Analysis with STM and AFM: Experimental and Theoretical Aspects of Image Analysis*; VCH Publishers: New York, 1996.
- Wiener, S. J.; Kollman, P. A.; Nguyen, D. T.; Case, D. A. *J. Comput. Chem.* **1986**, *7*, 230.
- Lazardis, T.; Archontis, G.; Karplus, M. *Adv. Protein Chem.* **1995**, *47*, 231.
- Dauber-Osguthorpe, P.; Roberts, V. A.; Osguthorpe, D. J.; Wolff, J.; Genest, M.; Hagler, A. T. *Proteins: Struct., Funct., Genet.* **1988**, *4*, 31.
- van Gunsteren, W. F.; Berendsen, H. J. *Groningen Molecular Simulation (GROMOS) Library Manual*; Biomos, Nijenborgh 16, 9747 AG Groningen, The Netherlands, 1987.
- Williams, E. R. *J. Mass Spectrom.* **1996**, *31*, 831.
- Green, M. K.; Lebrilla, C. B. *Mass Spectrom. Rev.* **1997**, *16*, 53.
- For a recent review of gas phase basicity and proton affinity measurements for amino acids and small peptides, see: Harrison, A. G. *Mass Spectrom. Rev.* **1997**, *16*, 201.
- Douglas, D. J. *J. Am. Soc. Mass Spectrom.* **1998**, *9*, 101.
- See: Kuntz, I. D.; Kauzmann, W. *Adv. Protein Chem.* **1974**, *28*, 239 and references therein.
- Rupley, J. A.; Careri, G. *Adv. Protein Chem.* **1991**, *41*, 37.
- Kim, P. S.; Baldwin, R. L. *Ann. Rev. Biochem.* **1990**, *49*, 631 and references therein.
- Dill, K. A. *Biochemistry* **1990**, *29*, 7133.
- Dill, K. A.; Chan, H. S. *Nature Struct. Biol.* **1997**, *4*, 10.
- Dobson, C. M.; Sali, A.; Karplus, M. *Angew. Chem. Int. Ed.* **1998**, *37*, 868.
- A comprehensive review of sequence-structure prediction methods is given in Benner, S. A.; Cannarozzi, G.; Gerloff, D.; Turcotte, M.; Chelvanayagam, G. *Chem. Rev.* **1997**, *97*, 2725.
- Sela, M.; White, F. H.; Anfinsen, C. B. *Science* **1957**, *125*, 691.
- Anfinsen, C. B. *Science* **1973**, *181*, 223.
- Lumry, R.; Eyring, H. *J. Phys. Chem.* **1954**, *58*, 110.
- Creighton, T. E. *Prog. Biophys. Mol. Biol.* **1978**, *33*, 231.
- Roder, H.; Elove, G. A.; Englander, S. W. *Nature* **1988**, *335*, 700.
- Englander, S. W. *Science* **1993**, *262*, 848.
- Richards, F. M. *Sci. Am.* **1991**, *Jan.*, 54.
- Creighton, T. E. *Proteins: Structures and Molecular Properties*, 2nd ed.; Freeman: New York, 1993.
- Woenckhaus, J.; Mao, Y.; Jarrold, M. F. *J. Phys. Chem. B* **1997**, *101*, 847.
- Makhatadze, G. I.; Privalov, P. L. *Adv. Protein Chem.* **1995**, *47*, 307.
- For a discussion of the derivation of these values, see endnote 1 of ref 43.
- Griebenow, K.; Klibanov, A. M. *Proc. Natl. Acad. Sci. U.S.A.* **1995**, *92*, 10969.
- Yeo, S. D.; DeBenedetti, P. G.; Patro, S. Y.; Przybycien, T. M. *J. Pharm. Sci.* **1994**, *83*, 1651 as cited in ref 46.
- Griebenow, K.; Klibanov, A. M. *J. Am. Chem. Soc.* **1995**, *117*, 3940.
- Miranker, A.; Robinson, C. V.; Radford, S. E.; Aplin, R. T.; Dobson, C. M. *Science* **1993**, *262*, 896.
- Kelly, J. W. *Curr. Opin. Struct. Biol.* **1998**, *8*, 101.
- Glenner, G. G.; Wong, C. W. *Biochem. Biophys. Res. Commun.* **1984**, *325*, 6865.
- Masters, C. L.; Simms, G.; Weinman, N. A.; Multhaup, G.; McDonald, B. L.; Beyreuther, K. *Proc. Natl. Acad. Sci. USA* **1985**, *82*, 4245.
- Prusiner, S. B. *Science* **1991**, *252*, 1515.
- Collinge, J.; Palmer, M. S. *Prion Diseases*; Oxford University Press: New York, 1997.
- Chiti, F.; Webster, P.; Taddei, N.; Clark, A.; Stefani, M.; Ramponi, G.; Dobson, C. M. *Proc. Natl. Acad. Sci. USA* **1999**, *96*, 3590.
- Dole, M.; Mack, L. L.; Hines, R. L. *J. Chem. Phys.* **1968**, *49*, 2240.
- Wolynes, P. G. *Proc. Natl. Acad. Sci.* **1995**, *92*, 2426.
- For a review, see: Hillenkamp, F.; Karas, M.; Beavis, R. C.; Chait, B. T. *Anal. Chem.* **1991**, *63*, 1193A.
- For a discussion of fast atom bombardment, see: Fenselau, C.; Cotter, R. J. *Chem. Rev.* **1987**, *87*, 501.
- Fenn, J. B. *J. Am. Soc. Mass Spectrom.* **1993**, *4*, 524.
- Hagar, D. B.; Dovichi, N. J.; Klassen, J.; Kebarle, P. *Anal. Chem.* **1994**, *66*, 3944.
- Smith, R. D.; Bruce, J. E.; Wu, Q.; Lei, Q. P. *Chem. Soc. Rev.* **1997**, *26*, 191.
- Smith, R. D.; Light-Wahl, K. J. *Biol. Mass Spectrom.* **1993**, *22*, 493.
- Mack, L. L.; Kralik, P.; Rheude, A.; Dole, M. *J. Chem. Phys.* **1970**, *52*, 4977.
- Clegg, G. A.; Dole, M. *Biopolymers* **1971**, *10*, 821.
- Nohmi, T.; Fenn, J. B. *J. Am. Chem. Soc.* **1992**, *114*, 3241.
- Fenn, J. B.; Mann, M.; Meng, C. K.; Wong, S. F.; Whitehouse, C. M. *Mass Spectrom. Rev.* **1990**, *9*, 37.
- Iribarne, J. V.; Thomson, B. A. *J. Chem. Phys.* **1976**, *64*, 2287.
- Gieniec, J.; Mack, L. L.; Nakamae, K.; Gupta, C.; Kumar, V.; Dole, M. *Biomed. Mass Spectrom.* **1984**, *11*, 259.
- Smith, R. D.; Loo, J. A.; Ogorzalek Loo, R. R.; Busman, M.; Udseth, H. R. *Mass Spectrom. Rev.* **1991**, *10*, 359.
- Chen, Y. H.; Hill, H. H., Jr.; Wittmer, D. P. *Int. J. Mass Spectrom. Ion Processes* **1996**, *154*, 1.
- Guevremont, R.; Siu, K. W. M.; Wang, J.; Ding, L. *Anal. Chem.* **1997**, *69*, 3959.
- Chowdhury, S. K.; Katta, V.; Chait, B. T. *Rapid Commun. Mass Spectrom.* **1990**, *4*, 81.
- Rodriguez-Cruz, S. E.; Klassen, J. S.; Williams, E. R. *J. Am. Soc. Mass Spectrom.* **1997**, *8*, 565.
- Lee, S.-W.; Freivogel, P.; Schindler, T.; Beauchamp, J. L. *J. Am. Chem. Soc.* **1998**, *120*, 11758.
- Covey, T. R.; Bonner, R. F.; Shushan, B. I.; Henion, J. *Rapid Commun. Mass Spectrom.* **1988**, *2*, 249.
- Smith, R. D.; Loo, J. A.; Edmonds, C. G.; Barinaga, C. J.; Udseth, H. R. *Anal. Chem.* **1990**, *62*, 882.
- For discussions of ionizable groups within proteins in condensed phase see: Rashin, A. A.; Honig, B. *J. Mol. Biol.* **1984**, *173*, 515.
- Handbook of Chemistry and Physics*; Weast, R. C., Ed.; CRC Press: Boca Raton, 1983.
- Rockwood, A. L.; Busman, M.; Smith, R. D. *Int. J. Mass Spectrom. Ion Processes* **1991**, *111*, 103.
- Mao, J.; Woenckhaus, J.; Ratner, M. A.; Jarrold, M. F. *J. Am. Chem. Soc.* **1999**, *121*, 2712.
- Schnier, P. D.; Gross, D. S.; Williams, E. R. *J. Am. Soc. Mass Spectrom.* **1995**, *6*, 1086.

- (83) Schnier, P. D.; Gross, D. S.; Williams, E. R. *J. Am. Chem. Soc.* **1995**, *117*, 6747.
- (84) Carbeck, J. D.; Severs, J. C.; Gao, J.; Wu, Q.; Smith, R. D.; Whitesides, G. M. *J. Phys. Chem. B* **1998**, *102*, 10596.
- (85) Loo, J. A.; Edmonds, C. G.; Udseth, H. R.; Smith, R. D. *Anal. Chem.* **1990**, *62*, 693.
- (86) Winger, B. E.; Light-Wahl, K. J.; Rockwood, A. L.; Smith, R. D. *J. Am. Chem. Soc.* **1992**, *114*, 5897.
- (87) Chowdhury, S. K.; Katta, V.; Chait, B. T. *J. Am. Chem. Soc.* **1990**, *112*, 9012.
- (88) Bushnell, G. W.; Louie, G. V.; Brayer, G. D. *J. Mol. Biol.* **1990**, *214*, 585.
- (89) Hamada, D.; Kuroda, Y.; Kataoka, M.; Aimoto, S.; Yoshimura, T.; Goto, Y. *J. Mol. Biol.* **1996**, *256*, 172.
- (90) Goto, Y.; Calciano, L. J.; Fink, A. L. *Proc. Natl. Acad. Sci. U.S.A.* **1990**, *87*, 573.
- (91) McDonald, C. C.; Phillips, W. D. *Biochemistry* **1973**, *27*, 3480.
- (92) Loo, J. A.; Ogorzalek Loo, R. R.; Udseth, H. R.; Edmonds, C. G.; Smith, R. D. *Rapid Commun. Mass Spectrom.* **1991**, *5*, 101.
- (93) Le Blanc, J. C. Y.; Beuchemin, D.; Siu, K. W.; Guevremont, R.; Berman, S. S. *Org. Mass Spectrom.* **1991**, *26*, 831.
- (94) Mirza, U. A.; Cohen, S. L.; Chait, B. T. *Anal. Chem.* **1993**, *65*, 1.
- (95) Mirza, U. A.; Chait, B. T. *Int. J. Mass Spectrom. Ion Processes* **1997**, *162*, 173.
- (96) Ogorzalek Loo, R. R.; Smith, R. D. *J. Am. Soc. Mass Spectrom.* **1994**, *5*, 207.
- (97) Covey, T. R.; Douglas, D. J. *J. Am. Soc. Mass Spectrom.* **1993**, *4*, 616.
- (98) Hudgins, R. R.; Woenckhaus, J.; Jarrold, M. F. *Int. J. Mass Spectrom. Ion Processes* **1997**, *165/166*, 497.
- (99) Suckau, D.; Shi, Y.; Beu, S. C.; Senko, M. W.; Quinn, J. P.; Wampler, F. M.; McLafferty, F. W. *Proc. Natl. Acad. Sci. U.S.A.* **1993**, *90*, 790.
- (100) Li, J.; Taraszka, J. A.; Counterman, A. E.; Clemmer, D. E. *Int. J. Mass Spectrom. Ion Processes* **1999**, *185/186/187*, 37.
- (101) Valentine, S. J.; Counterman, A. E.; Clemmer, D. E. *J. Am. Soc. Mass Spectrom.* **1997**, *8*, 954.
- (102) Gross, D. S.; Zhao, Y.; Williams, E. R. *J. Am. Soc. Mass Spectrom.* **1997**, *8*, 519.
- (103) Aue, D. H.; Bowers, M. T. In *Gas Phase Ion Chemistry*; Bowers, M. T., Ed.; Academic Press: New York, 1979; Vol 2, pp 1–51.
- (104) Bartmess, J. E.; McIver, R. T., Jr. In *Gas Phase Ion Chemistry*; Bowers, M. T., Ed.; Academic Press: New York, 1979; Vol. 2, pp 88–121.
- (105) Cooks, R. G.; Kruger, T. L. *J. Am. Chem. Soc.* **1977**, *99*, 1279.
- (106) Beauchamp, J. L.; Buttrill, S. E. *J. Chem. Phys.* **1968**, *48*, 178.
- (107) Long, J.; Munson, B. *J. Am. Chem. Soc.* **1973**, *95*, 2427.
- (108) Locke, M. J.; McIver, R. T. *J. Am. Chem. Soc.* **1983**, *105*, 4226.
- (109) Bojeson, G. *J. Chem. Soc., Chem. Commun.* **1986**, 244.
- (110) Bojeson, G. *J. Am. Chem. Soc.* **1987**, *109*, 5557.
- (111) Gorman, G. S.; Speir, J. P.; Turner, C. A.; Amster, I. J. *J. Am. Chem. Soc.* **1992**, *114*, 3986.
- (112) Li, X. P.; Harrison, A. G. *Org. Mass Spectrom.* **1993**, *28*, 366.
- (113) Wu, Z.; Fenselau, C. *Rapid Commun. Mass Spectrom.* **1992**, *6*, 403.
- (114) Wu, Z.; Fenselau, C. *Tetrahedron* **1993**, *49*, 9197.
- (115) Bojeson, G.; Breindahl, T. *J. Chem. Soc., Perkins Trans. 2* **1994**, 1029.
- (116) Lias, S. G.; Liebman, J. F.; Levin, R. D. *J. Phys. Chem. Ref. Data* **1984**, *13*, 695.
- (117) Hunter, E. P. L.; Lias, S. G. *J. Phys. Chem. Ref. Data* **1998**, *27*, 413.
- (118) NIST Chemistry WebBook, <http://webbook.nist.gov/chemistry>.
- (119) Dawson, R. M. C.; Elliott, D. C.; Elliott, W. H.; Jones, K. M. *Data for Biochemical Research*, 3rd ed.; Oxford Science Publications: New York, 1986; pp 1–31.
- (120) Bouchonnet, S.; Hoppilliard, Y. *Org. Mass Spectrom.* **1992**, *27*, 71.
- (121) Jensen, F. *J. Am. Chem. Soc.* **1992**, *114*, 9533.
- (122) Somogyi, A.; Wysocki, V. H.; Mayer, I. *J. Am. Soc. Mass Spectrom.* **1994**, *5*, 704.
- (123) Zhang, K.; Zimmerman, D. M.; Chung-Phillips, A.; Cassady, C. *J. J. Am. Chem. Soc.* **1993**, *115*, 10812.
- (124) Wu, Z.; Fenselau, C. *Rapid Commun. Mass Spectrom.* **1994**, *8*, 777.
- (125) Bliznyuk, A. A.; Schaefer, H. F., III; Amster, I. J. *J. Am. Chem. Soc.* **1993**, *115*, 5149.
- (126) Wu, Z.; Fenselau, C. *J. Am. Soc. Mass Spectrom.* **1992**, *3*, 863.
- (127) Wu, J.; Lebrilla, C. B. *J. Am. Chem. Soc.*, **1993**, *115*, 3270.
- (128) Cheng, X.; Wu, Z.; Fenselau, C. *J. Am. Chem. Soc.*, **1993**, *115*, 4844.
- (129) Kaltashov, I. A.; Fenselau, C. C. *Int. J. Mass Spectrom. Ion Processes* **1995**, *146/147*, 339.
- (130) Kaltashov, I. A.; Fabris, D.; Fenselau, C. C. *J. Phys. Chem.* **1995**, *99*, 10046.
- (131) Kaltashov, I. A.; Fenselau, C. C. *J. Am. Chem. Soc.* **1995**, *117*, 9906.
- (132) Wu, J.; Lebrilla, C. B. *J. Am. Soc. Mass Spectrom.* **1995**, *6*, 91.
- (133) McLuckey, S. A.; van Berkel, G. J.; Glish, G. L. *J. Am. Chem. Soc.* **1990**, *112*, 5668.
- (134) Ikonomou, M. G.; Kebarle, P. *Int. J. Mass Spectrom. Ion Processes* **1992**, *117*, 283.
- (135) Ogorzalek Loo, R. R.; Udseth, H. R.; Smith, R. D. *J. Am. Soc. Mass Spectrom.* **1992**, *3*, 695.
- (136) Ogorzalek Loo, R. R.; Winger, B. E.; Smith, R. D. *J. Am. Soc. Mass Spectrom.* **1994**, *5*, 1064.
- (137) Gross, D. S.; Schnier, P. D.; Rodriguez-Cruz, S. E.; Fagerquist, C. K.; Williams, E. R. *Proc. Natl. Acad. Sci. USA* **1996**, *93*, 3143.
- (138) Valentine, S. J.; Anderson, J.; Ellington, A. E.; Clemmer, D. E. *J. Phys. Chem. B*, **1997**, *101*, 3891.
- (139) Sullivan, P. A.; Axelsson, J.; Altmann, S.; Quist, A. P.; Sundqvist, B. U. R.; Reimann, C. T. *J. Am. Soc. Mass Spectrom.* **1996**, *7*, 329.
- (140) Reimann, C. T.; Sullivan, P. A.; Axelsson, J.; Quist, A. P.; Altmann, S.; Roepstorff, P.; Velazquez, I.; Tapia, O. *J. Am. Chem. Soc.* **1998**, *120*, 7608.
- (141) Ogorzalek Loo, R. R.; Smith, R. D. *J. Mass Spectrom.* **1995**, *30*, 339.
- (142) Zhang, X.; Cassady, C. J. *J. Am. Soc. Mass Spectrom.* **1996**, *7*, 1211.
- (143) Gronert, S. *J. Am. Chem. Soc.* **1996**, *118*, 3525.
- (144) Cassady, C. J.; Wronka, J.; Kruppa, G. H.; Laukien, F. H. *Rapid Commun. Mass Spectrom.* **1994**, *8*, 394.
- (145) Cassady, C. J.; Carr, S. R. *J. Mass Spectrom.* **1996**, *31*, 247.
- (146) Cassady, C. J. *J. Am. Soc. Mass Spectrom.* **1998**, *9*, 716.
- (147) Gross, D. S.; Williams, E. R. *J. Am. Chem. Soc.* **1995**, *117*, 883.
- (148) Gross, D. S.; Williams, E. R. *J. Am. Chem. Soc.* **1996**, *118*, 202.
- (149) Wong, S. F.; Meng, C. K.; Fenn, J. B. *J. Phys. Chem.* **1988**, *92*, 546.
- (150) Gilson, M. K.; Honig, B. *Biopolymers* **1986**, *25*, 2097.
- (151) Pethig, R. *Dielectric and Electronic Properties of Biological Materials*; John Wiley and Sons: New York, 1979, as cited in ref 82.
- (152) Wyttenbach, T.; von Helden, G.; Bowers, M. T. *J. Am. Chem. Soc.* **1996**, *118*, 8355.
- (153) Hudgins, R. R.; Ratner, M. A.; Jarrold, M. F. *J. Am. Chem. Soc.* **1998**, *120*, 12974.
- (154) Hudgins, R. R.; Mao, Y.; Ratner, M. A.; Jarrold, M. F. *Biophys. J.* **1999**, *76*, 1591.
- (155) Samuelson, S.; Martyna, G. J. *J. Chem. Phys.* **1999**, *103*, 1752.
- (156) Smith, D. L.; Zhang, Z. *Mass Spectrom. Rev.* **1994**, *13*, 411.
- (157) Katta, V.; Chait, B. T. *Rapid Commun. Mass Spectrom.* **1991**, *5*, 214.
- (158) Katta, V.; Chait, B. T. *J. Am. Chem. Soc.* **1993**, *115*, 6317.
- (159) Anderegg, R. J.; Wagner, D. S.; Stevenson, C. L.; Borchardt, R. T. *J. Am. Soc. Mass Spectrom.* **1994**, *5*, 425.
- (160) Wagner, D. S.; Anderegg, R. J. *Anal. Chem.* **1994**, *66*, 706.
- (161) Winston, R. L.; Fitzgerald, M. C. *Mass Spectrom. Rev.* **1997**, *16*, 165.
- (162) Zhang, Z.; Li, W.; Logan, T. M.; Li, M.; Marshall, A. G. *Protein Science* **1997**, *6*, 2203.
- (163) Brauman, J. L. In *Kinetics of Ion-Molecule Reactions*; Ausloos, P., Ed.; Plenum Press: New York, 1979; pp 153–164.
- (164) Lias, S. G. *J. Phys. Chem.* **1984**, *88*, 4401.
- (165) Campbell, S.; Rodgers, M. T.; Marzluff, E. M.; Beauchamp, J. L. *J. Am. Chem. Soc.* **1994**, *116*, 9765.
- (166) Campbell, S.; Rodgers, M. T.; Marzluff, E. M.; Beauchamp, J. L. *J. Am. Chem. Soc.* **1995**, *117*, 12840.
- (167) Cheng, X.; Fenselau, C. *Int. J. Mass Spectrom. Ion Processes* **1992**, *122*, 109.
- (168) Gard, E.; Green, M. K.; Bregar, J.; Lebrilla, C. B. *J. Am. Soc. Mass Spectrom.* **1994**, *5*, 623.
- (169) Green, M. K.; Lebrilla, C. B. *Int. J. Mass Spectrom. Ion Processes* **1998**, *175*, 15.
- (170) Wyttenbach, T.; Bowers, M. T. *J. Am. Soc. Mass Spectrom.* **1999**, *10*, 9.
- (171) Zhang, Z.; Li, W.; Guan, S.; Marshall, A. G. *Proceedings of the 44th ASMS Conference on Mass Spectrometry and Allied Topics*, Portland, OR, 1996; p 1061.
- (172) Lee, S.-W.; Lee, H.-N.; Kim, H. S.; Beauchamp, J. L. *J. Am. Chem. Soc.* **1998**, *120*, 5800.
- (173) McLafferty, F. W.; Guan, Z.; Haupts, U.; Wood, T. D.; Kelleher, N. L. *J. Am. Chem. Soc.* **1998**, *120*, 4732.
- (174) Valentine, S. J.; Clemmer, D. E. *J. Am. Chem. Soc.* **1997**, *119*, 3558.
- (175) Wood, T. D.; Chorush, R. A.; Wampler, F. M.; Little, D. P.; O'Connor, P. B.; McLafferty, F. W. *Proc. Natl. Acad. Sci. U.S.A.* **1995**, *92*, 2451.
- (176) Freitas, M. A.; Marshall, A. G. *Int. J. Mass Spectrom. Ion Processes* **1999**, *182/183*, 221.
- (177) Freitas, M. A.; Hendrickson, C. L.; Emmett, M. R.; Marshall, A. G. *J. Am. Soc. Mass Spectrom.* **1998**, *9*, 1012.
- (178) Li, J.; Clemmer, D. E. Unpublished results.
- (179) Robinson, J. M.; Greig, M. J.; Griffey, R. H.; Mohan, V.; Laude, D. A. *Anal. Chem.* **1998**, *70*, 3566.
- (180) Freitas, M. A.; Shi, S. D.-H.; Hendrickson, C. L.; Marshall, A. G. *J. Am. Chem. Soc.* **1998**, *120*, 10187.

- (181) Cheng, X.; Fenselau, C. *J. Am. Chem. Soc.* **1993**, *115*, 10327.
- (182) Weiske, T.; Bohme, D. K.; Hrusak, J.; Kratschmer, W.; Schwartz, H. *Angew. Chem., Int. Ed. Engl.* **1991**, *30*, 884.
- (183) Caldwell, K. A.; Giblin, D. E.; Hsu, C. S.; Cox, D.; Gross, M. L. *J. Am. Chem. Soc.* **1991**, *113*, 8519.
- (184) Ross, M. M.; Callahan, J. H. *J. Phys. Chem.* **1991**, *95*, 5720.
- (185) Wei, S.; Shi, Z.; Castleman, A. W., Jr. *J. Chem. Phys.* **1991**, *94*, 3268.
- (186) Svanberg, M.; Pettersson, J. B. C. *J. Phys. Chem. A* **1998**, *102*, 1862.
- (187) Stephenson, J. L., Jr.; McLuckey, S. A. *J. Am. Chem. Soc.* **1997**, *119*, 1688.
- (188) Stephenson, J. L., Jr.; McLuckey, S. A. *Anal. Chem.*, **1997**, *69*, 281.
- (189) Zhan, D.; Rosell, J.; Fenn, J. B. *J. Am. Soc. Mass Spectrom.* **1998**, *9*, 1241.
- (190) Counterman, A. E.; Valentine, S. J.; Srebalus, C. A.; Henderson, S. C.; Hoaglund, C. S.; Clemmer, D. E. *J. Am. Soc. Mass Spectrom.*, **1998**, *9*, 743.
- (191) Przybylski, M.; Glocker, M. O. *Angew. Chem. Int. Ed. Engl.* **1996**, *35*, 806.
- (192) Loo, J. A. *Mass Spectrom. Rev.* **1997**, *16*, 1.
- (193) Loo, J. A.; Udseth, H. R.; Smith, R. D. *Rapid Commun. Mass Spectrom.* **1988**, *2*, 207.
- (194) Johnson, R. S.; Martin, S. A.; Biemann, K. *Int. J. Mass Spectrom. Ion Processes* **1988**, *86*, 137.
- (195) Martin, S. A.; Biemann, K. *Int. J. Mass Spectrom. Ion Processes* **1987**, *78*, 213.
- (196) Tang, X.; Thibault, P.; Boyd, R. K. *Anal. Chem.* **1993**, *65*, 2824.
- (197) Mabud, Md. A.; DeKrey, M. J.; Cooks, R. G. *Int. J. Mass Spectrom. Ion Processes* **1985**, *67*, 285.
- (198) Jones, J. L.; Dongre, A. R.; Somogyi, A.; Wysocki, V. H. *J. Am. Chem. Soc.* **1994**, *116*, 8368.
- (199) Dongre, A. R.; Jones, J. L.; Somogyi, A.; Wysocki, V. H. *J. Am. Chem. Soc.* **1996**, *118*, 8365.
- (200) Dongre, A. R.; Somogyi, A.; Wysocki, V. H. *J. Mass Spectrom.* **1996**, *31*, 339.
- (201) Vachet, R. W.; Asam, M. R.; Glish, G. L. *J. Am. Chem. Soc.* **1996**, *118*, 6252.
- (202) Loo, J. A.; Edmonds, C. G.; Smith, R. D. *Science* **1990**, *248*, 201.
- (203) Wu, Q.; Van Orden, S.; Cheng, X.; Bakhtiar, R.; Smith, R. D. *Anal. Chem.* **1995**, *67*, 2498.
- (204) Zubarev, R. A.; Kelleher, N. L.; McLafferty, F. W. *J. Am. Chem. Soc.* **1998**, *120*, 3265.
- (205) Dunbar, R. C. In *Gas Phase Ion Chemistry*; Bowers, M. T., Ed.; Academic Press: New York, 1979; Vol. 2, pp 181–220.
- (206) Dunbar, R. C. In *Gas Phase Ion Chemistry*; Bowers, M. T., Ed.; Academic Press: New York, 1984; Vol. 3; pp 129–166.
- (207) Ballew, R. M.; Sabelko, J.; Gruebele, M. *Nature: Struct. Biol.* **1996**, *3*, 923.
- (208) Herzberg, G. *Atomic Spectra and Atomic Structure*, 2nd ed.; Dover: New York, 1944.
- (209) Herzberg, G. *Molecular Spectra and Molecular Structure*, 2nd ed.; Van Nostrand: New York, 1950.
- (210) Little, D. P.; Speir, J. P.; Senko, M. W.; O'Connor, P. B.; McLafferty, F. W. *Anal. Chem.* **1994**, *66*, 2809.
- (211) Little, D. P.; McLafferty, F. W. *J. Am. Chem. Soc.* **1995**, *117*, 6783.
- (212) Little, D. P.; Aaserud, D. J.; Valaskovic, G. A.; McLafferty, F. W. *J. Am. Chem. Soc.* **1996**, *118*, 9352.
- (213) Tholmann, D.; Tonner, D. S.; McMahon, T. B. *J. Phys. Chem.* **1994**, *98*, 2002.
- (214) Dunbar, R. C. *J. Phys. Chem.* **1994**, *98*, 8705.
- (215) Price, W. D.; Schnier, P. D.; Williams, E. R. *Anal. Chem.* **1996**, *68*, 859.
- (216) Schnier, P. D.; Price, W. D.; Jockusch, R. A.; Williams, E. R. *J. Am. Chem. Soc.* **1996**, *118*, 7178.
- (217) These ranges do not include the Arg-deleted forms that reported in Table 1 of ref 216.
- (218) Rockwood, A. L.; Busman, M.; Udseth, H. R.; Smith, R. D. *Rapid Commun. Mass Spectrom.* **1991**, *5*, 582.
- (219) Busman, M.; Rockwood, A. L.; Smith, R. D. *J. Phys. Chem.* **1992**, *96*, 2397.
- (220) Meot-Ner, M.; Dongre, A. R.; Somogyi, A.; Wysocki, V. H. *Rapid Commun. Mass Spectrom.* **1995**, *9*, 829.
- (221) Cooks, R. G.; Beynon, J. H.; Caprioli, R. M.; Lester, G. R. *Metastable Ions*; Elsevier: New York, 1973.
- (222) Kaltashov, I. A.; Fenselau, J. *J. Phys. Chem.* **1995**, *99*, 19946.
- (223) Adams, J.; Strobel, F.; Reiter, A. *J. Am. Soc. Mass Spectrom.* **1996**, *7*, 30.
- (224) Kaltashov, I. A.; Fenselau, C. *Proteins: Struct., Funct., Genet. Suppl.* **1997**, *27*, 165.
- (225) Kaltashov, I. A.; Fenselau, C. C. *Int. J. Mass Spectrom. Ion Processes* **1997**, *160*, 331.
- (226) Dempsey, C. E. *Biochim. Biophys. Acta* **1990**, *1031*, 143.
- (227) Terwilliger, T. C.; Eisenberg, D. *J. Biol. Chem.* **1982**, *257*, 6010.
- (228) Jarrold, M. F. Presented at the 46th ASMS Conference on Mass Spectrometry and Allied Topics, 1998, Orlando, FL.
- (229) Li, A.; Fenselau, C.; Kaltashov, I. A. *Proteins: Struct., Funct., Genet. Suppl.* **1998**, *22*.
- (230) Futrell, J. F.; Tiernan, T. O. In *Ion-Molecule Reactions*; Franklin, J. L., Ed.; Plenum Press: New York, 1972; Chapter 11.
- (231) Yost, R. A.; Enke, C. G. *J. Am. Chem. Soc.* **1978**, *100*, 2274.
- (232) Cox, K. A.; Julian, R. K., Jr.; Cooks, R. G.; Kaiser, R. E., Jr. *J. Am. Soc. Mass Spectrom.* **1994**, *5*, 127.
- (233) Douglas, D. J. *J. Am. Soc. Mass Spectrom.* **1994**, *5*, 17.
- (234) Chen, Y.-L.; Collings, B. A.; Douglas, B. J. *J. Am. Soc. Mass Spectrom.* **1997**, *8*, 681.
- (235) Collings, B. A.; Douglas, D. J. *J. Am. Chem. Soc.*, **1996**, *118*, 4488.
- (236) Nesatyi, V.; Chen, Y.-L.; Collings, B. A.; Douglas, D. J. *Rapid Commun. Mass Spectrom.* **1998**, *12*, 40.
- (237) Chen, Y.-L.; Campbell, J. M.; Collings, B. A.; Konermann, L.; Douglas, D. J. *Rapid Commun. Mass Spectrom.* **1998**, *12*, 1003.
- (238) Javahery, G.; Thomson, B. J. *Am. Mass Spectrom.* **1997**, *8*, 697.
- (239) Whitby, K. T.; Clark, W. E. *Tellus* **1966**, *18*, 573.
- (240) Sanders, T. M.; Forest, S. R. *J. Appl. Phys.* **1989**, *66*, 3317.
- (241) Hagen, D. F. *Anal. Chem.* **1979**, *51*, 870.
- (242) Jarrold, M. F.; Bower, J. E.; Creegan, K. *J. Chem. Phys.* **1989**, *90*, 3615.
- (243) Jarrold, M. F. *J. Phys. Chem.* **1995**, *99*, 11.
- (244) Radi, P. P.; von Helden, G.; Hsu, M. T.; Kemper, P. R.; Bowers, M. T. *Int. J. Mass. Spectrom. Ion Processes* **1991**, *109*, 49.
- (245) von Helden, G.; Hsu, M.-T.; Kemper, P. R.; Bowers, M. T. *J. Chem. Phys.* **1991**, *93*, 3835.
- (246) von Helden, G.; Hsu, M.-T.; Gotts, N.; Bowers, M. T. *J. Phys. Chem.* **1993**, *97*, 8182.
- (247) Shelimov, K. B.; Hunter, J. M.; Jarrold, M. F. *Int. J. Mass Spectrom. Ion Processes* **1994**, *138*, 17.
- (248) Hunter, J. M.; Jarrold, M. F. *J. Am. Chem. Soc.* **1995**, *117*, 103.
- (249) Mason, E. A.; McDaniel, E. W. *Transport Properties of Ions in Gases*; Wiley: New York, 1988.
- (250) A historical overview of cross section calculations is given by Lin, S. N.; Griffin, G. W.; Horning, E. C.; Wentworth, W. E. *J. Chem. Phys.* **1974**, *60*, 4994.
- (251) Mesleh, M. F.; Hunter, J. M.; Shvartsburg, A. A.; Schatz, G. C.; Jarrold, M. F. *J. Phys. Chem.* **1996**, *100*, 16082.
- (252) Mack, E., Jr. *J. Am. Chem. Soc.* **1925**, *47*, 2468.
- (253) Melaven, R. M.; Mack, E., Jr. *J. Am. Chem. Soc.* **1932**, *54*, 888.
- (254) Wyttenbach, T.; von Helden, G.; Batka, J. J., Jr.; Carlat, D.; Bowers, M. T. *J. Am. Soc. Mass Spectrom.* **1997**, *8*, 275.
- (255) Shvartsburg, A. A.; Jarrold, M. F. *Chem. Phys. Lett.* **1996**, *261*, 86.
- (256) Shvartsburg, A. A.; Schatz, G. C.; Jarrold, M. F. *J. Chem. Phys.* **1998**, *108*, 2416.
- (257) Viehland, L. A.; Dickinson, A. S. *Chem. Phys.* **1995**, *193*, 255.
- (258) Clemmer, D. E.; Hudgins, R. R.; Jarrold, M. F. *J. Am. Chem. Soc.* **1995**, *117*, 10141.
- (259) Jarrold, M. F.; Honea, E. C. *J. Phys. Chem.* **1991**, *95*, 9181.
- (260) Jarrold, M. F.; Constant, V. A. *Phys. Rev. Lett.* **1991**, *67*, 2994.
- (261) Liu, Y.; Clemmer, D. E. *Anal. Chem.* **1997**, *69*, 2504.
- (262) Shelimov, K. B.; Jarrold, M. F. *J. Am. Chem. Soc.* **1997**, *119*, 2987.
- (263) Shelimov, K. B.; Clemmer, D. E.; Hudgins, R. R.; Jarrold, M. F. *J. Am. Chem. Soc.* **1997**, *119*, 2240.
- (264) Taraszka, J. T.; Clemmer, D. E. Unpublished results.
- (265) Shelimov, K. B.; Jarrold, M. F. *J. Am. Chem. Soc.* **1996**, *118*, 10313.
- (266) Kieffhaber, T. *Proc. Natl. Acad. Sci. U.S.A.* **1995**, *92*, 9029.
- (267) Itzhaki, L. S.; Evans, P. A.; Dobson, C. M.; Radford, S. E. *Biochemistry* **1994**, *33*, 5212.
- (268) Radford, S. E.; Dobson, C. M.; Evans, P. A. *Nature* **1992**, *358*, 302.
- (269) Chaffotte, A. F.; Guillou, Y.; Goldberg, M. E. *Biochemistry* **1992**, *31*, 9694.
- (270) Reimann, C. T.; Velazquez, I.; Tapia, O. *J. Phys. Chem. B* **1998**, *102*, 2277.
- (271) Reimann, C. T.; Velazquez, I.; Tapia, O. *J. Phys. Chem. B* **1998**, *102*, 9344.
- (272) Arteca, G. A.; Valazquez, I.; Reimann, C. T.; Tapia, O. *Phys. Rev. E* **1999**, *59*, 5981.
- (273) Gas-phase basicity values for these bases are from ref 116 and Decouzon, M.; Gal, J. F.; Maria, P. C.; Raczynska, E. D. *Rapid Commun. Mass Spectrom.* **1993**, *7*, 599.
- (274) Li, J.; Clemmer, D. E. Unpublished results.
- (275) Lau, Y. K.; Ikuta, S.; Kebarle, P. *J. Am. Chem. Soc.* **1982**, *104*, 1462.
- (276) Klassen, J. S.; Blades, A. T.; Kebarle, P. *J. Phys. Chem.* **1995**, *99*, 15509.
- (277) Woenckhaus, J.; Hudgins, R. R.; Jarrold, M. F. *J. Am. Chem. Soc.* **1997**, *119*, 9586.
- (278) Fye, J. L.; Woenckhaus, J.; Jarrold, M. F. *J. Am. Chem. Soc.* **1998**, *120*, 1327.
- (279) McCammon, J. A.; Gelin, B. R.; Karplus, M. *Nature* **1977**, *267*, 585.
- (280) Levitt, M.; Sharon, R. *Proc. Natl. Acad. Sci. U.S.A.* **1988**, *85*, 7557.

- (281) Deisenhofer, J.; Steigemann, W. *Acta Crystallogr. B* **1975**, *31*, 238.
- (282) Wlodawer, A.; Walter, S.; Huber, R.; Sjölin, L. *J. Mol. Biol.* **1984**, *180*, 301.
- (283) Wlodawer, A.; Nachman, J.; Gilliland, G. L.; Gallagher, W.; Woodward, C. *J. Mol. Biol.* **1987**, *198*, 469.
- (284) Otting, G.; Wüthrich, K. *J. Am. Chem. Soc.* **1989**, *111*, 1871.
- (285) von Helden, G.; Wyttenbach, T.; Bowers, M. T. *Science* **1995**, *267*, 1483.
- (286) Pearlman, D. A.; Case, D. A.; Caldwell, J. C.; Seibel, G. L.; Singh, U. C.; Weiner, P.; Kollman, P. A. *AMBER 4.0*; University of California, San Francisco, 1991.
- (287) Wyttenbach, T.; Bushnell, J. E.; Bowers, M. T. *J. Am. Chem. Soc.* **1998**, *120*, 5098.
- (288) Li, J.; Clemmer, D. E. Unpublished results.
- (289) Henderson, S. C.; Li, J.; Counterman, A. E.; Clemmer, D. E. *J. Phys. Chem. B* **1999**, accepted for publication.
- (290) Pauling, L.; Corey, R. B.; Branson, H. R. *Proc. Natl. Acad. Sci. U.S.A.* **1951**, *37*, 205.
- (291) Chakarbartty, A.; Baldwin, R. L. *Adv. Protein Chem.* **1995**, *46*, 141.
- (292) Marqusee, S.; Robbins, V. H.; Baldwin, R. L. *Proc. Natl. Acad. Sci. U.S.A.* **1989**, *86*, 5286.
- (293) O'Neil, K. T.; DeGrado, W. F. *Science* **1990**, *250*, 646.
- (294) Shoemaker, K. R.; Kim, P. S.; York, E. J.; Stewart, J. M.; Baldwin, R. L. *Nature* **1987**, *326*, 563.
- (295) Sundaralingam, M.; Sekharudu, Y. C. *Science* **1989**, *244*, 1333.
- (296) Hudgins, R. R.; Jarrold, M. F. Submitted for publication.
- (297) Samuelson, S. O.; Martyna, G. J. *J. Chem. Phys.* **1998**, *109*, 11061.
- (298) Millhauser, G. L.; Stenland, C. J.; Bolin, K. A.; van de Ven, J. M. *J. Biomol. NMR* **1996**, *7*, 331.
- (299) Fiori, W. R.; Millhauser, G. L. *Biopolymers* **1995**, *37*, 243.
- (300) Yoder, G.; Pancoska, P.; Keiderling, T. A. *Biochemistry* **1997**, *36*, 15123.
- (301) Groebke, K.; Renold, P.; Tsang, K. Y.; Allen, T. J.; McClure, K. F.; Kemp, D. S. *Proc. Natl. Acad. Sci. U.S.A.* **1996**, *93*, 4025.
- (302) Smythe, M. L.; Nakaie, C. R.; Garland, R. M. *J. Am. Chem. Soc.* **1995**, *117*, 10555.
- (303) Counterman, A. E.; Clemmer, D. E. Unpublished results.
- (304) Hoaglund, C. S.; Valentine, S. J.; Clemmer, D. E. *Anal. Chem.* **1997**, *69*, 4156.
- (305) Hoaglund, C. S.; Valentine, S. J.; Sporleder, C. R.; Reilly, J. P.; Clemmer, D. E. *Anal. Chem.* **1998**, *70*, 2236.
- (306) Henderson, S. C.; Valentine, S. J.; Counterman, A. E.; Clemmer, D. E. *Anal. Chem.* **1999**, *71*, 291.
- (307) Valentine, S. J.; Counterman, A. E.; Hoaglund, C. S.; Reilly, J. P.; Clemmer, D. E. *J. Am. Soc. Mass Spectrom.* **1998**, *9*, 1213.
- (308) Valentine, S. J.; Counterman, A. E.; Hoaglund Hyzer, C. S.; Clemmer, D. E. *J. Phys. Chem.* **1999**, *103*, 1203.
- (309) Leon, S. J. *Linear Algebra with Applications*, 3rd ed.; Macmillan: New York, 1990; pp 208–211.
- (310) Voet, D.; Voet, J. G. *Biochemistry*, 2nd ed.; Wiley: New York, 1995; p 58–60.
- (311) Dudek, M. J.; Ramnarayan, K.; Ponder, J. W. *J. Comput. Chem.* **1998**, *19*, 548.
- (312) Counterman, A. E.; Clemmer, D. E. *J. Am. Chem. Soc.* **1999**, *121*, 4031.
- (313) Connolly, M. L. *J. Am. Chem. Soc.* **1985**, *107*, 1118.
- (314) Harpaz, Y.; Gerstein, M.; Chothia, C. *Structure* **1994**, *2*, 641.
- (315) Richards, F. M. *J. Mol. Biol.* **1974**, *82*, 1.
- (316) Voronoi, G. F. *J. Reine Angew. Math.* **1908**, *134*, 198.
- (317) Horz, D. E.; Brownlee, D. E.; Fechtig, H.; Hartung, J. B.; Morrison, D. A.; Neukum, G.; Schneider, E.; Fedder, J. F.; Gault, D. E. *Planet. Space Sci.* **1975**, *23*, 151.
- (318) Szenes, G. *Phys. Rev. B* **1995**, *51*, 8026.
- (319) Reimann, C. T.; Quist, A. P.; Kopniczky, J.; Sundqvist, B. U. R.; Erlandsson, R.; Tengvall, P. *Nucl. Instrum. Methods Phys. Res., Sect. B* **1994**, *88*, 29.
- (320) Quist, A. P.; Ahlbom, J.; Reimann, C. T.; Sundqvist, B. U. R. *Nucl. Instrum. Methods Phys. Res., Sect. B* **1994**, *88*, 164.
- (321) Light-Wahl, K. J.; Springer, D. L.; Winger, B. E.; Edmonds, C. G.; Camp, D. G., II; Thrall, B. D.; Smith, R. D. *J. Am. Chem. Soc.* **1993**, *115*, 803.
- (322) Doktycz, M. J.; Habibi-Gougarzi, S.; McLuckey, S. A. *Anal. Chem.* **1994**, *66*, 3416.
- (323) Ding, J.; Anderegg, R. J. *J. Am. Soc. Mass Spectrom.* **1995**, *6*, 159.
- (324) Gentil, E.; Banoub, J. *J. Mass Spectrom.* **1996**, *31*, 83.
- (325) Aaserud, D. J.; Kelleher, N. L.; Little, D. P.; McLafferty, F. W. *J. Am. Soc. Mass Spectrom.* **1996**, *7*, 1266.
- (326) Klassen, J. S.; Schnier, P. D.; Williams, E. R. *J. Am. Soc. Mass Spectrom.* **1998**, *9*, 1117.
- (327) Schnier, P. D.; Klassen, J. S.; Strittmatter, E. F.; Williams, E. R. *J. Am. Chem. Soc.* **1998**, *120*, 9605.
- (328) Hoaglund, C. S.; Liu, Y.; Ellington, A. D.; Pagel, M.; Clemmer, D. E. *J. Am. Chem. Soc.* **1997**, *119*, 9051.
- (329) Robinson, J. M.; Greig, M. J.; Griffey, R. H.; Mohan, V.; Laude, D. A. *Anal. Chem.* **1998**, *70*, 3566.
- (330) Freitas, M.; Shi, S. D.-H.; Hendrickson, C. L.; Marshall, A. G. *J. Am. Chem. Soc.* **1998**, *120*, 19187.
- (331) Lee, S.; Wyttenbach, T.; Bowers, M. T. *Int. J. Mass Spectrom. Ion Processes* **1997**, *167*, 605.
- (332) Green, M. K.; Penn, S. G.; Lebrilla, C. B. *Am. Soc. Mass Spectrom.* **1995**, *6*, 1247.
- (333) Imperiali, B. *Acc. Chem. Res.* **1997**, *30*, 452.
- (334) Loo, J. A. *Eur. Mass Spectrom.* **1997**, *3*, 93.
- (335) Mann, M.; Meng, C. K.; Fenn, J. B. *Anal. Chem.* **1989**, *61*, 1702.
- (336) Reinhold, B. B.; Reinhold V. N. *J. Am. Soc. Mass Spectrom.* **1992**, *3*, 207.
- (337) Ashton, D. A.; Beddell, C. R.; Cooper, D. J.; Green, B. N.; Oliver, R. W. A. *Org. Mass Spectrom.* *28*, 721.
- (338) Winger, B. E.; Light-Wahl, K. J.; Smith, R. D. *J. Am. Soc. Mass Spectrom.* **1992**, *3*, 624.
- (339) Ogorzalek Loo, R. R.; Udseth, H. R.; Smith, R. D. *J. Phys. Chem.* **1991**, *95*, 6412.
- (340) Stephenson, J. L., Jr.; McLuckey, S. A. *J. Am. Soc. Mass Spectrom.* **1998**, *9*, 585.
- (341) McLuckey, S. A.; Stephenson, J. L., Jr.; Asano, K. G. *Anal. Chem.* **1998**, *70*, 1198.
- (342) Scalf, M.; Westphall, M. S.; Krause, J.; Kaufman, S. L.; Smith, L. M. *Science* **1999**, *283*, 194.
- (343) Kaufman, S. L.; Skogen, J. W.; Dorman, F. D.; Zarrin, F. *Anal. Chem.* **1996**, *68*, 1895.
- (344) Schnier, P. D.; Williams, E. R. *Anal. Chem.* **1998**, *70*, 3033.
- (345) Gill, L. A.; Wells, M.; Patterson, G. E.; Amy, J. W.; Cooks, R. G. *Anal. Chem.* **1998**, *70*, 4448.
- (346) Wells, J. M.; Plass, W. R.; Patterson, G. E.; Ouyang, Z.; Badman, E. R.; Cooks, R. G. *Anal. Chem.* **1999**, *71*, 3405.
- (347) Buryakov, K. A.; Krylov, E. V.; Nazarov, E. G.; Rasulev, U. K. *Int. J. Mass Spectrom. Ion Processes* **1993**, *128*, 143.
- (348) Guevremont, R.; Purves, R. W. *Rev. Sci. Instrum.* **1999**, *70*, 1370.
- (349) Krylov, E. V. *Tech. Phys.* **1999**, *44*, 113.
- (350) Purves, R. W.; Guevremont, R.; Day, S.; Pipich, C. W.; Matyjaszczyk, M. S. *Rev. Sci. Instrum.* **1998**, *69*, 4094.
- (351) Purves, R. W.; Guevremont, R. *Anal. Chem.* **1999**, *71*, 2346.

CR980139G

